



저작자표시-비영리-변경금지 2.0 대한민국

이용자는 아래의 조건을 따르는 경우에 한하여 자유롭게

- 이 저작물을 복제, 배포, 전송, 전시, 공연 및 방송할 수 있습니다.

다음과 같은 조건을 따라야 합니다:



저작자표시. 귀하는 원저작자를 표시하여야 합니다.



비영리. 귀하는 이 저작물을 영리 목적으로 이용할 수 없습니다.



변경금지. 귀하는 이 저작물을 개작, 변형 또는 가공할 수 없습니다.

- 귀하는, 이 저작물의 재이용이나 배포의 경우, 이 저작물에 적용된 이용허락조건을 명확하게 나타내어야 합니다.
- 저작권자로부터 별도의 허가를 받으면 이러한 조건들은 적용되지 않습니다.

저작권법에 따른 이용자의 권리는 위의 내용에 의하여 영향을 받지 않습니다.

이것은 [이용허락규약\(Legal Code\)](#)을 이해하기 쉽게 요약한 것입니다.

[Disclaimer](#)

공학박사학위논문

A Study on the Mechanical Deformation
dependent Electrical Property Change in
PEDOT:PSS Conductive Polymer for
Stretchable Electronic Conductor

신축성 전극 개발을 위한 전도성 고분자
PEDOT:PSS 의 기계적 변형에 따른
전기적 특성 변화 연구

2016년 2월

서울대학교 대학원

재료공학부

이 유 용

ABSTRACT

A Study on the Mechanical Deformation dependent Electrical Property Change in PEDOT:PSS Conductive Polymer for Stretchable Electronic Conductor

Yoo-Yong Lee

Department of Materials Science and Engineering

The Graduate School

Seoul National University

Recently, conducting polymers have been widely used to produce flexible and stretchable electronics, which are exposed to large amounts of mechanical strains. In contrast to elastic strain regions, extrinsic contributions such as defect generation, microstructural and dimensional changes, and neighboring materials can influence the change of electrical properties in concerted ways under large and plastic deformation. Therefore, systematically extinguishing each extrinsic factor and understanding the mechanism of change in the resistivity of a material subject to mechanical deformation is becoming increasingly important for the realization of stretchable electronic conductors. Here, we investigated the use of a poly(3,4-ethylenedioxythiophene):poly(styrene sulfonate) (PEDOT:PSS) conductive

polymer as an electrode material and developed two classes of stretchable electronic conductors that could endure large amounts of mechanical stretch. First, we suggested the use of a film-type PEDOT:PSS conductor by applying a polyimide (PI) substrate that had matching mechanical properties (Poisson's ratio and elastic modulus). The PEDOT:PSS films successfully stretched above 60% strain without any generation of defects (buckles or cracks). Interestingly, upon stretching the films, the resistivity of the pristine PEDOT:PSS decreased by 80%, however, it exhibited almost invariant change for dimethyl sulfoxide (DMSO)-doped PEDOT:PSS, which were directly caused by a morphological change in PEDOT:PSS. Due to the dissolution of PEDOT chains after doping with DMSO, the electrical path was not changed under mechanical strain. In case of the pristine films, the equivalent growth of conductive PEDOT-rich cores led to significant enhancements in charge conductivity. For the first time, we revealed a mechanism for the strain-induced growth of PEDOT-rich cores and discovered the mechanically tunable conductivity of PEDOT:PSS films. Secondly, we developed a new class of soft material-based electronic conductors based on PEDOT:PSS organogel. Due to its natural softness and compatibility with human-skin, this material enabled the stable transport of electrical signals upon severe mechanical deformation. Even under large amounts of stretch, the electrical resistance increased insensitively when the strain up to 350% and became lower than the

theoretical increase in resistance resulting from geometrical shape changes. This was because of the formation of a polymeric conducting path that had closely packed PEDOT:PSS in the gel. The resistance change in response to strain was invariant even when the material was stretched to 50% strain in a cyclic deformation. Furthermore, by using ethylene glycol as a liquid constituent for the organogel, purely electrical conduction was enabled without the use of any electrochemical reactions, successfully resulting in long-term environmental stability. The PEDOT:PSS stretchable electronic conductors can be widely applied to electrical interconnection applications such as human wearable and attachable devices that cover any arbitrary curved surface or three-dimensional structures that require large amounts of stretchability. This work is a multidisciplinary project that includes studies in materials science, polymer science, and electronics and will enable researchers to design and tailor entirely new classes of conductive organic hybrid materials; such materials will also lead into a new area of biocompatible electronic devices.

Keywords: Conductive polymer; PEDOT:PSS; Morphological change; Mechanical-electrical correlation; Stretchable electronic conductor; Strain insensitivity;

Student Number: 2010-20623

Table of Contents

Abstract	i
Table of Contents	iv
List of Tables	viii
List of Figures	ix

Chapter 1. Introduction

1.1. Electronic conductors for stretchable electronics	1
1.1.1. Stretchable electronic conductors	1
1.1.2. Soft stretchable conductors consisting of PEDOT conductive polymers	5
1.2. Issues on PEDOT:PSS-based stretchable conductors	5
1.3. Objective of the thesis	11
1.4. Organization of the thesis	12

Chapter 2. Theoretical Background

2.1. PEDOT:PSS conductive polymers	13
2.1.1. Introduction	13
2.1.2. Synthesis	14
2.1.3. Morphology	17
2.1.4. Mechanical properties	21

2.1.5. Electrical properties	23
2.1.6. Secondary doping	26

Chapter 3. Experimental Methods

3.1. Sample preparation	31
3.1.1. Thin film-type PEDOT:PSS	31
3.1.2. Soft gel-type PEDOT:PSS	32
3.2. Characterization	34
3.2.1. Mechanical properties	34
3.2.2. Electrical properties	34
3.2.3. Morphological analyses	38

Chapter 4. Strong Correlation between the Resistivity and Tensile Strain of PEDOT:PSS films

4.1. Introduction	39
4.2. Methods	41
4.3. Effect of substrates under large amounts of stretch	42
4.3.1. Mismatch of mechanical properties	42
4.3.2. Substrate dependence of defect generation	47
4.4. Electrical properties of PEDOT:PSS under large stretch	54
4.4.1. Morphology of PEDOT:PSS film	54
4.4.2. Resistivity changes with tensile strain	56
4.5. Stretch-induced growth of PEDOT-rich cores	59
4.6. Application of the variable range hopping model	64

4.7. Resistivity changes induced by morphological changes	65
4.8. Summary	71

**Chapter 5. Growth Mechanism of Strain-dependent Morphological Changes
in PEDOT:PSS Films**

5.1. Introduction	72
5.2. Methods	76
5.3. Resistivity changes dependent on PEDOT:PSS thickness	78
under tensile strain	
5.4. Evolution of PEDOT:PSS morphology under tensile strain	83
5.4.1. Growth procedure of PEDOT cores with strain	83
5.4.2. Mechanism of the local rearrangement of PEDOT	87
5.5. Changes in the chemical environment induced by PEDOT	90
rearrangement	
5.6. Dependence of changes in resistivity on the weight ratio of	95
PEDOT to PSS	
5.7. Summary	99

**Chapter 6. Strain-insensitive stretchable electronic conductors:
PEDOT-PSS/Acrylamide organogels**

6.1. Introduction	100
6.2. Methods	102
6.3. Electronic conductor of PEDOT:PSS-PAAm organogel	105
6.3.1. Demonstration of stretchable LED arrays	105

6.3.2. Electrical conduction under DC voltage	111
6.4. Fabrication of the organogel with a PEDOT:PSS polymeric path	119
6.4.1. Formation of polymeric conducting path	119
6.4.2. Microstructure	122
6.5. Mechanical and electrical response under tensile deformation	126
6.5.1. Mechanical properties	126
6.5.2. Tensile fatigue insensitive changes of electrical properties	129
6.6. Environmental stabilities of the organogels	132
6.7. Summary	135

Chapter 7. Conclusion

7.1. Conclusion	136
7.2 Future work and recommendations	138

References	141
-------------------	-----

Abstract (In Korean)	154
-----------------------------	-----

Curriculum Vitae	156
-------------------------	-----

LIST OF TABLES

- Table 4.1.** The mechanical properties of PEDOT:PSS, PDMS, and PI films.
- Table 4.2.** Comparison between increased area by geometrical change from the extension in length and the contraction in width direction and the resultant change in average area of each PEDOT-rich cores as a function of strain of the films.
- Table 5.1.** Representative FT-IR absorption band for PEDOT:PSS and PI films.

LIST OF FIGURES

- Figure 1.1.** Mechanical and electrical requirements of stretchable electronic conductors for the realization of human wearable or attachable devices.
- Figure 1.2.** Typical conductive polymers and their structures in undoped forms
- Figure 1.3.** The evolution of the utilization of PEDOT:PSS conductive polymers ranging from a charge transport layer to a stretchable electrode.
- Figure 1.4.** Response of electrical properties of PEDOT:PSS under large amounts of mechanical stretching: (i) Stretch-response, (ii) Electrical reversibility, (iii) Recovery behavior, and (iv) Rupture mode.
- Figure 2.1.** The synthetic procedure for generating PEDOT:PSS. Sodium persulfate is used as an oxidizing agent for EDOT, and PSS acts as charge-balancing counter-ions for positively charged PEDOT.
- Figure 2.2** Schematic illustration of PEDOT:PSS morphology. The morphology is primarily composed of a PEDOT-rich core and a PSS shell.

- Figure 2.3** AFM phase images of PEDOT:PSS films. The bright and dark fields indicate the PEDOT-rich core and PSS shell, respectively. The image was obtained by tapping-mode AFM at a scale of $1 \times 1 \mu\text{m}^2$.
- Figure 2.4** The mechanical properties of PEDOT:PSS films. (a) Stress-strain curves, (b) Young's modulus, (c) elastic strain, and (d) Poisson's ratio of PEDOT:PSS films at different levels of humidity^[1].
- Figure 2.5** Temperature-dependent conductivity changes in PEDOT:PSS films measured in (a) lateral and (b) vertical directions^[2].
- Figure 2.6** Electrical conductivities of PEDOT:PSS films as a function of DMSO concentration.
- Figure 2.7** Crystal structure PEDOT, in projections along the b-axis and c-axis for upper and lower conformations, respectively^[20].
- Figure 2.8** (a) WAXS profiles of PEDOT:PSS solid films and water dispersion with 3 wt.% of EG. (b) Comparison of WAXS profiles of PEDOT:PSS films for pristine samples and those with added water, ethanol, and ethylene glycol^[21].

Figure 3.1 I (Current) - V (Voltage) sweep of PEDOT:PSS-PAAm gel using the four-point probe method. Four electrical contacts were made at each end of the gel and the middle of two points with silver paste.

Figure 4.1 Origins of extrinsic resistance changes in PEDOT:PSS films deposited on substrates under tensile deformation. There are two contributions: (i) Geometrical shape changes and (ii) Defect (i.e., buckles and cracks) generation.

Figure 4.2 Experimental set-up for the *in-situ* measurement of the electrical resistance of PEDOT:PSS films during the tensile stretching of films coated on PI or PDMS substrates.

Figure 4.3 Relative resistance changes ($\Delta R/R_0$ (%)) of PEDOT:PSS films doped with 5 wt. % DMSO as a function of tensile strains of the PDMS and PI substrates. For comparison, the resistance changes calculated from the changes in the geometry of the PI substrates are presented as dotted lines.

Figure 4.4 Schematics and optical/SEM images of PEDOT:PSS films on PDMS and PI substrates during substrate stretching according to the difference in the Poisson's ratio between the films and the substrates at (a) $\nu_f < \nu_s$ and (b) $\nu_f \cong \nu_s$, where ν_f and ν_s are the Poisson's ratios of the $\nu_f < \nu_f$ films and the substrates, respectively. The stretching direction is indicated by arrows in the micrographs.

Figure 4.5 In-situ optical microscopy/SEM images of PEDOT:PSS films on (a) PDMS and (b) PI substrates at specific tensile strains and when released to their load-free states. The arrows indicate the stretching directions.

Figure 4.6 AFM phase images of pristine (a)-(d) and 5 wt. % DMSO-doped (e), (f) PEDOT:PSS films at each strain denoted in the images. The arrow indicates the stretching direction, and all the images were obtained by tapping-mode AFM at a scale of $1 \times 1 \mu\text{m}^2$.

Figure 4.7 (a) Relative resistance changes of PEDOT:PSS films doped with various concentrations of DMSO (0, 5, and 10 wt. %) on O_2 -plasma-treated PI substrates during stretching of up to 60 % strain. (b) The resistivity and (c) relative changes in resistivity of the PEDOT:PSS films as a function of strain. The orange spheres denote the resistivities calculated from the 3D VRH model.

Figure 4.8 Reproduced AFM phase images of pristine PEDOT:PSS films at each strain using image analyzing software. The black and white regions in the images indicate tangled PEDOT-rich cores and excess PSS shells, respectively. All images were obtained with tapping mode AFM at a scale of $1 \times 1 \mu\text{m}^2$. The arrow indicates the direction of stretching.

Figure 4.9 (a) Relative resistivity changes ($\Delta\rho/\rho_0$ (%)) of PEDOT:PSS films as a function of strain (9, 17, 26, and 35 %) for the pristine and 5 wt. % DMSO-doped films. (b) The change in resistivity parallel and perpendicular to the stretching direction of pristine films.

Figure 4.10 AFM phase images and reproduced images of pristine PEDOT:PSS films (a) at a strain of 42 % and (b) released to their load-free states (28 %).

Figure 4.11 Relative resistivity change ($\Delta\rho/\rho_0$ (%)) of pristine PEDOT:PSS films on PI substrates as a function of time during stretching and releasing. Blue and black arrows indicate that strain at the onset of releasing (9, 17, 26, and 35 %) and load-free states after releasing, respectively.

Figure 5.1 (a) Electrical resistivities of PEDOT:PSS films as a function of the RPM of a spin-coater. (b) Thickness of PEDOT:PSS films as a function of the RPM of a spin-coater.

Figure 5.2 Mechano-resistivity changes of PEDOT:PSS films. (a) The resistance changes of PEDOT:PSS films with tensile strains according to the thickness of the films. (b) Relative changes in the resistances ($\Delta R/R_0$) with strain. Gray circles indicate the theoretical increases in resistance based on geometrical changes. (c) Relative changes in resistivity ($\Delta\rho/\rho_0$) as a function of tensile strain.

Figure 5.3 Morphological changes of PEDOT:PSS according to the applied amounts of tensile strain. (a) AFM phase images of PEDOT:PSS films at each strain denoted in the images. Bright field and dark field images represent the PEDOT-rich cores and the PSS shells, respectively. The arrow indicates the stretching direction, and all the images were obtained using tapping-mode AFM at a scale of $1 \times 1 \mu\text{m}^2$. (b) Distribution of cumulative density as a function of PEDOT-rich core area using a log-normal distribution function. (c) The change in the areas of PEDOT-rich cores at 5%, 50%, and 95% of cumulative density as a function of tensile strain.

Figure 5.4 Schematic illustration of the evolution procedure of PEDOT-rich cores by mechanical tensile stretching. During the stretching process, a local rearrangement of PEDOT chains occurred, and the PEDOT chains locally migrated to the vicinity of the PSS shells to reduce the electro-repulsive force among the PSS chains. The areas of the PEDOT-rich cores increased after stretching.

Figure 5.5 Spectroscopic analysis of the changes in bonding energy with tensile strain: (a) XPS spectra of S 2p for PEDOT:PSS films as a function of applied strain (0, 16, 28, and 42%). (b) The change in binding energy of S 2p in PEDOT according to the strain. (c) FT-IR absorption spectra for PEDOT:PSS films with tensile strain and PI substrates. The inset shows the peak shift of C-S bonding. (d) The change in carbon-sulfur (C-S) bonding energy in PEDOT chains as a function of the strain.

Figure 5.6 Mechano-resistivity changes in PEDOT:PSS films depending on the weight ratio of PEDOT to PSS. (a) Resistance changes of PEDOT:PSS films with tensile strain for PEDOT to PSS ratios of 1:6 and 1:2.5. (b) Relative changes in resistivity as a function of the strain for the 1:6 and 1:2.5 weight ratios. (c) Schematic illustration of the evolution of PEDOT-rich cores with strain dependency on the weight ratio of PEDOT to PSS.

Figure 6.1 Schematic illustration of PEDOT:PSS-PAAm organogel microstructures. Conductive and soluble PEDOT:PSS polymers are dispersed in PAAm matrix polymers, and ethylene glycol organic solvent is the liquid constituent of the organogels.

Figure 6.2 Electrical interconnection with PEDOT:PSS-PAAm organogels. (a) LED operation with interconnections containing the organogels while being (b) stretched, twisted by (c) 360° and (d) 720°, and (e) stretched in a twisted state.

Figure 6.3 Strain-insensitive electronic conductor of a PEDOT:PSS-PAAm organogel without electrochemical reactions. (a) Schematic illustration of the LED integrated circuit. (b) and (c) Optical images of the circuit before and after stretching up to 200% strain, respectively. The LED light interconnected with PEDOT:PSS-PAAm organogel was still operational even with large deformations.

Figure 6.4 Stretchable LED arrays and their response to biaxial stretching on a balloon. (a) Optical image of a stretchable 2×3 array of LEDs interconnected with PEDOT:PSS-PAAm organogels on an Ecoflex substrate. (b) Optical image of the 2×3 LED array showing the emission of the LEDs in a flatted state. (c) Optical images of the stretchable array of LEDs (2×3) attached to a balloon under biaxial expansion (80% and 167%).

- Figure 6.5** I (current) - V (voltage) measurements of (a) PEDOT:PSS-PAAm organogels according to the weight ratio of PEDOT:PSS relative to PEDOT:PSS plus PAAm, which exhibited ohmic electronic conductivity. (b) Electrical resistivity of the organogels as a function of weight ratios.
- Figure 6.6** Impedance curves of (a) PEDOT:PSS hydrogel and (b) organogel (9.06%) with a frequency ranging from 100 kHz to 0.1 Hz at 10 mV.
- Figure 6.7** Measurement of a I (current) - V (voltage) sweep of the PEDOT:PSS-PAAm hydrogel. Non-ohmic conduction occurred during the current (I) – voltage (V) sweep.
- Figure 6.8** Normalized resistance change (R/R_0) plotted during the stretching of PEDOT:PSS organogels with various weight ratios showing insensitive resistance increases under extension. The inset shows increases in resistance changes when the strain was under 100%. The dotted grey line indicates the theoretical resistance change with the change in dimension.

Figure 6.9 Formation of polymeric conducting paths of PEDOT:PSS distributed PAAm organogels. Synthetic procedure of the electrically conductive PEDOT:PSS-PAAm organogels. Closely packed PEDOT:PSS was obtained from freeze drying the as-received PEDOT:PSS aqueous solution. For the gelation process, the PEDOT:PSS solute was mixed with ethylene glycol (EG) diluted with DI water and acrylamide (AAm) matrix monomer. Ammonium persulphate (APS) and TEMED (tetramethylethylenediamine) were used as the initiator and accelerator for the polymerization of acrylamide (AAm) and the N,N'-methylenebisacrylamide (MBAAm) cross-linker, respectively. The conductive paths were formed inside the gels with PEDOT:PSS. The gels were swelled in EG diluted with DI water for dialysis and were then dried in an oven to selectively evaporate the water inside the gels.

Figure 6.10 SEM images of the cross sections of the PEDOT:PSS-PAAm organogels made from (a) the as-received PEDOT:PSS solution and (b) the freeze-dried PEDOT:PSS solution, respectively. The polymeric conductive path was well formed inside densely packed pores for the organogels made from the freeze-dried PEDOT:PSS solution.

Figure 6.11 Microstructure of an organogel made from freeze-dried PEDOT:PSS solute. Cross-sectional SEM images of the gels at three different points. The magnified images are shown to the right of each image, which correspond to the dotted box.

Figure 6.12 (a) A strip of PEDOT:PSS-PAAm organogel in the undeformed state (left) and stretched state up to 300% strain (right). (b) Stress-strain curves for the PEDOT:PSS-PAAm organogels for various weight ratios of PEDOT:PSS until mechanical fracture of each sample occurred. (c) The Young's modulus and rupture strains of the organogels as a function of weight ratios.

Figure 6.13 Fatigue tests for PEDOT:PSS (9.06%)-PAAm organogels after 1000 cycles of repeated tensile deformations of up to 50% strain. d) Stress-strain curves from the 1st, 10th, 100th, 500th and 1000th cycles. e) Resistance changes as a function of fatigue cycle up to the 1000th cycle. f) Resistance change-strain curves from the 1st, 10th, 100th, 500th and 1000th cycles, which exhibited stretch-insensitive resistance change up to 50% strain within a cycle.

Figure 6.14 Environmentally stable PEDOT:PSS-PAAm organogels. (a) Photographs of the PEDOT:PSS-PAAm hydrogel and organogel before and after being dried in air for 1 day. (b) Schematic illustration of the experimental set-up for measurements of the weight changes of the gels in a vacuum chamber (0.013 atm). (c) Relative changes in the solvent weight (w/w_0 (%)) inside the PEDOT:PSS-PAAm hydrogel and PEDOT:PSS-PAAm organogels of various weight ratios in a vacuum chamber as a function of time at room temperature. The weights of the initial and present amounts of solvent are indicated with w_0 and w , respectively. The organogels contained above 60% of EG, even after 22 hr in the vacuum chamber.

Figure 7.1 Integration of PEDOT:PSS-PAAm organogel-based electronics, including interconnects, a strain sensor, wireless power transfer (WPT), battery, temperature detector, actuator, and other devices on soft elastomeric substrates.

CHAPTER 1

Introduction

1.1. Electronic conductors for stretchable electronics

1.1.1. Stretchable electronic conductors

With a rapid increase in demand for new technologies, electronics are rapidly evolving and being incorporated into human devices. The emergence of stretchable electronics has resulted in its use in an enormous range of applications in human wearable and attachable devices^[3-6]. As an essential component of such devices, conducting materials are required to transport electrical signals between each functional component of the devices even after being subjected to large mechanical deformations. To accomplish successful electrical conductivity, mechanical and electrical considerations for conductive materials should be preceded (Figure 1.1). Conductive materials should not only be mechanically and biologically compatible but should also be electrically functional after experiencing large deformations.

Chapter 1: Introduction

However, the development of stretchable electronic conductors has been hindered by the fundamental challenge of maintaining stable electrical conductivity under severe mechanical deformations.

Conventionally, metallic nanomaterials-based electrical conductors have been widely used for stretchable electronic conductors. The applied nanomaterials have high electrical conductivity, including gold, silver, copper, and carbon nanotube (CNT). Excellent electrical functionality is expected from products using such materials due to their high conductivities. However, concerning mechanical considerations, physical deformabilities are very limited to below approximately 1% of strain in the bulk state. Hence, two typical strategies are used to render the stiff nanomaterials to their stretchable forms by i) generating metallic composites with polymers^[7–11] and ii) modifying the structural design of the nanomaterials^[4,12–16]. First, by using soft polymers as a matrix for metallic nanomaterials (e.g., Ag nanowires, nanoparticles, and CNT), the deformability of materials is secured with the polymeric matrices, and their electrical conductivities are enabled through metallic percolation inside the matrix upon mechanical deformation. Secondly, by designing the structure of metallic conductors in different shapes, such as mesh, coils, or wavy structures, areas of mechanical deformation can be obtained when the conductors are subjected to strain. The electrical conductivities of such conductors are also maintained upon straining due to the lack of plastic deformations.

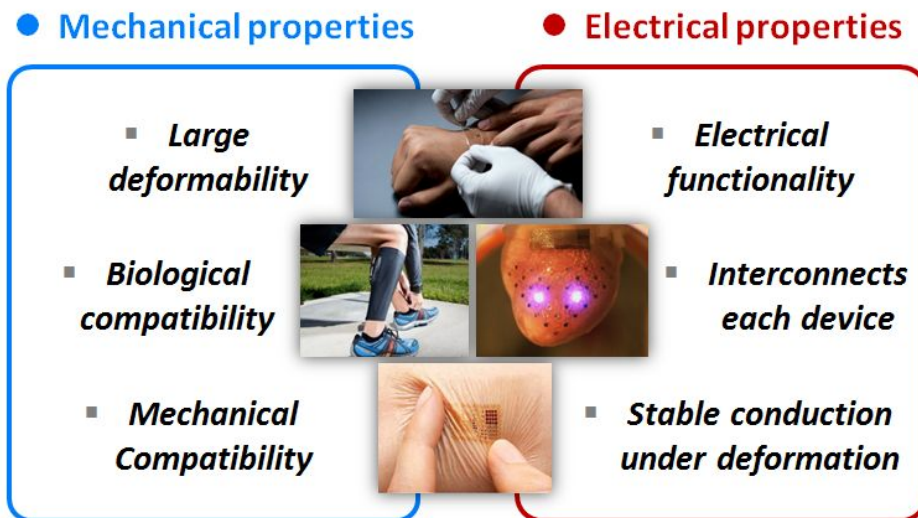


Figure 1.1. Mechanical and electrical requirements of stretchable electronic conductors for the realization of human wearable or attachable devices.

Chapter 1: Introduction

Although metallic nanomaterials-based stretchable conductors have high electrical conductivity, the mechanical stretchability of such conductors are very constrained by the materials and their structural design. For metallic composite conductors, structural collapse and defect generation of the composites can occur by the introduction of mechanical deformations. Moreover, even plastic deformations of nanomaterials occur when the conductors experience large amounts of stretch. When mechanical deformation processes are repeated, it leads to the degradation of electrical percolation paths and an irreversible increase in electrical conductivity. In the case of structured conductors with mesh, wavy, or coiled shape materials, the stretchable areas are directly limited to the structural design of the conductors. When the expandable regions are fully stretched, mechanical and electrical rupture of the conductors occur beyond the strain. Furthermore, due to the mechanical and biological incompatibilities of rigid metallic nanomaterials with soft human skin, severe instability, including interfacial delamination and crack generation, arises during when mechanical deformation occurs on the skin. Therefore, for the realization of intrinsically stretchable electronic conductors compatible with human skin is necessary, and we suggested the development of soft electronic materials-based conductive polymers. In spite of their relatively low conductivity, conductive polymers have several advantages for use in stretchable electronics. Due to the intrinsic nature of these polymers, they are mechanically soft and are compatible with human skin. The Young's modulus of conductive polymers (1 MPa ~ 1GPa) are much lower than those of metallic nanomaterials (100 GPa ~ 500 GPa). In addition, the use of solution processes, such as spin coating, spray coating, and inkjet printing, is possible to form a conductive thin films or bulk materials. Hence, conductive polymers can be widely applied to generate stretchable organic and bioelectronic devices.

1.1.2. Soft stretchable conductors consisting of PEDOT conductive polymers

Conductive polymers are organic materials that can transport electrical charges. They consist of polymeric backbone chains with extended π -conjugations, and their conductivity can be modulated from semiconductive to metallic states by doping them with chemical oxidants. P-doping is usually conducted by partially oxidizing polymers with a chemical oxidant or using an electrochemical method, and mobile holes are generated by depopulation of the bonding π orbital. There are many types of conductive polymers, including polyaniline, polypyrrole, polythiophenes, poly(p-phenylene vinylene)s, and polyethylenedioxythiophene (PEDOT), as shown in Figure 1.2. Among these types of conductive polymers, PEDOT is mostly used in conductive materials due to its high stability in air and relatively high conductivity (550 S/cm) compared to other conductive polymer materials^[17]. As a soft polymeric material, the Young's modulus of PEDOT is in the 3 GPa range, which is much lower than those of metal materials. In its the initial state, PEDOT is a water insoluble polymer, but this solubility problem can be solved by using water-soluble and charge-balancing counter ions such as poly(4-styrenesulfonic acid) (PSS). By combining PEDOT with such counter ions, water-soluble and conductive PEDOT:PSS polymers can be synthesized, and the processability can be greatly improved. With advantages such as mechanical flexibility, high electrical conductivity, excellent stability in air, and good solution processability, PEDOT:PSS polymers can be used to generate stretchable conductors as soft conductive materials.

1.2. Issues on PEDOT:PSS-based stretchable conductors

Chapter 1: Introduction

To utilize PEDOT:PSS polymers as electric conductors, PEDOT must be positively doped and water-soluble. Hence, negatively charged and soluble PSS polyelectrolytes are required to maintain PEDOT:PSS in its proper form in solution. The combination of PEDOT and PSS enables the generation of water-soluble conductive polymers with excellent film forming properties. PEDOT:PSS conductors have mainly been used to develop hole transport layers at the anodes of organic solar cells or organic light emitting diodes. The usage of PEDOT:PSS is limited to early stage applications due to its relatively low conductivity (~ 1 S/cm). However, by mixing these polymers with organic solvents, which have high dielectric constants, or polyalcohols, such as dimethyl sulfoxide (DMSO), ethylene glycol (EG), and sorbitol, the conductivities of PEDOT:PSS polymers can be enhanced by approximately three orders of magnitude. With a large increase in the electrical conductivity of PEDOT:PSS, its utilization has gradually widened (Figure 1.3). PEDOT:PSS layers can be used in organic electrodes for organic devices in place of conventionally used ITO electrodes. Because ITO is rigid and brittle, it is easily ruptured through the generation of cracks upon receiving a small amount of mechanical strain^[18,19]. By using soft PEDOT:PSS electric conductors, organic flexible electronics fields are open, allowing for PEDOT:PSS to be widely utilized in organic or perovskite solar cells. Furthermore, PEDOT:PSS polymers have recently been utilized to generate stretchable electronic conductors by enhancing their mechanical flexibility. For example, stretchable mechanical sensors or organic solar cells have been developed using PEDOT:PSS stretchable conductors.

Following the expansion of the application of PEDOT:PSS in stretchable electronics, PEDOT:PSS conductors have gradually been exposed to large mechanical deformations. When PEDOT:PSS is deformed by the application of stress, its

Chapter 1: Introduction

electrical properties are significantly influenced by configuration and conformation changes of the polymer chains upon being subjected to strain. In situations that require the stretchable conductors to be subjected to large deformations, it is essential to understand changes in the polymers' electrical properties upon being mechanically stretched or released. Mechanical strain is an inevitable factor that conductors experience when they are used in stretchable devices. Hence, the direct responses in the electrical properties of PEDOT:PSS must be elucidated under large deformations for their proper utilization in stretchable conductors.

It is important to figure out how mechanical stretch directly influences the electrical behavior of PEDOT:PSS. As shown in Figure 1.4, the electrical properties of these polymers can be plotted as a function of mechanical stretch. The response of the electrical properties of PEDOT:PSS under large amounts of mechanical stretching can be categorized into four factors: (i) Stretch-response electrical properties, (ii) Electrical reversibility, (iii) Recovery behavior, and (iv) Rupture modes. It is necessary to determine these factors in stretchable system. For example, the available strain range of a material is determined by quantifying its electrical reversibility, and the recovery behavior and rupture of a materials' electrical properties upon being stretched and released influences the reliability of the corresponding stretchable conductors. Therefore, an in-depth understanding of the mechanical strain responsive electrical behaviors of PEDOT:PSS materials will allow us to define the applicable region for stretchable electronics and result in the further development of PEDOT:PSS-based stretchable organic conductors.

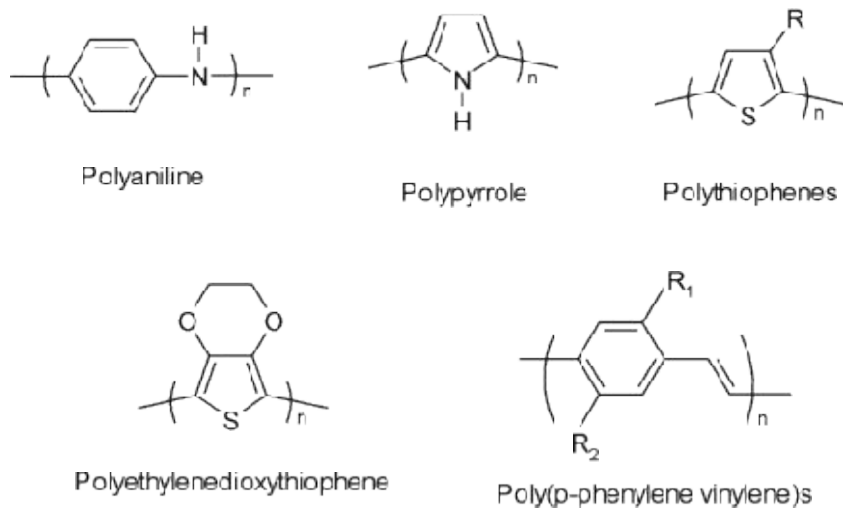


Figure 1.2. Typical conductive polymers and their structures in undoped forms

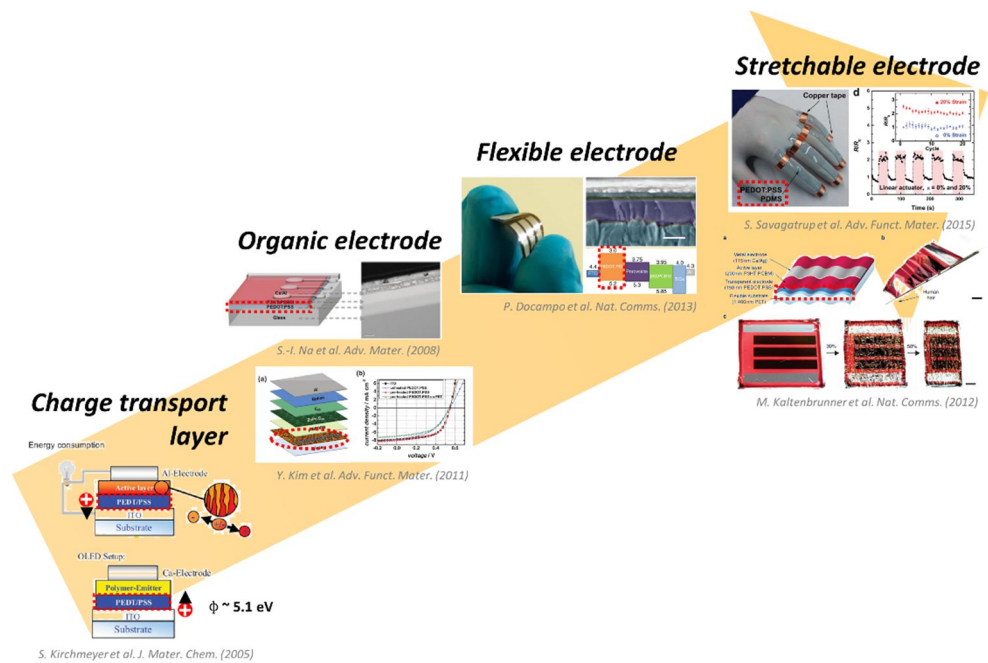


Figure 1.3. The evolution of the utilization of PEDOT:PSS conductive polymers ranging from a charge transport layer to a stretchable electrode.

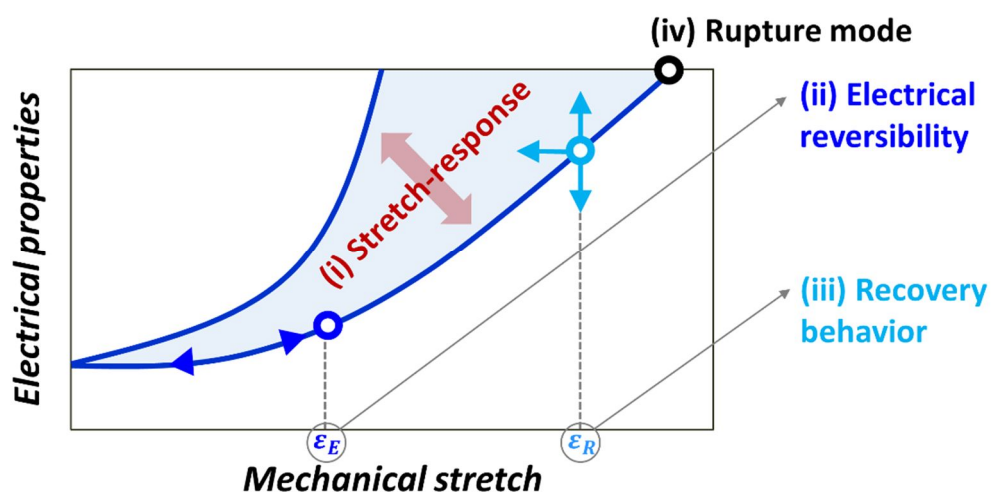


Figure 1.4. Response of electrical properties of PEDOT:PSS under large amounts of mechanical stretching: (i) Stretch-response, (ii) Electrical reversibility, (iii) Recovery behavior, and (iv) Rupture mode.

1.3. Objective of the thesis

PEDOT:PSS is one of the most promising materials in the field of stretchable electronic devices, specifically in stretchable electrodes or electrical interconnections. This thesis has two primary objectives. The first is an in-depth investigation on the correlation between mechanical deformations and the consequent electrical properties changes of PEDOT:PSS films. Change in the electrical properties of these films under strain have critical effects on the utilization of PEDOT:PSS films in stretchable conductors. The reliability and durability of PEDOT:PSS was determined by measuring the responses of its electrical properties, which are reversibility, recovery, and rupture behavior under large amounts of mechanical strain. In addition, to investigate the origin of electrical property changes with the application of strain, we also investigated the scope of molecular structural change of PEDOT:PSS. By correlating the changes in the mechanical and electrical properties of the material, we could predict suitable application areas and the limitations of using PEDOT:PSS as stretchable conductors.

The second objective of this thesis was to develop intrinsically stretchable PEDOT:PSS electronic conductors. We aimed to generate a highly stretchable and human-compatible PEDOT:PSS-based electronic conductor that was not a solid-state material but in a soft gel state. Based understandings of the electrical and structural properties of PEDOT:PSS, we used PEDOT:PSS to generate freestanding and highly stretchable electronic gel conductors. By incorporating highly hydrated polymeric materials with PEDOT:PSS, soft materials-based PEDOT:PSS gel conductors were obtained. PEDOT:PSS gel conductors have the potential to be used in many applications, such as human-wearable and attachable electronics that require

resistance against large amounts of stretching and biocompatibility, as well as electrical functionality.

1.4. Organization of the thesis

This thesis consists of seven chapters. In Chapter 2, basic background information on PEDOT:PSS is introduced, which contains the synthesis, morphology, and descriptions of the mechanical and electrical properties of PEDOT:PSS. Chapter 3 describes the experimental procedures, including PEDOT:PSS sample preparation, characterization of its mechanical and electrical properties and descriptions of its morphology. In Chapter 4, the strong correlation between resistivity and tensile strain on PEDOT:PSS films is introduced. Chapter 5 discusses the mechanism of strain-dependent morphological changes for the PEDOT:PSS films. Chapter 7 introduces the development of highly stretchable PEDOT:PSS-based soft gel electronic conductors. Finally, Chapter 8 summarizes the results of this study.

CHAPTER 2

Theoretical background

2.1. PEDOT:PSS conductive polymers

2.1.1. Introduction

PEDOT:PSS conductive polymers are widely utilized in various electronics fields. Two major advantages of PEDOT:PSS are their high electrical conductivity and good solution processability. To transport mobile electrical carriers, PEDOT should be in a positively doped state that has unpaired π electrons. Simultaneously, it requires an additive to be in a water-soluble form of the doped state of PEDOT due to the hydrophobicity of PEDOT. In this respect, PSS is the most suitable additive that meets the requirements for PEDOT. PSS is a highly water-soluble and a negatively charged state in an aqueous solution. By combining PSS with PEDOT, the positive charge of PEDOT can be maintained and dispersed in a solution to form a polymeric dispersion. This enables the electronic application of PEDOT:PSS due to a large enhancement in its solution processability.

Chapter 2: Theoretical background

To understand the overall function of PEDOT:PSS, this Chapter starts with a description of the chemical synthetic procedure to generate PEDOT:PSS. The formation of PEDOT:PSS significantly influences its morphologies in solution and film states. This is followed by descriptions of the morphology, mechanical, and electrical properties of PEDOT:PSS films and improvements in their electrical conductivity by introducing additional treatment to PEDOT:PSS solutions.

2.1.2. Synthesis

PEDOT:PSS is synthesized by oxidatively polymerizing EDOT (monomer of PEDOT) in the presence of PSS negatively charged counter-ions. The polymerized and positively charged PEDOT is combined with PSS, which forms a PEDOT:PSS polymeric dispersion. PSS is used in excess as the counter-ions for PEDOT. Typically, the weight ratio of PEDOT to PSS in PEDOT:PSS dispersions ranges from 1:2.5 to 1:20. Hence, PEDOT can be well dispersed in a solution in a positively charged state that is found for every three to four thiophene rings. Cationic PEDOT chains can only be obtained by combining PEDOT with polyanions of PSS chains.

The solvent used for the synthesis of PEDOT:PSS polymeric dispersions is water. Water is non-toxic, inert, and a good polar solvent for PSS. In contrast, EDOT monomers have poor solubility in water. Only a small amount of EDOT dissolves in water; typically, 0.2 g of EDOT dissolves in 100 mL water at 20 °C. The polymerization of EDOT is conducted in the aqueous PSS solution. The pH of water is important for the polymerization of EDOT in the PSS solution. An acidic environment is helpful for PEDOT polymerization due to the catalytic effect of acid for the polymerization reaction. The most critical agent for the reaction is the oxidant

Chapter 2: Theoretical background

used to convert EDOT to a PEDOT polymer.

Of the various oxidizing agents available, peroxodisulfates are the most commonly used versatile oxidant. For example, sodium, potassium, and ammonium persulfate are mainly used. Figure 2.1 shows a conventional procedure used to synthesize PEDOT:PSS. First, PSS is fully dissolved in water and ionized to negatively charged moieties for the generation of appropriate counter-ions. Subsequently, EDOT monomer and the oxidizing agent, sodium persulfate, are dispersed in the solution, and a small amount of HCl solution is added to catalyze the polymerization reaction. During the reactions, the EDOT monomers are oxidized, and oxidative polymerization of the monomers occurs to generate PEDOT. The positively charged PEDOT chains balance the charge state by bonding with negatively charged PSS counter-ions. The synthesized PEDOT:PSS can fully dissolve in an aqueous solution and remains in a charged state for electrical conduction.

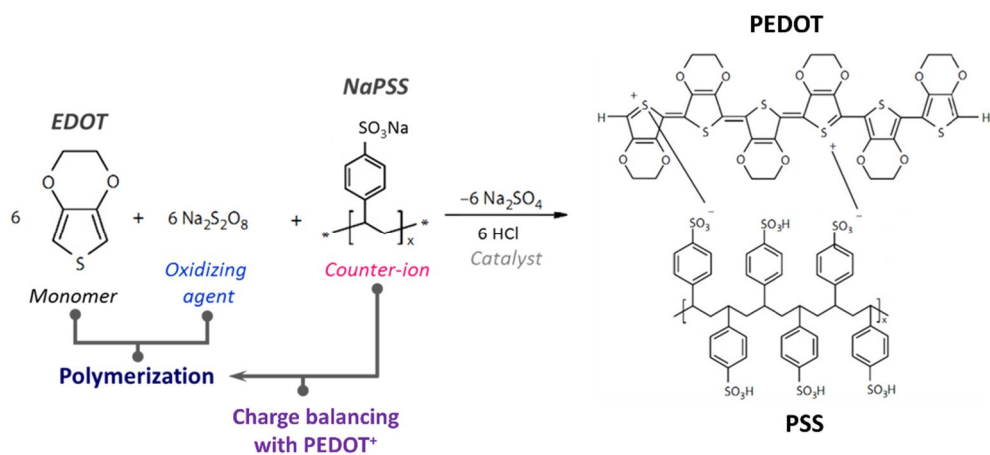


Figure 2.1. The synthetic procedure for generating PEDOT:PSS. Sodium persulfate is used as an oxidizing agent for EDOT, and PSS acts as charge-balancing counter-ions for positively charged PEDOT.

2.1.3. Morphology

The PEDOT:PSS has a particular structure because it is a combination of positively charged PEDOT with an excess amount of negatively charged PSS. Polymerized PEDOT has relatively short chains compared to PSS polyanions. The molecular weight of PEDOT is approximately 1,000 to 2,500 Da, which translates to the structuring having 6 to 18 repeating monomers with oligomeric segments. The molecular weights of PSS polyanions are approximately 400,000 Da, which is much higher than those of PEDOT segments. Because the PSS chains are dissolved in water in negatively charged states, the positively charged PEDOT segments bond to PSS through Coulomb interactions. For the dispersion of PEDOT:PSS in water, relatively high amounts of PSS chains are used compared to PEDOT in the synthesis of PEDOT:PSS. Hence, excess amounts of PSS chains that are not bonded to PEDOT segments are dispersed by bonding with each other through hydrogen bonds. Due to the chemical conformations of PEDOT to PSS and PSS to PSS chains, core and shell-like morphologies have been observed.

The morphology of PEDOT:PSS is shown in Figure 2.1. PEDOT:PSS forms a core and shell, which consist of PEDOT segments and PSS chains. The core is mainly composed of PEDOT segments bonded with PSS chains, which is called a PEDOT-rich core. The shell is a polymeric layer of excess PSS chains, which is called a PSS shell. Inside the PEDOT-rich core, highly entangled PEDOT segments are randomly distributed. The PSS shells are strongly bonded with excess amounts of PSS chains, which form the outside layers of PEDOT-rich cores. The sizes of the core and shell are dependent on the weight ratio of PEDOT and PSS. In case of conventionally used PEDOT:PSS that has a weight ratio of 1:2.5, the diameter of the cores are 40 ~100 nm

Chapter 2: Theoretical background

and the thicknesses of the shells are 5 ~ 10 nm; these values change according to the weight ratios of PEDOT and PSS. The morphology of PEDOT:PSS can be observed with phase imaging using atomic force microscope (AFM) in tapping mode. The phase images of PEDOT:PSS films (Figure 2.3) demonstrate that the PEDOT-rich cores (bright field) and the PSS shells (dark field) can be clearly observed due differences in viscosity of the cores and shells.

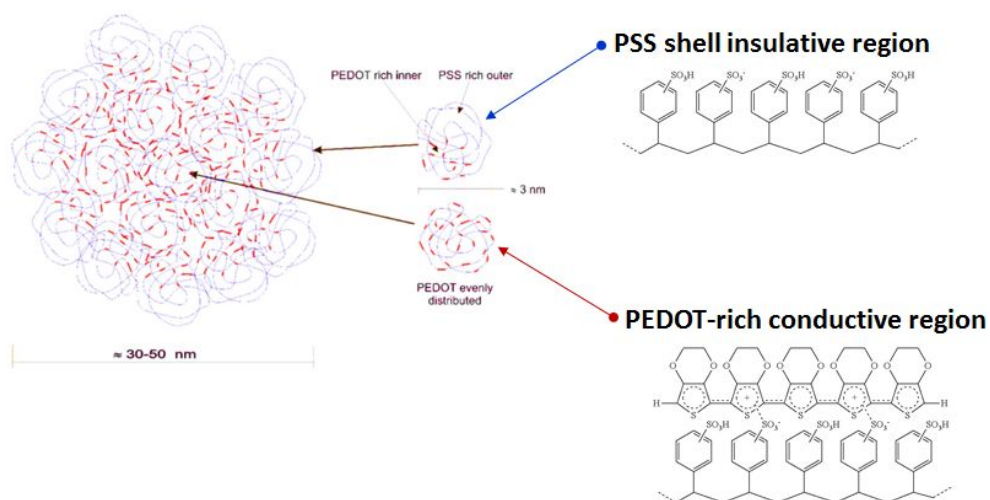


Figure 2.2. Schematic illustration of PEDOT:PSS morphology. The morphology is primarily composed of a PEDOT-rich core and a PSS shell.

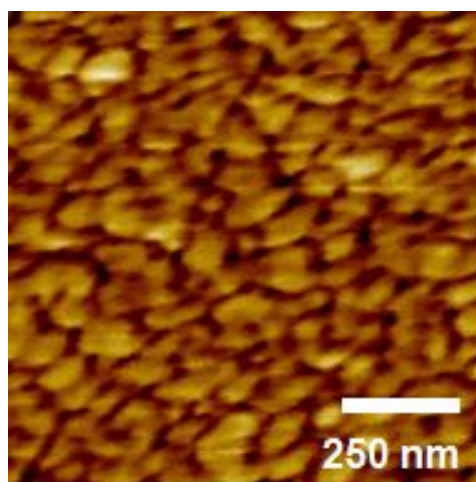


Figure 2.3. AFM phase images of PEDOT:PSS films. The bright and dark fields indicate the PEDOT-rich core and PSS shell, respectively. The image was obtained by tapping-mode AFM at a scale of $1 \times 1 \mu\text{m}^2$.

2.1.4. Mechanical properties

To utilize soft polymeric PEDOT:PSS in stretchable electronics, understanding the mechanical properties of PEDOT:PSS is important. Its mechanical properties, including tensile strength, elastic modulus, and the Poisson's ratio of PEDOT:PSS films, were obtained using a tensile test^[1]. The stress-strain curves are shown in Figure 2.4. The tensile stress was found to gradually increase and become saturated with an increase in the tensile strain. The curves were dependent on the relative humidity of the air because hygroscopic PSS swells by soaking the moisture in the air. When the humidity increased in the air, the stress-strain curves shifted down due to the weak bonding strengths of the swelled PSS chains. These stress-strain curves exhibited the mechanical properties of the PEDOT:PSS films (Figure 2.5). At room humidity (30%), the Young's modulus of PEDOT:PSS was 3 Gpa, which was similar to the corresponding values for typical compliant polymers such as PI and PET. Other mechanical properties such as elastic strain and Poisson's ratio were 2% and 0.34, respectively, which were identical to those of other flexible and compliant polymers.

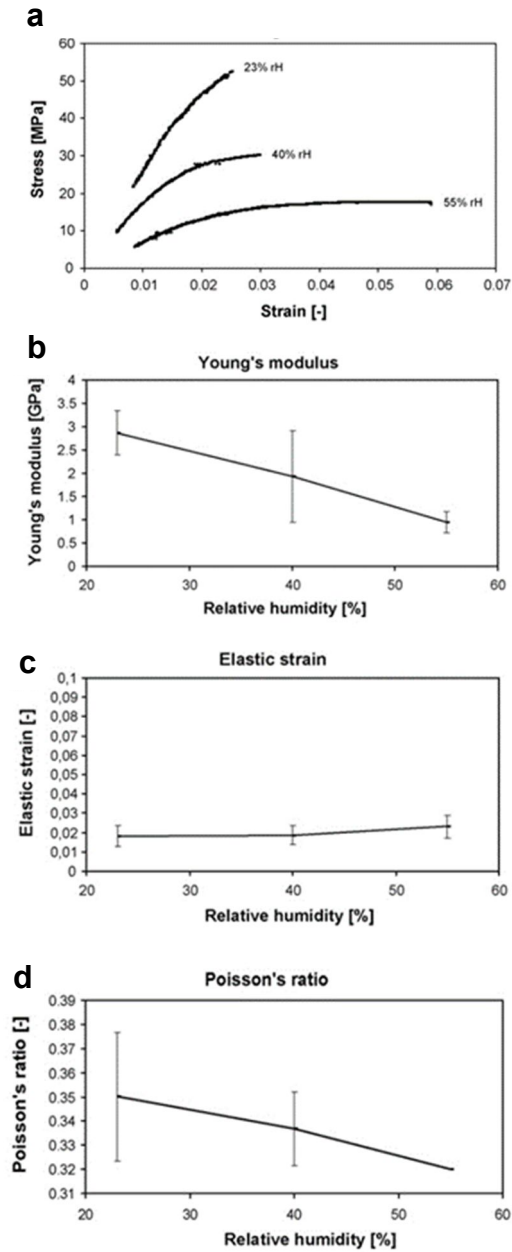


Figure 2.4. The mechanical properties of PEDOT:PSS films. (a) Stress-strain curves, (b) Young's modulus, (c) elastic strain, and (d) Poisson's ratio of PEDOT:PSS films at different levels of humidity[1].

2.1.5. Electrical properties

As an intrinsic conductive polymer, PEDOT:PSS can transport free charge carriers through its thiophene rings. Due to the positively charged PEDOT chains, unpaired π electrons can freely migrate and allows for electrical conductivity. The negatively charged PSS chains work as a counterions for PEDOT to maintain the positively charged state of PEDOT and allow for the solution process of film formation due to their hydrophilicity.

Electrical conduction was primarily observed in PEDOT. In spite of the counterion role of PSS for PEDOT, the PSS chains are electrically insulative and act as barriers for the charge carriers. As discussed in a previous section, the morphology of PEDOT:PSS is composed of conductive PEDOT-rich cores and insulated PSS shells. The charge carriers can migrate freely inside the conductive cores. However, the insulated shells of PSS act as obstacles for the migration of the carriers. The barriers must be overcome for successful electrical conduction. Because of the presence of insulated barriers, the electrical resistivity of PEDOT:PSS films typically ranges from 0.1 to 1 Ωcm , which are very low values.

The transport of charge carriers occurs by a temperature-dependent hopping process, which is called the variable range hopping (VRH) model^[2]. It shows a temperature-dependent increase in a material's conductivity by enhancing hopping conduction (Figure 2.5). The equation is described as follows,

$$\rho$$

where ρ_0 is the resistivity at an infinite temperature (T_0), $T_0 = 16/(k_b N(E_f) \xi^3)$ for $\alpha = 1/4$, ξ is the localization length, and $N(E_f)$ is the density of the states at the Fermi

Chapter 2: Theoretical background

energy. This model is normally applied to describe low-temperature conduction in strongly disordered systems with localized charge carrier states. The PEDOT conductive segments are highly disordered due to chemical bonding with the entangled and negatively charged PSS chains, and the charge carriers are localized inside the PEDOT segments. Due to the random distribution of PEDOT segments inside the PEDOT-rich cores, the conduction of charge carriers is relatively low. In addition, the transport of charge carriers is significantly hindered by the insulated PSS barriers, which is a main obstacle for electrical conduction. Therefore, the electrical conductivity of pristine PEDOT:PSS is extremely low due to the disordered conformation of the PEDOT and PSS insulated barriers.

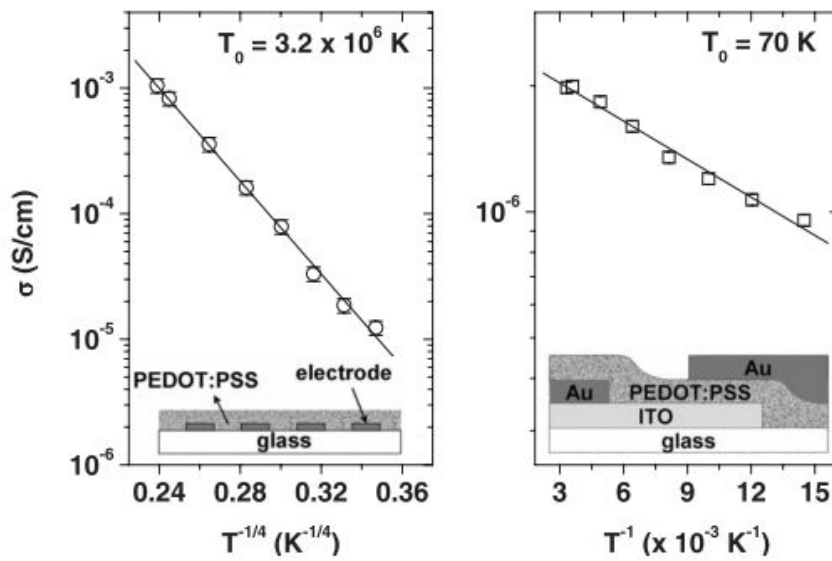


Figure 2.5. Temperature-dependent conductivity changes in PEDOT:PSS films measured in (a) lateral and (b) vertical directions^[2].

2.1.6. Secondary doping

The electrical conductivity of PEDOT:PSS can be highly enhanced by the addition of chemical additives, which is called secondary doping. The secondary doping of already doped PEDOT:PSS was found to improve its conductivity by several orders of magnitude. The chemical additives were organic solvents that had high dielectric constants (e.g., dimethyl sulfoxide (DMSO) and dimethylformamide (DMF)) or polar groups (e.g., ethylene glycol, glycerol, or sorbitol). By adding small amounts of such chemical additives, the electrical conductivity of a material can be greatly enhanced. As shown in Figure 2.6, we measured the electrical conductivities of PEDOT:PSS films upon adding DMSO. The conductivity of these materials increased by approximately three orders of magnitude. At a concentration of 5 wt.% DMSO, the conductivity was almost 800 S/cm, which was 1600 times higher than those of pristine PEDOT:PSS films.

This large enhancement of electrical conductivity was primarily caused by a conformational change of PEDOT:PSS. Conductive PEDOT segments were previously found to be randomly distributed in the PEDOT-rich cores. This was because PEDOT was bonded to highly entangled PSS chains through electrostatic effects. By adding chemical additives such as DMSO, DMF, and ethylene glycol, these electrostatic effects were shielded by the chemical solvents and resulted in weakening of the attractive forces. Hence, the PEDOT segments freely moved and crystallized through π - π interactions with each other because of the intrinsic nature of the linear and planar characteristics of the PEDOT segments (Figure 2.7)^[20,21]. The crystal structure of PEDOT was investigated using a Wide-angle X-ray scattering (WAXS) method^[21,22]. As shown in Figure 2.8, the crystallinity of the PEDOT:PSS

Chapter 2: Theoretical background

films significantly increased after the addition of ethylene glycol. The crystal structure was orthorhombic with lattice parameters of $a = 14.0 \text{ \AA}$, $b = 6.8 \text{ \AA}$ and $c = 7.8 \text{ \AA}$. The increase in crystallinity of the PEDOT:PSS films led to the enhancement in the migration of charge carriers and the electrical conductivity was highly improved. The effect of secondary doping permanently remained even after the chemical additives were removed. Therefore, the crystalline structures of the PEDOT segments were maintained after secondary doping with chemical additives.

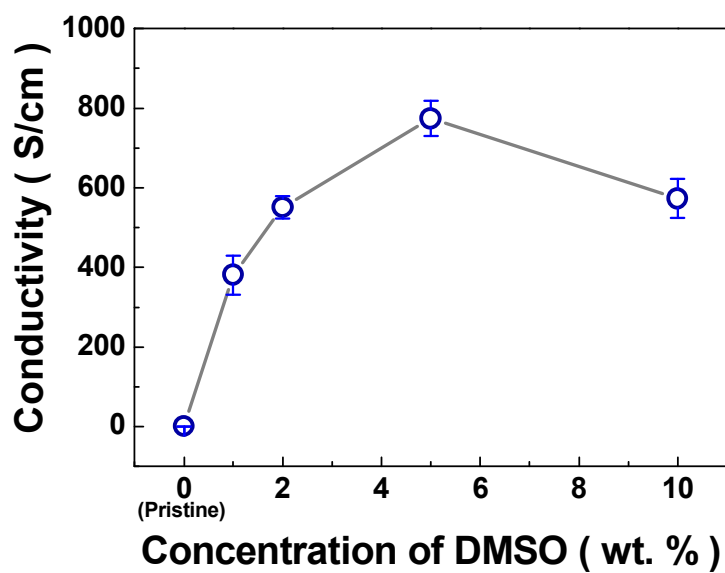


Figure 2.6. Electrical conductivity of PEDOT:PSS films as a function of DMSO concentration.

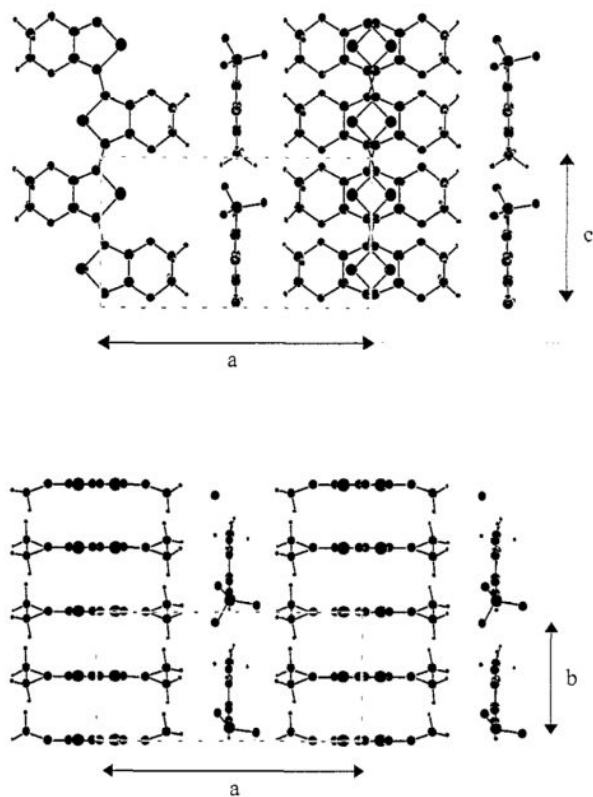


Figure 2.7. Crystal structure PEDOT, in projections along the b-axis and c-axis for upper and lower conformations, respectively^[20].

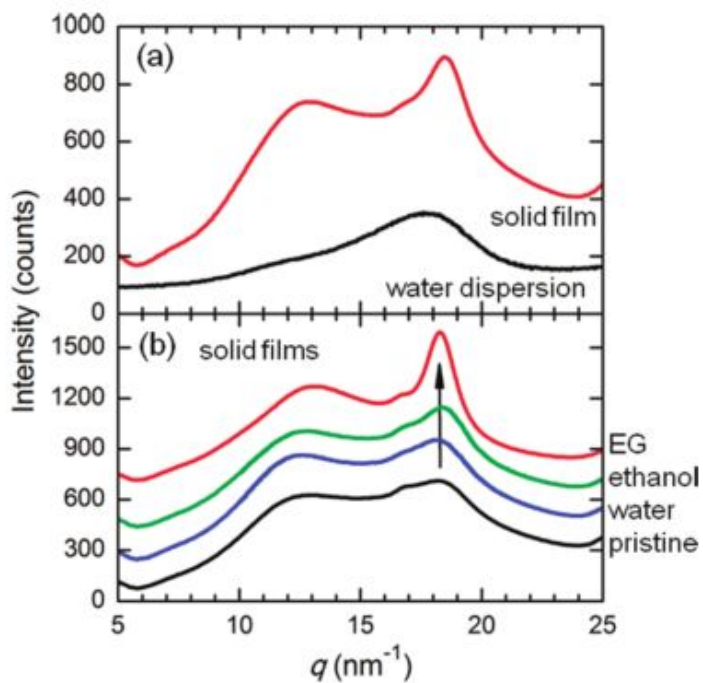


Figure 2.8. (a) WAXS profiles of PEDOT:PSS solid films and water dispersion with 3 wt.% of EG. (b) Comparison of WAXS profiles of PEDOT:PSS films for pristine samples and those with added water, ethanol, and ethylene glycol^[21].

CHAPTER 3

Experimental methods

3.1. Sample preparation

3.1.1. Thin film-type PEDOT:PSS

PEDOT:PSS solutions were prepared with different weight concentrations of dimethyl sulfoxide (DMSO) as a secondary doping material. The weight ratios of DMSO mixed in the PEDOT:PSS solution were 0, 5, and 10 wt. %. The PEDOT:PSS/DMSO solutions were stirred for 24 hours at room temperature in a N₂ glove box and filtered with polypropylene filters (0.45 μm pore size). The PEDOT:PSS films were formed by spin-coating at 1000, 2000, and 3000 rpm for 30 s onto polyimide (PI) substrates (Kapton 300 HN, DuPontTM) treated with oxygen plasma (100 W, 75 mTorr O₂, 120 s by RIE 80 PLUS, Oxford Instrument) and onto PDMS (Sylgard 184, Base/Cross-linker = 10:1, Dow Corning) substrates under the same conditions. The spin-coated films were annealed on a hot plate for 15 min at 130°C in a N₂ ambient glove box and were then cooled to room temperature in the

glove box. Subsequently, the PEDOT:PSS films coated on O₂-plasma-treated PI substrates and PDMS substrates were cut into rectangles that were 10 mm in width and 30 mm in length.

3.1.2. Soft gel-type PEDOT:PSS

To fabricate PEDOT:PSS-based soft materials, gelation of a PEDOT:PSS solution was conducted. Two types of PEDOT:PSS solutions were prepared: (i) an as-received PEDOT:PSS solution and (ii) a PEDOT:PSS solute. The as-received PEDOT:PSS aqueous solution (Clevios P, Heraeus) was mixed with EG with a volume ratio of 8:1. The PEDOT:PSS solute was obtained by freeze-drying the PEDOT:PSS solution. The freeze-drying methods used sublimation of the solution and did not use evaporation by heat. Damage did not occur on the samples, and the internal structures were mostly maintained because the samples were frozen. The PEDOT:PSS aqueous solution was frozen in a freezer (-20 °C) for one day. Subsequently, the frozen solution was placed in a freeze-drying machine (FD5508, ilShinBioBase) equipped with a vacuum chamber. The vacuum was lowered to 5 mTorr inside the chamber. The solution was freeze-dried for 3 days to afford the fully dried PEDOT:PSS solute. This product was dissolved in DI water and EG (8:1) with weights of 0.105, 0.13, 0.155, and 0.18 g for 12 mL solutions. Acrylamide (AAm, Sigma-Aldrich) monomer was added to these solutions to reach a concentration of 2.12 M. The concentration of PEDOT:PSS to PEDOT:PSS plus AAm was varied to 5.49%, 6.83%, 7.90%, and 9.06% for the freeze-dried solutions and 6.72% for the as-received solution. The cross-linker, N,N'-methylenebisacrylamide (MBAAm, Sigma-Aldrich) initiator, ammonium persulphate,

Chapter 3: Experimental methods

(APS, Sigma-Aldrich), and N,N,N',N'-tetramethylethylenediamine (TEMED) accelerator, whose weight ratios were 0.38 wt. %, 0.55 wt. %, and 0.39 wt. % relative to AAm, respectively, were added into the solution. Subsequently, the solution was poured into a glass mold with dimensions of 50 mm × 75 mm × 1 mm (w × l × t). Then, the gelation was conducted on a hotplate at 90 °C for 2 hr. To remove the extra ions and impurities, the synthesized gels were washed in DI water mixed with EG (8:1) for 3 days, and the solution was changed every day. To selectively evaporate the DI water inside the swelled gels, the samples were dried in an oven at 60 °C for 4 hr, resulting in the generation of PEDOT:PSS-PAAm organogels containing EG.

3.2. Characterization

3.2.1. Mechanical properties

The mechanical properties of the PEDOT:PSS-PAAm organogels were measured using a tensile machine (Instron 3343). The dimensions of the rectangular gels were 10 mm × 10 mm ($w \times l$) with thicknesses of 1 mm; these samples were glued onto acrylic clamps. The samples were placed and fixed between two jigs at both ends of the machine. The displacement rate of the samples was 3 mm/min and all the tensile tests were conducted at room temperature. We obtained the loads and displacement rates of the organogels, and the geometric dimensions of the organogels allowed for the stress-strain curves to be plotted for each of the samples. In addition, tensile fatigue tests were also conducted from 50% strain to 0% strain for 1000 cycles at 0.05 Hz. The displacement rate was 15 mm/min. All tests were conducted in air at room temperature.

3.2.2. Electrical properties

The electric resistivity of PEDOT:PSS film is normally determined by multiplying the sheet resistance (R_s) and the thickness (t) of a film ($\rho = R_s \times t$). By separating the paths of current-flow and voltage-sensing, we could measure the electrical resistance of the PEDOT:PSS without the contact resistance (R_c) between electrodes and the samples. As shown in Figure 3.1, an electrical current (I_1) was applied at the end of a sample, and a drop in voltage (V) was measured at two points in the middle of the sample with a high impedance voltmeter. The voltage (V) can be expressed by

Chapter 3: Experimental methods

equation (1).

$$V = 2I_2R_c + (I_1 + I_2)R_g \quad (1)$$

Because the current (I_2) that flows in the voltmeter is negligible compared to I_1 ($I_2 \ll I_1$), the equation (1) can be expressed by equation (2).

$$V = I_1R_g \quad (2)$$

Therefore, the contact resistance can be ignored by using the four-point probe method, and I_1 -V sweeps were successfully conducted for all the gels. To measure the currents across the samples as functions of voltage, I-V sweeps were conducted for the gels with dimensions of 20 mm \times 3 mm \times 1 mm ($w \times l \times t$) using a four-point probe (Keithley 6487 picoammeter, 2000 multimeter, and 6220 current source). The four electrical contacts with the probe tips were made with silver paste, and the I-V curves were measured in voltages ranging from -5 to +5 V. The electrical resistance was calculated using the results from the resistance, which was extracted from the inverse of the slope of the I-V curves and the dimensions of the samples.

Changes in the electrical resistances of the PEDOT:PSS films and PAAm organogels during stretching were measured. Uniaxial stretching tests were conducted using a tensile machine (MMT-500N, Shimadzu) equipped with an electrically contactable jig for *in situ* resistance measurements (Agilent 34410A multimeter). The films and gels were cut into dimensions of 10 mm \times 10 mm \times 0.125 mm and 8 mm \times 5 mm \times 1 mm ($w \times l \times t$), respectively. Electrical contacts were formed with copper foil at each end of the gels before the gels were glued onto the acrylic clamps. The samples were placed and fixed between two jigs at both ends in the tensile machine. All tests were conducted at room temperature at a displacement rate of 3 mm/min. As the gels were stretched, and the electrical resistance of each sample was measured once per second until the samples ruptured. To measure the change in resistance

Chapter 3: Experimental methods

during high cycle tensile fatigue, each sample was also fixed with the machine, deformed uniaxially up to 50% strain and released to 0% strain for 1000 cycle at 0.05 Hz. The displacement rate was 15 mm/min, and the resistance was measured once per second.

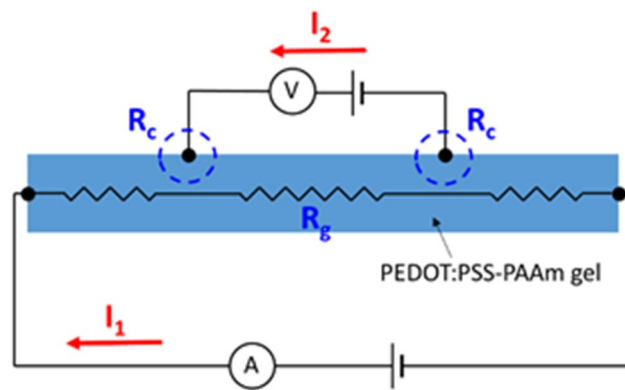


Figure 3.1. I (Current) - V (Voltage) sweep of PEDOT:PSS-PAAm gel by using four-point probe method. Four electrical contacts were made at each end of the gel and the middle of two points with silver paste.

3.2.3. Morphological analyses

The morphology of PEDOT:PSS could be observed using AFM. For the pristine and DMSO-doped PEDOT:PSS films, the surface phases of the PEDOT-rich portion and the PSS-rich portion could be distinguished due to differences in viscosity. The AFM phase images were obtained with a NANO Station II instrument operating in non-contact tapping mode under ambient conditions. We scanned the PEDOT:PSS films for $1 \times 1 \mu\text{m}$ surface areas, and the morphologies were obtained for the pristine and DMSO-doped PEDOT:PSS films as a function of the strain of the films (0, 16, 28, and 42% strain).

In case of the microstructures of the PEDOT:PSS-PAAm gels, the internal structures of the PEDOT:PSS-PAAm gels were observed using a field-emission scanning electron microscope (FESEM, Carl Zeiss, SUPRA 55VP). The freeze-drying method allowed the liquid constituents to totally dry up inside the gel. The gels were freeze-dried for 4 days, and cross-sections of the gels were cut. The gels were coated with 3 nm of Pt before the cross sections were imaged.

CHAPTER 4

Strong Correlation between the Resistivity and Tensile Strain of PEDOT:PSS films

4.1. Introduction

The electrical conductivity of materials generally decreases under mechanical deformation. However, in several materials, such as n-doped silicon, the mobility can be enhanced under tensile strain because of a change in the materials' electronic band structure^[23]. This change in conductivity, which is an intrinsic material property, is valid only within the elastic strain region, whereas under huge deformations, extrinsic factors such as the generation of defects^[24,25], microstructural and dimensional changes^[26,27], and neighboring materials^[28-30] can influence the conductivity in concerted ways. For stretchable electronics in particular, these factors should be controlled and restrained to develop conductors or interconnects that endure high applied strain. Previous approaches to overcoming this challenge for stretchable conductors can be categorized into two types of methods. The first is the hybridization of metallic and organic materials that can withstand large strains without rupturing^{[31-}

Chapter 4: Strong Correlation between the Resistivity and Tensile Strain of PEDOT:PSS films

^{33]}. The second is the design of structures, such as wavy-, net-, or arc-shaped conductors, that can undergo larger strains than plane-shaped structures due to their ability to be stretched^[34–36]. To develop further improvements, understanding the mechanism governing the change in electrical properties and decoupling the contribution of each influencing factor are highly important. In this study, we chose the conducting polymer poly(3,4-ethylenedioxythiophene):poly(styrenesulfonate) (PEDOT:PSS) to produce films that have innate flexibility under mechanical strain. The resistivity response of PEDOT:PSS films to an applied tensile strain was directly investigated, and the key parameters that control the strain-response behavior were identified. By selecting mechanically suitable substrates for the PEDOT:PSS films, each factor that influences the resistance change in a complex manner was distinguished. Moreover, we demonstrated that the resistivity of the films can be modulated, which may be useful in developing conducting polymer electrodes for stretchable electronics.

The conductivity of as-deposited pristine PEDOT:PSS films is approximately $< 1 \text{ S cm}^{-1}$, but it can be improved by controlling the PEDOT-to-PSS ratio^[37], UV radiation^[38], thermal treatment^[39], or, more dramatically, by secondary doping with the addition of solvents^[39–42]. Although previous data have shown that the conductivity of such films also depends on the applied strain, there is no consistency between the range of values over which the resistance changes and the mechanisms that have been proposed for this change. The relative change in the resistance under elastic strain, which is known as the gauge factor, has been reported to be 5.2 and 17.8, indicating positive piezoresistivity^[43,44]. It should be noted that these measurements were performed using the bending strain test with applied strains of less than 1 %. In contrast, several previous studies have shown that the resistivity decreases by 15 %

Chapter 4: Strong Correlation between the Resistivity and Tensile Strain of PEDOT:PSS films

when small and finite tensile strains of less than 10 % are applied^[45,46]. However, the continuous increase in the tensile strain ultimately resulted in an abrupt increase in the resistance due to the cracking of the films. These changes in resistance are associated with different complex factors that originate from not only a change in intrinsic properties with strain but also from extrinsic factors, such as dimensional changes and the generation of defects in the films. Additionally, there are no previous reports regarding the observation of resistance changes at large strains greater than 30 % due to the cracking of PEDOT:PSS films or the rupturing of the underlying substrates.

In this study, we successfully investigated the change in the resistivity of PEDOT:PSS films up to strains of 60 % by matching the Poisson's ratio and elastic modulus between the substrates and the films and decoupled the changes into several underlying mechanisms. We then demonstrated how the resistivity can be modulated under mechanical strain from invariant values to “decreasing” values up to 90 %. Surprisingly, the irreversible growth of conductive PEDOT-rich cores is the primary mechanism for the enhancement of conductivity purely induced by applied strain.

4.2. Methods

Preparation of PEDOT:PSS Solution and Films: PEDOT:PSS (CleviosTM PH 1000, Heraeus) solutions with different concentrations (by weight) of dimethyl sulfoxide (DMSO) solvent (>99.9 %, Sigma-Aldrich) as a doping material were prepared. The weight fractions of DMSO contained in the PEDOT:PSS solution were 0, 5, and 10 wt. %. The PEDOT:PSS/DMSO solutions were stirred for 24 hours at room temperature in a N₂ glove box and filtered with polypropylene filters (0.45 μm pore

Chapter 4: Strong Correlation between the Resistivity and Tensile Strain of PEDOT:PSS films

size). The PEDOT:PSS films were formed by spin-coating at 1000 rpm for 30 s onto polyimide (PI) substrates (Kapton 300 HN, DuPontTM) treated with oxygen plasma (100 W, 75 mTorr O₂, 120 s by RIE 80 PLUS, Oxford Instrument) and onto PDMS (Sylgard 184, Base/Cross-linker = 10:1, Dow Corning) substrates under the same conditions. The spin-coated films were annealed on a hot plate for 15 min at 130°C in a N₂ ambient glove box and then cooled to room temperature in the glove box. Subsequently, the PEDOT:PSS films cast on O₂-plasma-treated PI substrates and PDMS substrates were cut into rectangles measuring 10 mm in width and 30 mm in length.

Characterization of Electrical and Morphological Properties of PEDOT:PSS Films by Stretching/Releasing Tests: Uniaxial stretching tests were conducted on the PEDOT:PSS films by using a micro tensile machine (MMT-500N, Shimadzu) equipped with an electrically contactable jig for *in-situ* resistance measurements (Figure 4.2). All tests were conducted at room temperature at a constant strain rate of $5 \times 10^{-5} \text{ s}^{-1}$. As the films were deformed by uniaxial tension, the electrical resistance of the films was measured with an Agilent 34410A multimeter. The initial electrical conductivities of the films were measured using the four-point probe technique. Surface images of the PEDOT:PSS films were taken using an optical microscope and SEM (FE-SEM S-4800, Hitachi) at each strain. Atomic force microscope (AFM) phase images were obtained with a NANO Station II instrument operating in non-contact tapping mode under ambient conditions.

4.3. Effect of substrates under large amounts of stretch

4.3.1. Mismatch of mechanical properties

In principle, the origins of extrinsic resistance changes in PEDOT:PSS films deposited on compliant substrates under tensile conditions can be divided into the following two major contributions (Figure 4.1). The first contribution is the change in the geometrical shape of PEDOT:PSS films resulting from tensile deformation. When a substrate is stretched along a longitudinal direction, the length (l) of the supported film increases but the width (w) and thickness (t) decrease. Given that the resistivity (ρ) is constant under tensile deformation, the variation in resistance ($\Delta R_G/R_0$) induced by the geometric change can be described by equation (1):

$$\frac{\Delta R_G}{R_0} = \frac{R_G - R_0}{R_0} = \left[\frac{l/l_0}{(w/w_0)(t/t_0)} - 1 \right] \quad (1)$$

where l/l_0 is the extension ratio of the film and w/w_0 and t/t_0 denote the contraction ratio of the width and the thickness, respectively. The above equation predicts that the resistance always increases as a result of such a geometrical change during tensile deformation.

The second contribution is the generation of defects (buckles and cracks) in PEDOT:PSS films. Generally, when a large strain ($> 10\%$) is applied, this mechanism becomes dominant, which results in an abrupt increase in electrical resistance. The cracks normally can form in the films with applied strain for free standing states and fractured at a small strain. However, the formation of the defects can be suppressed when the PEDOT:PSS film is deposited to a compliant substrate. Furthermore, the abrupt fracture of the film can be retarded at even higher strain by matching the elastic modulus and Poisson's ratio between the film and the substrate. For example, poly(dimethylsiloxane) (PDMS) is conventionally used as a substrate for stretchable

Chapter 4: Strong Correlation between the Resistivity and Tensile Strain of PEDOT:PSS films

devices. However, the Poisson's ratio, elastic modulus, and elastic strain limit of PDMS are quite different from those of PEDOT:PSS, as listed in Table 4.1^[1]. Such huge differences in mechanical properties result in a local instability at the interface, which generates cracks in the films during stretching. For example, in a previous experiment, cracks started to form at 12 % strain and the resistance increased abruptly at approximately 30 % strain as a result of the accumulation of cracks^[45]. Moreover, the treatment of PDMS with O₂ plasma or UV/O₃ to activate the surface generates thin SiO_x layers^[47,48], which leads to the brittle fracture of the films, even at extremely low strains. It seems that the abrupt and irreversible increase in resistance is inevitable after stretching and releasing PEDOT:PSS deposited on PDMS.

To eliminate or minimize the effects of defects, we chose polyimide (PI) as a substrate material instead of PDMS. As shown in Table 4.1, the Poisson's ratio and elastic strain limit of PI are exactly the same as those of PEDOT:PSS (0.35 and 2 %, respectively), and the materials' elastic modulus are also similar^[1,49]. Thus, we expect that using a PI substrate would allow us to observe the intrinsic behavior of PEDOT:PSS by preventing the generation of cracks or buckles.

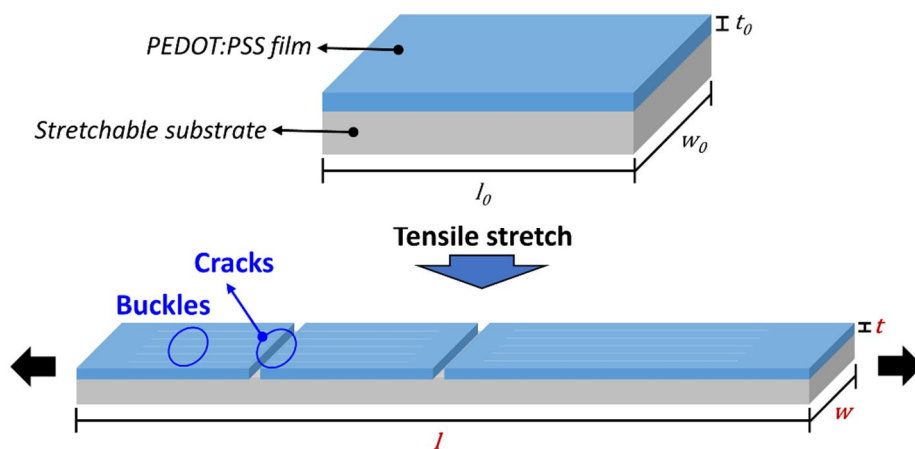


Figure 4.1. Origins of extrinsic resistance changes in PEDOT:PSS films deposited on substrates under tensile deformation. There are two contributions: (i) Geometrical shape changes and (ii) Defect (i.e., buckles and cracks) generation.

Chapter 4: Strong Correlation between the Resistivity and Tensile Strain of PEDOT:PSS films

Table 4.1. The mechanical properties of PEDOT:PSS, PDMS, and PI films.

	PEDOT:PSS	PDMS	PI
Poisson's ratio	0.34-0.35	0.5	0.34
Elastic modulus (MPa)	2000	0.1-3	3200
Elastic strain limit (%)	2	~ 160	2

4.3.2. Substrate dependence of defect generation

To examine the effects induced by substrate type, PEDOT:PSS films were deposited on PI substrates and PDMS substrates. The change in the electrical resistance of the PEDOT:PSS films on the PDMS and PI substrates with tensile strain was investigated using the *in-situ* resistance measurement tensile test system schematically shown in Figure 4.2. The strain of the samples was monitored by optically measuring the distance between markers on the samples. The relative resistance changes ($(R-R_0)/R_0$ (%)) in PEDOT:PSS films doped with 5 wt. % dimethyl sulfoxide (DMSO) on PI and PDMS substrates with tensile strain are shown in Figure 4.3 as the representative cases. In the case of the PDMS substrate, an abrupt increase in resistance was observed at small tensile strain (< 3 %). The formation of cracks in the film is responsible for such a rapid increase in resistance in the film because it facilitates the local delamination of the films, as indicated by the *in-situ* observation of the film surfaces by microscopy during stretching and releasing (Figure 4.4a). When the Poisson's ratio of the substrates is larger than that of the films, a compressive force perpendicular to the stretching direction is exerted on the films during stretching. This leads to the formation of dense lateral buckles on the surface. These dense buckles at the interface induce instabilities in local adhesion, and cracking subsequently occurs perpendicular to the stretching direction. These cracks are permanent defects and do not disappear after deformation. Furthermore, the elastic strain limit of PEDOT:PSS is approximately 2%; therefore, plastic deformation occurs in PEDOT:PSS at these strains. As the substrates were released, the lateral buckles disappeared, but vertical buckles formed due to the previous plastic deformation of the PEDOT:PSS film. The *in-situ* morphologies of the films during this process are shown in greater detail in

Chapter 4: Strong Correlation between the Resistivity and Tensile Strain of PEDOT:PSS films

Figure 4.5.

A completely different behavior was observed for the PI substrates. The change in the resistance of the films increased gradually with strain, and we could successfully stretch the film up to 60 % strain without generating buckles or cracks. No damage was observed on the surface of the PEDOT:PSS films deposited on the PI substrates during or after the stretching of the sample up to 60 % strain (Figure 4.4b and Figure 4.5). The Poisson's ratio of the films is similar to that of the substrates; therefore, the films and the substrates are uniformly deformed and experience the same Poisson's compression perpendicular to the stretching direction. Tensile testing was terminated at 60 % strain due to the rupture of the substrate. To our knowledge, a gradual increase in resistance at strains of up to 60 % has never been observed before in PEDOT:PSS films. Because the PI substrate allowed the PEDOT:PSS films to remain crack-free up to 60 % strain, we believe that the intrinsic behavior of the films could be observed.

The gradual increase in the resistance of the PEDOT:PSS films on the PI substrates is completely attributed to the change in the geometry ($\Delta R_G/R_0$) of the films during tensile testing, as formulated in equation (1). We plotted ($\Delta R_G/R_0$) in Figure 4.3, where the extension in the length and contraction in the width were optically measured by monitoring a marker's movement on the substrates. The contraction in thickness can be calculated, assuming that the film undergoes Poisson's compression, $(1-\nu_f \epsilon_l)$, where ν_f is the Poisson's ratio of PEDOT:PSS (0.35) and ϵ_l is longitudinal strain. The measured resistance change matches well with the expected increase due to a change in geometry, which confirms that there was no contribution from cracking when using the PI substrates. Because the two major extrinsic contributions to the resistance change were eliminated, we could identify the purely intrinsic factors affecting the change in resistance by in-situ electrical measurements

Chapter 4: Strong Correlation between the Resistivity and Tensile Strain of PEDOT:PSS films

conducted over a wide range of deformation states, from small elastic strain to 60 % strain.

In-situ observation was performed with the optical microscopy which is equipped with tensile testing stage. For SEM, it was difficult to conduct *in-situ* testing with a large strain. Hence, stretched samples were fixed to silicon wafers with an adhesive tape and subsequently loaded on SEM holders. When tensile strain is applied on PEDOT:PSS films on PDMS substrate (Figure 4.5a), cracks are generated at strain below 15 %. As the strain increases, lateral buckles are formed parallel to the stretched direction and cracks gradually increased because of a large difference in Poisson's ratio between each other. After the films are released completely, the cracks are permanently remains and a direction of buckles is changed from lateral to vertical to the films. It is because plastic deformation of the PEDOT:PSS films. However, for the PEDOT:PSS films on the PI substrates (Figure 4.5b), there is no damage is observed on the surface of the films during or after the stretching the substrates up to strain of 42 %. In case of PI substrates, Poisson's ratio and elastic strain limit are very similar each other. Therefore, the PEDOT:PSS films can be deformed uniformly according to the applied strain on the substrates. We can obtain buckle and crack-free PEDOT:PSS films even stretching up to 60 % strain.

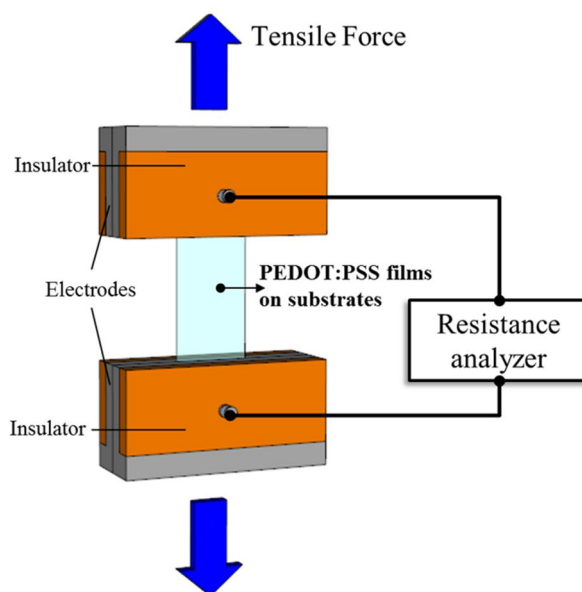


Figure 4.2. Experimental set-up for the in-situ measurement of the electrical resistance of PEDOT:PSS films during the tensile stretching of films coated on PI or PDMS substrates.

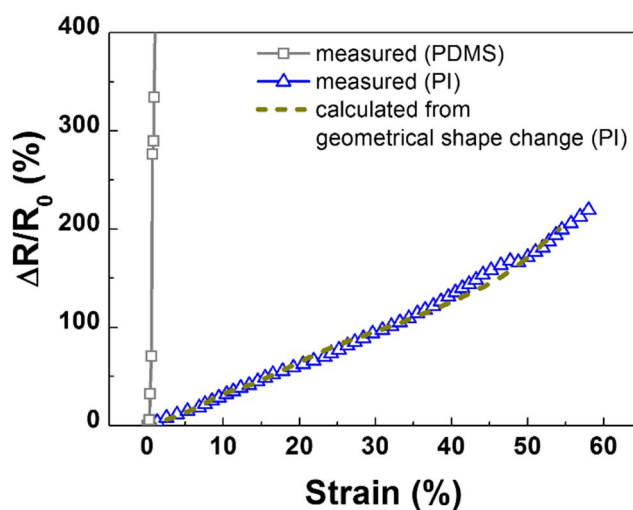


Figure 4.3. Relative resistance changes ($\Delta R/R_0$ (%)) of PEDOT:PSS films doped with 5 wt. % DMSO as a function of tensile strains of the PDMS and PI substrates. For comparison, the resistance changes calculated from the changes in the geometry of the PI substrates are presented as dotted lines.

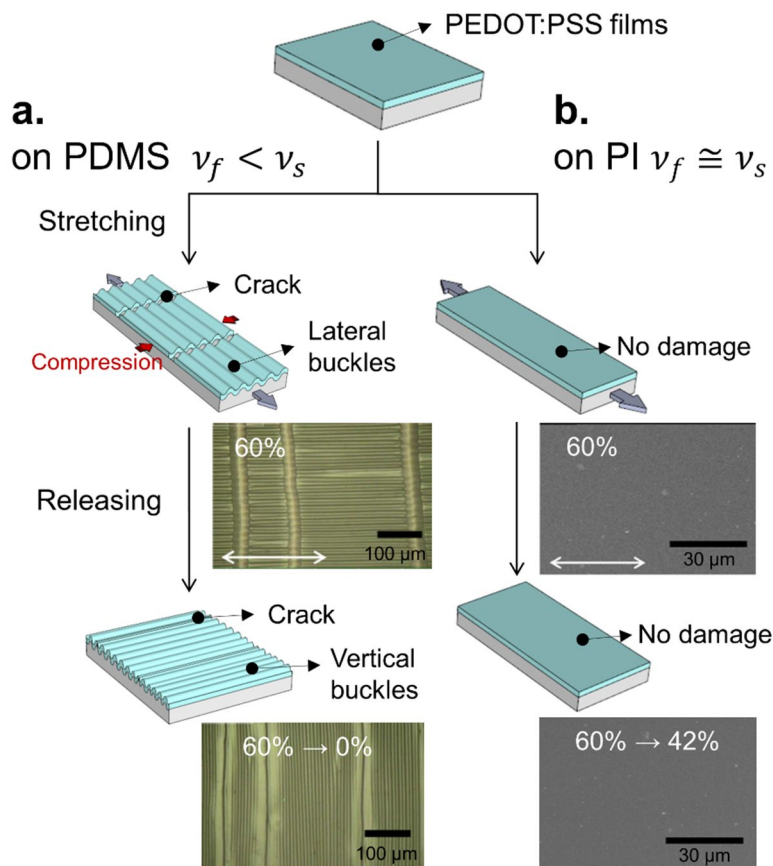


Figure 4.4. Schematics and optical/SEM images of PEDOT:PSS films on PDMS and PI substrates during substrate stretching according to the difference in the Poisson's ratio between the films and the substrates at (a) $\nu_f < \nu_s$ and (b) $\nu_f \approx \nu_s$, where ν_f and ν_s are the Poisson's ratios of the films and the substrates, respectively. The stretching direction is indicated by arrows in the micrographs.

Chapter 4: Strong Correlation between the Resistivity and Tensile Strain of PEDOT:PSS films

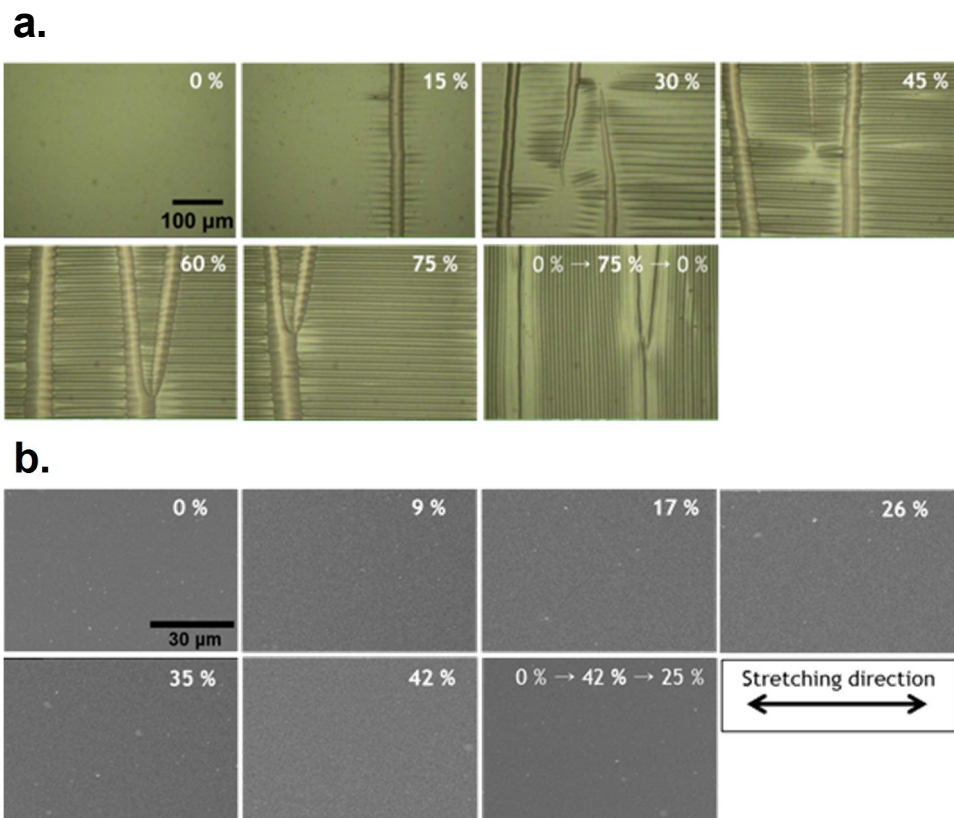


Figure 4.5. In-situ optical microscopy/SEM images of PEDOT:PSS films on (a) PDMS and (b) PI substrates at specific tensile strains and when released to their load-free states. The arrows indicate the stretching directions.

4.4. Electrical properties of PEDOT:PSS under large stretch

4.4.1. Morphology of PEDOT:PSS film

After we confirmed that PI substrates are suitable in providing a crack-free condition, we investigated how the doping of PEDOT:PSS films with DMSO affects the strain-resistance response. It is well known that secondary doping with DMSO can enhance the conductivity of PEDOT:PSS by about three orders of magnitude. The initial morphology of pristine PEDOT:PSS (Figure 4.6c) consists of conductive and tangled PEDOT-rich cores (bright regions in the images) surrounded by insulating shells composed of excess PSS chains (dark region in the images)^[17]. The conductivity is very low ($< 1 \text{ S cm}^{-1}$) because the PSS shells serve as barriers to charge transport. However, when doped with DMSO (Figure 4,6a), the cores and the insulating shells were wholly dissolved. According to previous studies, the main effect of doping is the transformation of the PEDOT chains' coiled conformation into a linear one and the homogeneous dispersion of the cores^[42,50-52]. This morphological change enhances the connectivity of the individual PEDOT chains, and the resulting enhancement increases the conductivity. Our question was how such a difference in morphology induced by DMSO doping affects the resistance change responding to the large applied strain.

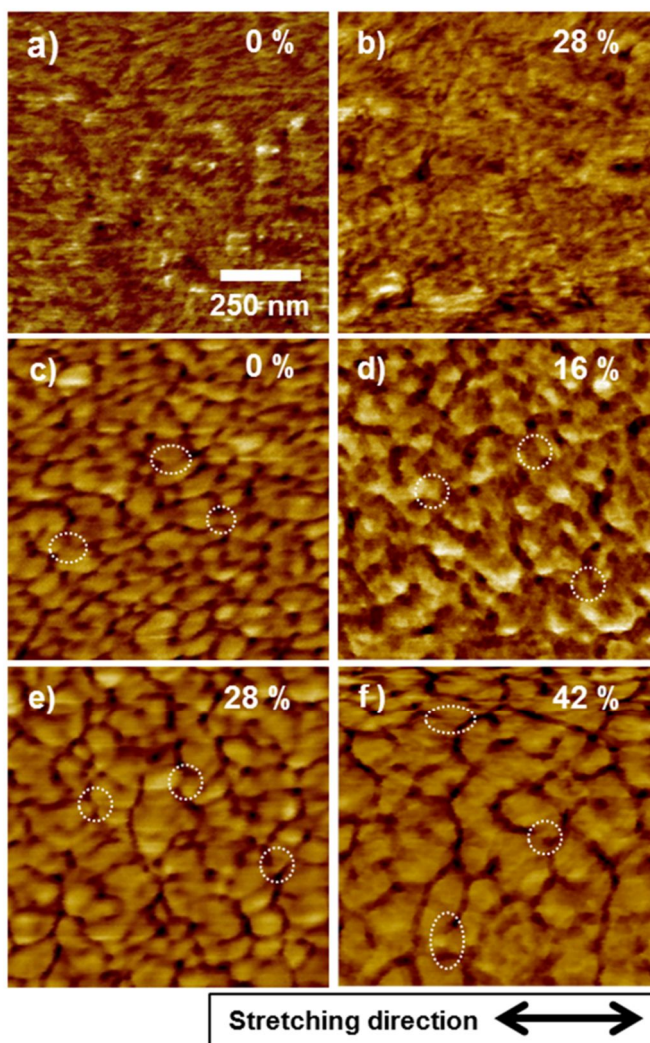


Figure 4.6. AFM phase images of pristine (a)-(d) and 5 wt. % DMSO-doped (e), (f) PEDOT:PSS films at each strain denoted in the images. The arrow indicates the stretching direction, and all the images were obtained by tapping-mode AFM at a scale of $1 \times 1 \mu\text{m}^2$.

4.4.2. Resistivity changes with tensile strain

We investigated the relative resistance changes of PEDOT:PSS films doped with 0, 5, and 10 wt. % DMSO as a function of strain, which are shown in Figure 4.7a. Pristine PEDOT:PSS films (0 wt. % DMSO) and DMSO-doped films (5 and 10 wt. %) exhibited completely opposite resistance responses to the applied strain. While the resistance increases with strain in the case of the DMSO-doped PEDOT:PSS, it decreases in the pristine film. This increasing and decreasing trend continues up to 60 % strain. The positive dependence of resistance on strain has been observed under many experimental conditions, regardless of the doping conditions. However, the negative dependence observed in the pristine film has never been observed before in PEDOT:PSS subject to such large strains. A previous study reported the observation of this negative dependence along the stretched direction only below 10 % strain^[28]. When the strain increased above 10 %, the resistance abruptly increased due to the generation of cracks, and the films ultimately ruptured. Because the formation of cracks were effectively retarded at the interface by using PI substrates, the observed strain dependence resulted only from the change in the geometry and the intrinsic properties of the films, i.e., the morphological transformation of the pristine PEDOT:PSS films with strain.

To determine the purely intrinsic resistivity change, the geometric contribution was calculated and subtracted from the measured resistance. The relationship between the relative resistance and the resistivity change can be expressed by equation (2):

$$\frac{R}{R_0} = \frac{\Delta R}{R_0} + 1 = \frac{\rho}{\rho_0} \cdot \left[\frac{l/l_0}{(w/w_0)(1 - \nu_f \varepsilon_l)} \right]$$

Chapter 4: Strong Correlation between the Resistivity and Tensile Strain of PEDOT:PSS films

where $\Delta R/R_0$ and $\Delta R_G/R_0$ are the normalized change in the measured resistance and that induced by a change in geometry, respectively. The equation can be rearranged to obtain the resistivity of the PEDOT:PSS films at each strain:

$$\rho$$

The values of $\Delta R/R_0$ and $\Delta R_G/R_0$ were obtained from Figure 4.7a. The resistivity is plotted as a function of the strain of the films in Figure 4.7b. The resistivity of the DMSO-doped films was invariant as a function of strain. On the other hand, interestingly, the resistivity of the pristine films gradually decreased as the strain increased. When we examined the relative change in the resistivity, shown in Figure 4.7c, the change in the DMSO-doped films was observed to remain constant and only fluctuated by approximately 10 % at maximum. However, the resistivity of the pristine films decreased by 90 % at a strain of 60 %. These changes are only caused by the morphological change of the PEDOT:PSS films induced by strain. This suggests that the change in resistivity can be modulated from invariant to negative values by controlling not only the DMSO doping conditions but also the mechanical strain. Now, we discuss the mechanism governing the change in resistivity, focusing on the correlation between the change in morphology and the film strain.

Chapter 4: Strong Correlation between the Resistivity and Tensile Strain of PEDOT:PSS films

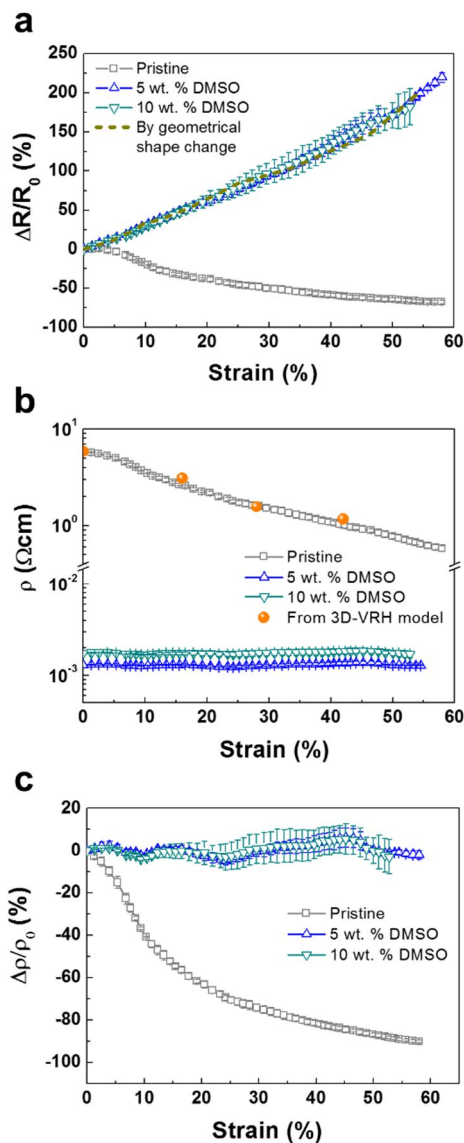


Figure 4.7. (a) Relative resistance changes of PEDOT:PSS films doped with various concentrations of DMSO (0, 5, and 10 wt. %) on O_2 -plasma-treated PI substrates during stretching of up to 60 % strain. (b) The resistivity and (c) relative changes in resistivity of the PEDOT:PSS films as a function of strain. The orange spheres denote the resistivities calculated from the 3D VRH model.

4.5. Stretch-induced growth of PEDOT-rich cores

To investigate the difference in the resistivity-strain response between 5 wt. % DMSO-doped and pristine PEDOT:PSS films, the morphological change of the films with tensile strain was investigated using AFM phase images (Figure 4.6). Comparing the initial morphology (Figure 4.6a) with the morphology of the DMSO-doped films after being strained 28 % (Figure 4.6b), no significant changes were observed. This result indicates that the connectivity between the PEDOT chains was not significantly degraded with respect to the tensile deformation because the initial morphology already showed fully delocalized and uniformly dispersed PEDOT chains. Hence, no changes in the resistivity were observed as a function of strain.

By contrast, for the pristine PEDOT:PSS films, the size of the PEDOT-rich cores increased and the number of PSS barriers decreased as the strain increased (Figure 4.6c-f). Image analysis provides more quantitative information regarding the increase in the surface area of the PEDOT-rich cores. In those AFM phase images, the scanned area is $1 \mu\text{m} \times 1 \mu\text{m}$. The average surface area of the cores increased to 0.88, 1.27, 2.00, and $2.50 \times 10^{-2} \mu\text{m}^2$ for strains of 0, 16, 28, and 42 %, respectively. The detail information is presented in Figure 4.8 and Table 4.2. Compared with the initial core size, the average size increased by more than 185 %. Such large growth of the PEDOT-rich cores is unexpected and cannot be explained by core elongation due to tensile stress. For example, in the 42 % strained film, if a single core is considered, the extension along the applied strain direction will be 42 % and the contraction perpendicular to the strain direction will be 18 %. This calculation indicates that the increase in surface area should be 16 %, which is much smaller than our measured value (185 %). Therefore, our analysis shows that core coalescence or agglomeration results in apparent core growth. Additional evidence shows

Chapter 4: Strong Correlation between the Resistivity and Tensile Strain of PEDOT:PSS films

that the cores were grown not only parallel but also perpendicular to the direction of tensile strain, as shown in Figure 4.6c-f.

To understand the effect of core coalescence, we took a close look at the boundaries between the PEDOT cores neighboring the PSS shells. As indicated by the dotted white circles, the PEDOT-rich cores were not fully enclosed by the PSS shells. The non-uniform contrast in the phase image indicates a variation in the local density. The PSS shells (dark brown) have different thicknesses and are not fully connected. It should be noted that the multiple PEDOT-rich cores are connected in a lasagna-like structure. It is that such morphology can be formed favorably during thermal treatment when the film is deposited by spin coating^[53]. In this structure, gel particles of PEDOT:PSS in the solution are shirked along the lateral and perpendicular direction, which results in the lasagna-like structure. Approximately 5-10 % of the circumference of the PEDOT cores is open to the neighboring cores, and the width of the connected channel is approximately 20 nm. The direction of the open sites is isotropic, and the number of sites per core is not uniform. In our AFM analysis, our observation was limited to the in-plane surface such that only two-dimensional connectivity could be observed. Because the spherical PEDOT-rich cores are wrapped three-dimensionally by PSS domains, the actual three-dimensional connectivity should be larger than that indicated by our observation. We believe that the PEDOT-rich cores start to coalesce together when the PEDOT chains are transported through the connected channels.

Our observation is the first demonstration of mechanically induced annealing for the growth of PEDOT-rich cores. It is known that thermal annealing can increase the size of cores. A previous study showed that when a PEDOT:PSS film was annealed from 100 °C to 200 °C, the growth of PEDOT-rich cores could be observed by the coalescence of the cores^[39]. However, there has been no prior observation of core growth induced by

Chapter 4: Strong Correlation between the Resistivity and Tensile Strain of PEDOT:PSS films

stretching. Energetically, a deformed system subject to excessive strain tends to minimize the strain energy. In case of the crack-free PEDOT-PSS films, large amount of applied strain cannot be relieved through the crack generation. The morphological transformation can be an alternative way to relieve the strain energy. Hence, in this study, the driving force of mechanical annealing should be the strain energy developed in the PEDOT:PSS films due to the large extent of deformation. Because the elastic modulus of the PEDOT-rich cores is theoretically lower than that of the PSS-rich shells^[54], the cores possibly develop a lower strain energy than that of the PSS-rich shells upon straining. Hence, the growth of PEDOT-rich cores is energetically favorable. Furthermore, the coalescence of the PEDOT-rich cores leads to an increase in configurational entropy in the core, which may also reduce the elastic modulus. However, the exact mechanism that explains how PEDOT-rich core growth minimizes the strain energy in films is still not clear; thus, further studies should be performed.

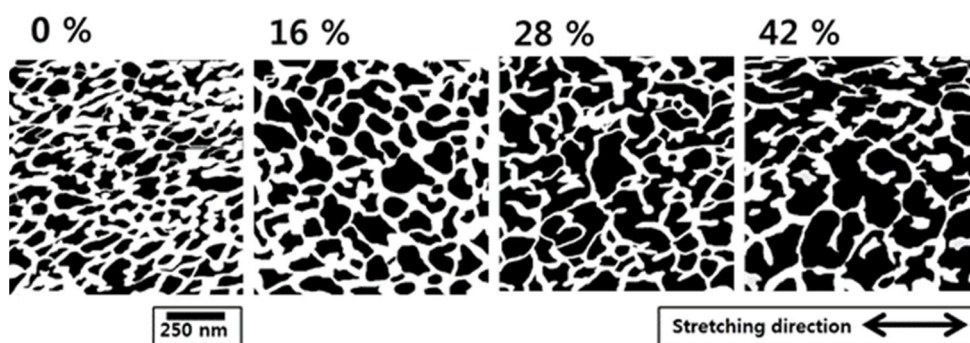


Figure 4.8. Reproduced AFM phase images of pristine PEDOT:PSS films at each strain using image analyzing software. The black and white regions in the images indicate tangled PEDOT-rich cores and excess PSS shells, respectively. All images were obtained with tapping mode AFM at a scale of $1 \times 1 \mu\text{m}^2$. The arrow indicates the direction of stretching.

Chapter 4: Strong Correlation between the Resistivity and Tensile Strain of PEDOT:PSS films

Table 4.2. Comparison between increased area by geometrical change from the extension in length and the contraction in width direction and the resultant change in average area of each PEDOT-rich cores as a function of strain of the films.

Extension in length direction	Contraction in width direction	Increased area due to elongation	Area of each PEDOT-rich cores ($10^{-2} \mu\text{m}^2$)	Increased area of the cores
0 %	0 %	-	0.88	-
16 %	4 %	11%	1.27	44%
28 %	9 %	16%	2.00	128%
42 %	18 %	16%	2.50	185%

4.6. Application of the variable range hopping model

The decrease in the resistivity of pristine PEDOT:PSS films was quantified from the size of conductive PEDOT-rich cores. Charge transport in PEDOT:PSS films can be modeled by a variable range hopping (VRH) process^[2]. Generally, the VRH model theorized the conduction in strongly disordered systems, which consist of insulating barriers and conducting region with localized states. In VRH, the resistivity (ρ) of the films is expressed by,

$$\rho = \rho_0 \cdot \exp \left[\left(\frac{T_0}{T} \right) \right]^\alpha \quad (4)$$

,where ρ_0 is the resistivity at infinite temperature and exponent α is equal to $1/(1+D)$ related to the signature of VRH in D dimensions. In the case of pristine PEDOT:PSS films, we used 3D VRH model for lateral charge hopping and the exponent α becomes $1/4$ ^[2]. T_0 is a material-dependent parameter represented by $T_0 = \beta/k_B N(E_F)\xi^3$, where ξ is the localization length, β is a numerical factor, k_B is the Boltzmann constant, and $N(E_F)$ is the density of states at the Fermi level. Among these parameters, the localization length, ξ , should be closely related to the dimensions of PEDOT-rich cores and can be expressed by $\xi = ad/s$, where a , d and s are the tunneling decay length in the barriers, the core diameter and the barrier thickness, respectively. Therefore, an increase in core size leads to an increase in the localization length of PEDOT:PSS films, which in turn leads to an enhancement in charge transport.

We then switched the change in the resistivity with the initial resistivity and the diameter of the cores before and after deformation at the same temperature by dividing

Chapter 4: Strong Correlation between the Resistivity and Tensile Strain of PEDOT:PSS films

equation (4).

$$\rho^* = \rho \cdot \left(\frac{\rho}{\rho_0}\right) \left[\left(\frac{d^* \cdot s}{d \cdot s^*}\right)^{-3/4} - 1 \right] \quad (5)$$

where ρ and ρ^* are the initial and the final resistivities and d^* and s^* are the core diameter and the barrier thickness after deformation, respectively. The cores diameters are 52, 64, 80, and 89 nm for strains of 0 %, 16 %, 28 %, and 42 %, respectively. We obtained these values from each area of the cores by assuming that these cores were circular in shape and that the PSS shell thickness and tunneling decay length were constant. By substituting the measured core diameters into the equation above, the resistivity at each strain of the films was plotted in Figure 4.7b as an orange spheres. These values match the experimental data quite well. Therefore, the growth in core size directly results in an increase in the localization length in a VRH process.

4.7. Resistivity changes induced by morphological changes

The resistivity change induced by the growth of PEDOT-rich cores under large strain is characteristically different from changes induced by elastic deformation under small strain. Figure 4.9 shows the change in the resistivity of the PEDOT:PSS films on PI substrates during stretching/releasing cycles as well as the anisotropic change in resistivity (resistivity parallel vs. perpendicular to the stretching direction of the films).

Figure 4.9a shows that the resistivity of the 5 wt. % DMSO-doped films did not change upon stretching and releasing the films, as expected. However, the pristine PEDOT:PSS films showed different behavior depending on the applied strain. First, the films were stretched and released under a small strain (less than 10 %); the

Chapter 4: Strong Correlation between the Resistivity and Tensile Strain of PEDOT:PSS films

resistivity recovered reversibly to the released strain. (Figure 4.9a). In the strain region between 2% and 10 %, the plastic deformation of the film occurred so that the film dimension was not fully recovered to the initial even after the releasing. Because of the plastic deformation, the resistivity was not also fully recovered to the initial value but returned to the value at the load-free state (4.6% strain). Interestingly, during the releasing, the resistivity change returned by following the path obtained during the stretching as shown in Figure 4.9a. However, for large deformation (above 17 % strain), the resistivity decreased permanently and was not recovered upon releasing. (Due to the plastic deformation of the PEDOT:PSS films and PI substrates, the samples were not recovered to the initial dimension after the releasing.)

Figure 4.9b shows that the resistivity parallel and perpendicular to the stretching direction. Upon stretching, the resistivity decreased along the parallel direction but increased along the perpendicular direction. Such anisotropy was maintained up to a strain of 7 %; however, under larger deformation, above 7 % strain, it disappeared. This anisotropic change and the recovery of the resistivity in the small-strain region (< 10 %) are caused by the elastic recovery of the single PEDOT-rich cores. The conductivity of the stretched conductive polymer may have been enhanced by a few possible mechanisms, such as an increase in inter-chain conductivity due to alignment and an increase in the degree of crystallinity^[55,56]. Regardless of the mechanism, the anisotropic change in resistivity has also been reported^[46]. During stretching, the diameter of the PEDOT-rich cores increased parallel to the stretching direction, which enhanced the conductivity along that direction. However, charge transport was retarded in the perpendicular direction because the core diameter decreased. Because this anisotropic deformation was elastically recovered when the films were released, the change in resistivity was observed to recover in this strain region.

Chapter 4: Strong Correlation between the Resistivity and Tensile Strain of PEDOT:PSS films

However, when the applied strain is larger, the change in the resistivity of the pristine films is caused by the coalescence of PEDOT-rich cores. The increase in core size caused by mechanical deformation is hardly recovered but is permanently maintained even after the films are completely released. Although the shrinkage occurs during the release of the films, the effect of the dimensional change on the cores size is small. For example, the core area decreased only 1 % by the dimensional change during the release from 42 % strain to the load-free state (28 % strain). AFM analysis (Figure 4.10) shows that the core area is $2.85 \times 10^{-2} \mu\text{m}^2$ for the sample of 42 % strain. After the strain releasing, the core area is still maintained at $2.70 \times 10^{-2} \mu\text{m}^2$. The altered resistivity is also maintained over time, as shown in Figure 4.11. Moreover, as shown in Figure 4.9b, the anisotropic-to-isotropic transition of the resistivity appears above 7 % strain. In the AFM phase images (Figure 4.6d-f), the equivalent growth of the cores can be observed independent of the stretching direction. Beyond 7 % strain, the slope of the change in resistivity in the perpendicular direction is nearly identical to that in the parallel direction. Therefore, the resistivity of the pristine films can be reduced permanently and isotropically because of the coalescence of the cores induced by large strain.

This isotropic and permanent nature of the electrical resistivity of PEDOT:PSS films induced by mechanical deformation provides another way in which the electrical properties of the films can be modulated. To date, only chemical doping has been used for such a purpose.

Chapter 4: Strong Correlation between the Resistivity and Tensile Strain of PEDOT:PSS films

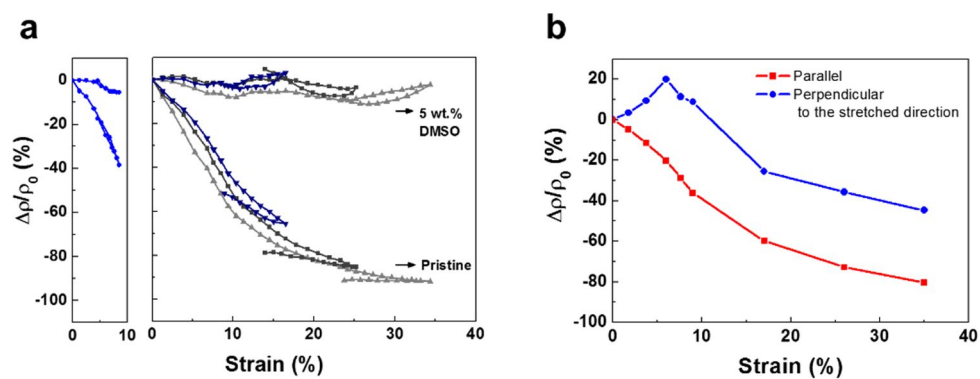


Figure 4.9. (a) Relative resistivity changes ($\Delta\rho/\rho_0$ (%)) of PEDOT:PSS films as a function of strain (9, 17, 26, and 35 %) for the pristine and 5 wt. % DMSO-doped films. (b) The change in resistivity parallel and perpendicular to the stretching direction of pristine films.

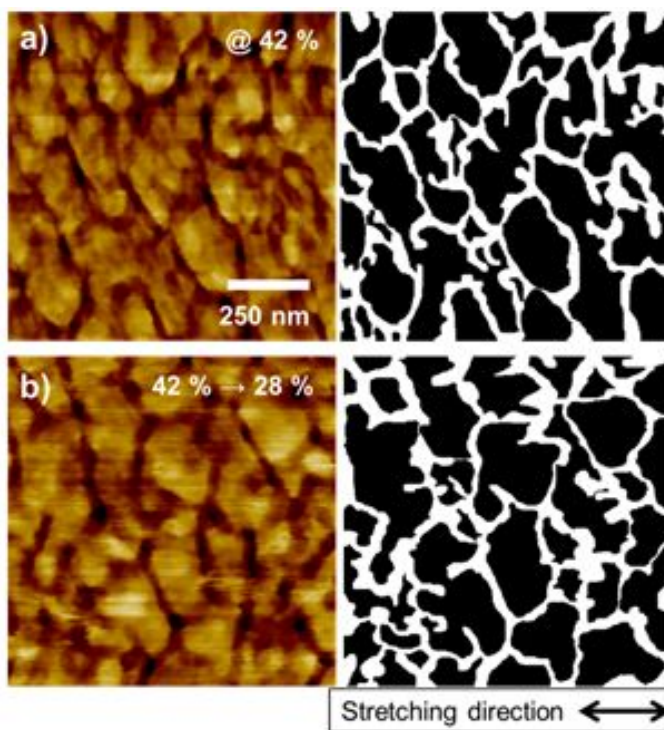


Figure 4.10. AFM phase images and reproduced images of pristine PEDOT:PSS films (a) at a strain of 42 % and (b) released to their load-free states (28 %).

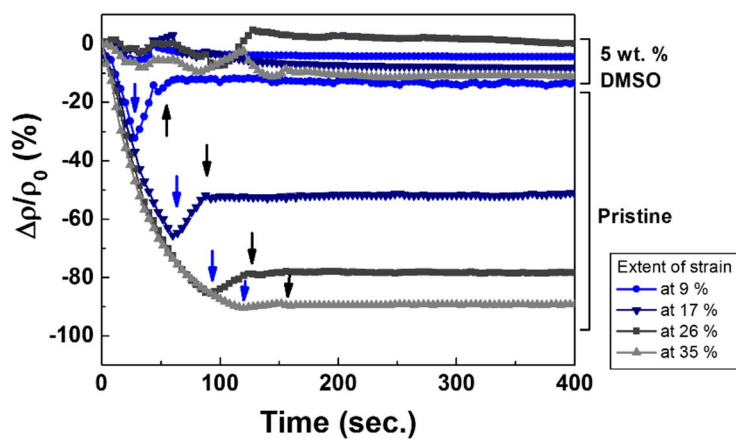


Figure 4.11. Relative resistivity change ($\Delta\rho/\rho_0$ (%)) of pristine PEDOT:PSS films on PI substrates as a function of time during stretching and releasing. Blue and black arrows indicate that strain at the onset of releasing (9, 17, 26, and 35 %) and load-free states after releasing, respectively.

4.8. Summary

In this study, we investigated the change in the resistivity of pristine and DMSO-doped PEDOT:PSS as a function of tensile deformation. We obtained crack-free PEDOT:PSS stretchable conductors at a strain of 60 % by using PI substrates, which have mechanical properties that are similar to those of PEDOT:PSS films. These results demonstrate that we can directly determine intrinsic changes in resistivity solely by studying morphological changes. The resistivity of DMSO-doped PEDOT:PSS films remains constant with respect to strain because conducting PEDOT chains are homogeneously dispersed and delocalized. In contrast, the resistivity of pristine PEDOT:PSS films was observed to decrease by up to 90 %. This decrease is primarily caused by the unique morphological changes of the pristine PEDOT:PSS films. Stretching to large tensile strains gives rise to the unusual coalescence of conductive PEDOT-rich cores. An increase in core size is permanently maintained during stretching and even after releasing the films, which results in an irreversible decrease in resistivity. We conclude that tensile strain in PEDOT:PSS films significantly influences the morphological changes of the films and is dependent on the DMSO doping concentration. The resulting morphological changes directly lead to changes in electrical properties. According to these results, the resistivity of PEDOT:PSS films can be modulated to be negative with the application of tensile strain due to the permanent deformation of the films' morphology.

CHAPTER 5

Growth Mechanism of Strain-Dependent Morphological Changes in PEDOT:PSS Films

5.1. Introduction

The resistance of materials generally increases under large amounts of mechanical strain and does not recover after deformation due to the generation of defects (buckles and cracks)^[27,57,58] and geometrical plasticity^[26,59]. However, within the elastic strain region, strain-dependent resistivity can increase or decrease depending on the intrinsic properties of a material. For example, the resistivity of n-doped silicon decreases^[23,60], whereas that of p-doped silicon^[60–62] and metals^[63] increase due to changes in the corresponding atomic lattices, which alter the electronic band structures. Such piezoresistive properties have been used in many applications, such as pressure sensors^[64], strain gauges^[65], and accelerometers^[66]. With the increasing demand for stretchable and flexible devices, the development of materials that exhibit reliable deformation-induced resistivity changes, even under large amounts of deformation, has become necessary^[59,67–71]. Thus, the underlying mechanism of resistivity changes under such large deformations must be understood.

Chapter 5: Growth Mechanism of Strain-Dependent Morphological Changes in PEDOT:PSS Films

As a flexible and stretchable electrode, soft polymeric PEDOT:PSS (poly(3,4-ethylenedioxythiophene):polystyrene sulfonate) conductors are widely applicable in electronic devices^[19,72-75]. However, its electrical behaviors in response to mechanical deformations have not been clearly elucidated. The relative change in the resistance of this material under 2% strain, known as the gauge factor, was previously reported to be 5.2^[43] and 17.8^[76]. These values indicate a positive increase in resistivity with strain. However, the opposite change in resistivity has also been observed when the applied strain was increased up to 10%; the measured resistivity was found to gradually decrease with an increase in strain^[45,46]. Above 10% strain, the resistivity change could not be observed due to the generation of defects (buckles and cracks) and because changes in resistivity may have occurred in a complex manner. Considering all the previous data, the range of values over which the resistivity changes and the mechanisms that have been proposed for these change are inconsistent. To understand the strain-dependent resistivity changes of PEDOT:PSS, this study focused on the morphological changes of PEDOT-rich cores, which are known to be a major determinant of the intrinsic conductivity of a material.

The morphology of PEDOT:PSS has a particular core-shell structure composed of conductive and tangled PEDOT-rich cores surrounded by shells with excess amounts of PSS chains^[2,53]. PEDOT has very short and lightweight segments compared with polymeric PSS chains^[53]. In the cores, positively charged PEDOT is electrostatically bound to negatively charged PSS chains via Coulomb interactions. The excess PSS chains that are not bonded to PEDOT surround the cores with a shell thickness of 5-6 nm^[2]. Because the cores have much higher conductivity than the PSS shells, their conductivity is predominantly determined by the size of the cores, phase distribution of the cores and shells in the films. The size and film resistivity of the PEDOT-rich

Chapter 5: Growth Mechanism of Strain-Dependent Morphological Changes in PEDOT:PSS Films

cores are highly correlated. For example, when the PSS content is increased, the core diameter and shell thickness decrease and increase, respectively; the intrinsic conductivity decreases due to a reduction in the diameter of the conductive cores. The morphology of such materials can be controlled by adjusting the mixing ratio of PEDOT-to-PSS^[37], UV irradiation^[38,77], and thermal treatment^[39], which cause changes in conductivity. In a more direct way, mechanical deformations induce morphological changes and can widely modulate a material's electrical properties. However, the detailed underlying mechanisms of the external strain-induced morphological changes of PEDOT:PSS have not been studied. In this regard, we investigated the origin of morphological changes in PEDOT-rich cores under large tensile deformations and the correlation of the resistivity changes induced by the resultant morphological changes.

In other conducting polymers, such as polyacetylene^[55], polyaniline^[56] and P3HT^[78], the resistivity always decreases during stretching. This behavior is primarily due to the directional alignment of polymer chains along the direction of the mechanical stress and the subsequent conformational changes of the polymers from entangled chains to linear chains. This phenomenon is more interesting for PEDOT:PSS, which consists of two types of polymers: a single PSS chain with adherent PEDOT segments. Uniquely, the conductive part of PEDOT is oligomeric and bonded to a relatively long PSS chain, but not all PSS chains contain PEDOT segments. Thus, the mechanism of decreasing strain-induced resistivity differs from that of single-component conducting polymers.

In this study, we investigated strain-dependent resistivity changes by achieving an in-depth understanding of the morphological evolution of PEDOT:PSS during stretching above 60% strain. The resistivity was decreased by following an identical decreasing path that was independent of the PEDOT:PSS film thickness, and the

Chapter 5: Growth Mechanism of Strain-Dependent Morphological Changes in PEDOT:PSS Films

decrease in resistivity could be explained by the growth of the conductive PEDOT-rich cores upon the application of tensile strain. The conductive cores gradually grew larger by consuming relatively smaller cores as the strain of the films increased. We further elucidated that the growth mechanism caused by the local rearrangement of PEDOT segments was near the PSS shells. The resultant rearrangement led to changes in the chemical environment in the cores, such as changes to the bonding energies and binding energies on PEDOT. We successfully examined the growth mechanism of the conductive cores induced by the local rearrangement of PEDOT segments, which directly modulated the electrical, morphological, and chemical properties that were dependent on the application of strain.

5.2. Methods

Preparation of PEDOT:PSS Solution and Films: PEDOT:PSS (CleviosTM PH 1000 and P VP Al 4083 Heraeus, Germany) solutions were prepared and then filtered through polypropylene filters (0.45- μm pore size). The PEDOT:PSS (PH 1000) films were formed by spin-coating at 1000, 2000, and 3000 rpm for 30 s onto polyimide (PI) substrates (Kapton 300 HN, DuPontTM) treated with air plasma (plasma cleaner PDC-32G, Harrick Plasma). The PEDOT:PSS (P VP Al 4083) films were also formed by spin coating at 1,000 rpm for 30 s on a PI substrate. The spin-coated films were annealed on a hot plate for 15 min at 130°C in an ambient N₂ glove box and were then cooled to room temperature in the glove box. Subsequently, the PEDOT:PSS films cast on the plasma-treated PI substrates were cut into rectangles measuring 10 mm in width and 30 mm in length.

Characterization: Uniaxial stretching tests were conducted on the PEDOT:PSS films using a micro tensile machine (MMT-500N, Shimadzu) equipped with an electrically contactable jig for *in-situ* resistance measurements. All the tests were conducted at room temperature at a constant strain rate of $5 \times 10^{-5} \text{ s}^{-1}$. As the films were deformed by uniaxial tension, and the electrical resistance of the films was measured with an Agilent 34410A multimeter. The initial electrical conductivities of the films were measured using the four-point probe technique. Surface images of the PEDOT:PSS films were acquired using an optical microscope and scanning electron microscopy (SEM, FE-SEM S-4800, Hitachi) at each strain level. AFM phase images were obtained with a NANO Station II instrument operating in non-contact tapping mode under ambient conditions. An X-ray photoelectron spectroscopy (XPS) survey spectrum was obtained using a PHI 5000 VersaProbeTM (ULVAC-PHI) with a

Chapter 5: Growth Mechanism of Strain-Dependent Morphological Changes in PEDOT:PSS Films

monochromatized Al K α , 1486.6 eV source. Fourier transform infrared (FT-IR) spectroscopy measurements were recorded on a Vertex 80 spectrometer (Bruker) in absorption mode.

5.3. Resistivity changes dependent on PEDOT:PSS thickness under tensile strain

PEDOT:PSS thin films were spin-coated on a PI substrate with a different RPM. The electrical resistivities and thicknesses of the PEDOT:PSS films are shown in Figure 5.1. The resistivity was independently varied from 6.5 Ωcm to 7.8 Ωcm on the spin-coating RPM. The thicknesses of the films were rapidly decreased with an increase in the RPM. The thicknesses were 74, 29, and 15 nm for 1000, 2000, and 3000 RPM, respectively.

To investigate the tensile strain responsive electrical behaviors of the PEDOT:PSS films, we observed the changes in resistance under tensile deformation that was dependent on the thickness of the PEDOT:PSS films. Figure 5.2a shows the resistance changes as a function of tensile strain for the different PEDOT:PSS films. The electrical resistance was monitored *in-situ* upon stretching the samples with up to 60% of strain. Tensile deformation was terminated after mechanical rupture of the films occurred. The initial resistance of the films increased due to the decrease in thickness. Notably, when the PEDOT:PSS films were stretched, the resistance of all the films gradually decreased even upon elongating the films above 50% strain. By mechanically stretching PEDOT:PSS for the different thickness films, a decrease in resistance was enabled regardless of the thickness of the sample.

To quantify the decrease in resistance of PEDOT:PSS films with tensile strain, we plotted the relative changes in resistance ($\Delta R/R_0$) as a function of the applied amount of strain (Figure 5.2b). Interestingly, despite a large difference in the initial resistance dependent on the thickness of the PEDOT:PSS films, the relative resistance change decreased along the same path as the strain applied to the films increased. The

Chapter 5: Growth Mechanism of Strain-Dependent Morphological Changes in PEDOT:PSS Films

resistance change with the strain gradually decreased and reached a saturation point, which was an 86% decrease in the resistance change for all the PEDOT:PSS films. The relative changes in resistance contains a theoretical resistance increase induced by a geometrical shape change of the films. We also plotted the theoretical increase term in Figure 5.2b using optical measurements of the length (l/l_0) and width changes (w/w_0) with the strain, and a calculation of the thickness change ($1-\nu_f \epsilon_l$) was assumed following Poisson's compression ratio. Despite the large increase in the relative resistance resulting from geometrical changes, the measured resistance changes decreased following the same path regardless of the thickness of the PEDOT:PSS films. This phenomenon has not been previously observed.

To observe an intrinsic electrical response with tensile strain, an electrical resistivity change was obtained by excluding a theoretical increase in resistance from a measured relative change in resistance. By rearranging the measured change in resistance ($\Delta R/R_0$) and the theoretical increase in resistance ($\Delta R_G/R_0$), the relative change in electrical resistivity ($\Delta \rho/\rho_0$) could be obtained. The equation is as follows:

$$\frac{\Delta \rho}{\rho_0}$$

We plotted the relative resistivity change as a function of tensile strain for the PEDOT:PSS films of different thickness as shown, in Figure 5.3c. The resistivity changes gradually decreased by as much as 95% with the strain of the films. They also followed the same decreasing path of resistivity with the strain independent of sample thickness. These decreasing behaviors were only induced by changes in the internal morphology of PEDOT:PSS with the introduction of strain. Mechanical deformation effected morphological changes and reduced the resistivity of PEDOT:PSS films regardless of their thickness. Hence, we investigated the

Chapter 5: Growth Mechanism of Strain-Dependent Morphological Changes in PEDOT:PSS Films

mechanism controlling this decrease in resistivity through an in-depth analysis of the morphological changes that occurred to PEDOT:PSS upon the application of strain.

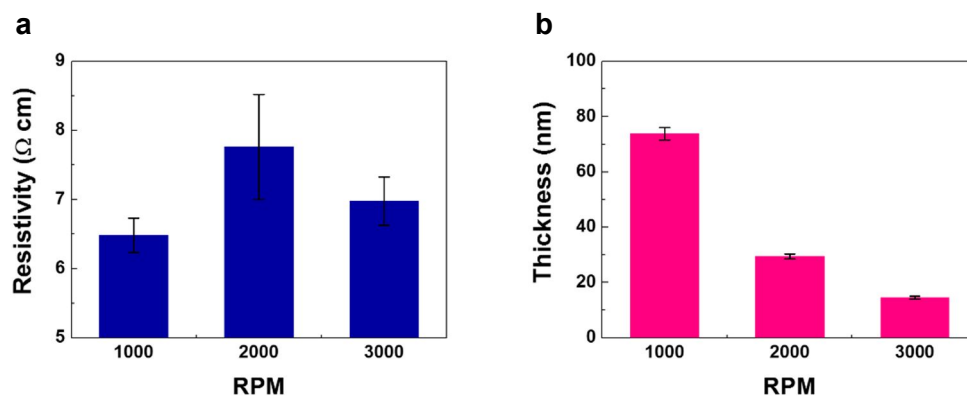


Figure 5.1. (a) Electrical resistivities of PEDOT:PSS films as a function of the RPM of a spin-coater. (b) Thickness of PEDOT:PSS films as a function of the RPM of a spin-coater.

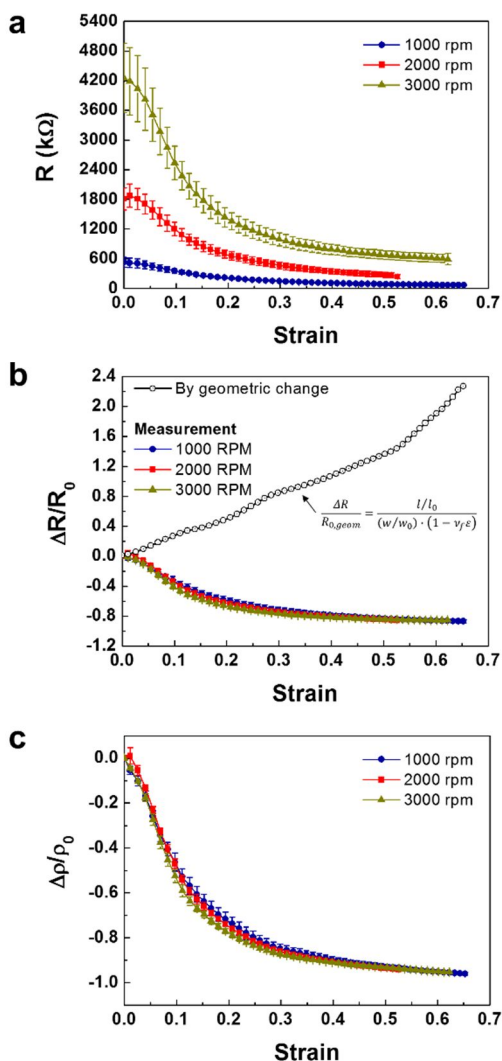


Figure 5.2. Mechano-resistivity changes of PEDOT:PSS films. (a) The resistance changes of PEDOT:PSS films with tensile strains according to the thickness of the films. (b) Relative changes in the resistances ($\Delta R/R_0$) with strain. Gray circles indicate the theoretical increases in resistance based on geometrical changes. (c) Relative changes in resistivity ($\Delta \rho/\rho_0$) as a function of tensile strain.

5.4. Evolution of PEDOT:PSS morphology under tensile strain

5.4.1. Growth procedure of PEDOT cores with strain

Mechanical strain directly causes morphological changes to PEDOT:PSS and decreases its electrical resistivity. The morphology of PEDOT:PSS consists of tangled and conductive PEDOT-rich cores that are surrounded by insulating shells composed of excess PSS chains. We examined the PEDOT:PSS morphology after tensile deformation by observing AFM phase images, which are presented in Figure 5.3a. The bright and dark fields in the images indicate PEDOT-rich cores and PSS shells, respectively. The sizes of the conductive cores mainly determines the electrical conductivity of PEDOT:PSS films^[50,79]. When the tensile strain was increased, the overall size of the cores increased independent of the direction of stretching. To easily differentiate between the cores and shells with strain, the AFM phase images were reproduced with binary contrast (black and white) using Photoshop (below Figure 5.3a). This showed large increases in the conductive cores and a reduction in the number of cores and shells per unit length (1 μm) with straining of the films. The increase in the conductive area and decrease in insulated barriers led to the enhancement of mobile charge transport. As previously confirmed, the decrease in resistivity occurred independent of the thickness of PEDOT:PSS. Based on the identical behavior of decreasing resistivity with strain, the growth of conductive cores were found to be the main mechanism for the improvement of electrical conductivity, regardless of the thickness of the samples.

The evolution procedure of PEDOT-rich cores is significantly influenced by the application of strain. To quantify the increase of the cores with the strain, we

Chapter 5: Growth Mechanism of Strain-Dependent Morphological Changes in PEDOT:PSS Films

measured each area of the cores with straightening of the PEDOT:PSS films, which are the black regions in the reproduced images (Figure 5.3a). The size of individual cores could be obtained using image analysis software (Scion Image Analyzer). We found that the distribution of the core area was plotted by the log-normal distribution function, which is widely used for presenting distribution function domains of living tissues or grain size of thin films. The cumulative equation of log-normal distribution is as follows:

$$\text{Cumulative density function (CDF)} = \frac{n - 0.3}{N + 0.4} \quad (2)$$

where n is each number of the core area, and N is the total core number. By using the size of the cores and their total number, we could obtain the cumulative density of the cores. The cumulative distribution as a function of the core areas is plotted at each strain level of the PEDOT:PSS films (Figure 5.3b). As shown in Figure 5.3b, the curves were shifted to the right, and the slope decreased with the strain, which not only indicated an increase in the median size but also the standard deviation of the cores. This demonstrated that non-uniform growth of the cores occurred with an increase in strain.

We observed the evolution procedure according to the initial PEDOT-rich core size at the sub-5% ($A_{5\%}$), median ($A_{50\%}$), and top-95% ($A_{95\%}$). The area change of each core was plotted as a function of the tensile strain (Figure 5.3c). The cores evolved with the strain regardless of their initial areas. The median of the core sizes were 0.23, 0.42, 0.51, and $0.61 \times 10^{-2} \mu\text{m}$ for strains of 0 %, 16 %, 28 %, and 42 %, respectively. This analysis clearly shows that the median size increased by 85 %, 119 %, and 164 % with the introduction of strain compared to the initial core sizes. This large increase of the conductive region is a major cause for the enhancement

Chapter 5: Growth Mechanism of Strain-Dependent Morphological Changes in PEDOT:PSS Films

electrical conductivity. Such a huge growth in the cores cannot be explained by mechanical elongation because of tensile stress. Interestingly, the non-uniform behavior of core growth was found to be dependent on the initial size as the strain increased above 16% of the films. The initially large cores ($A_{95\%}$) gradually became larger as the strain increased. On the other hand, for the small sized cores ($A_{5\%}$), the occupied areas steadily decreased with the increase in strain. This means that the evolution of PEDOT-rich cores was exhibited by consuming the small cores into the large cores with the application of strain. The overall increase in conductive areas was mainly caused by the growth of large-sized cores according to the increase in tensile strain.

Chapter 5: Growth Mechanism of Strain-Dependent Morphological Changes in PEDOT:PSS Films

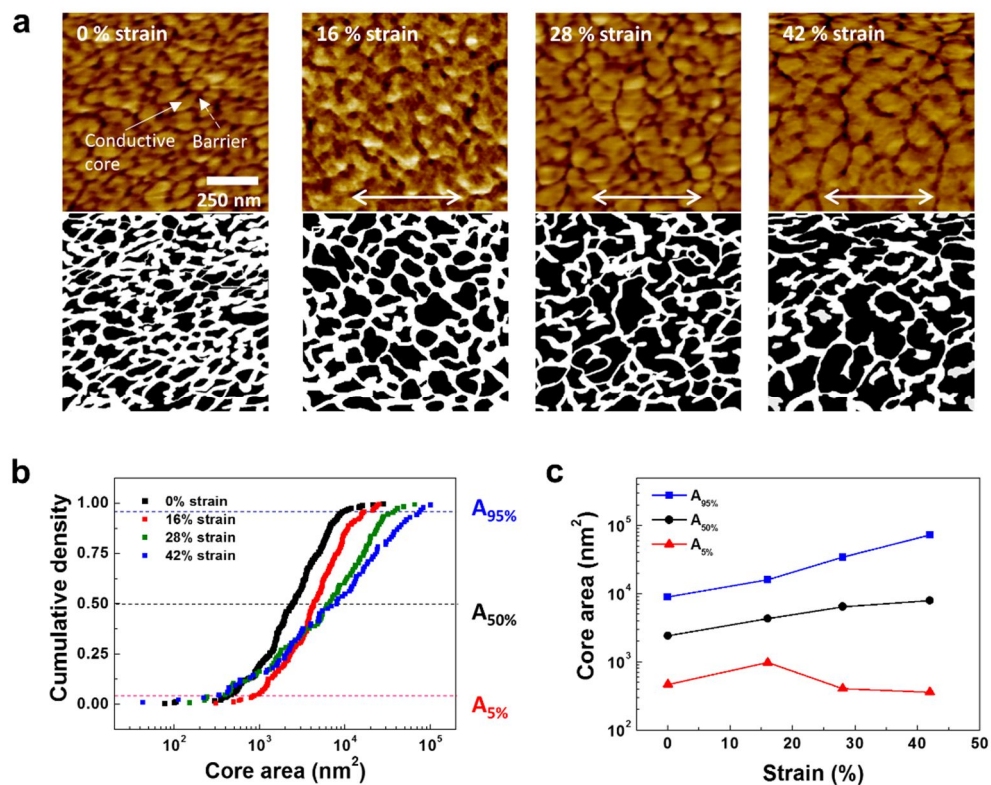


Figure 5.3. Morphological changes of PEDOT:PSS according to the applied amounts of tensile strain. (a) AFM phase images of PEDOT:PSS films at each strain denoted in the images. Bright field and dark field images represent the PEDOT-rich cores and the PSS shells, respectively. The arrow indicates the stretching direction, and all the images were obtained using tapping-mode AFM at a scale of $1 \times 1 \mu\text{m}^2$. (b) Distribution of cumulative density as a function of PEDOT-rich core area using a log-normal distribution function. (c) The change in the areas of PEDOT-rich cores at 5%, 50%, and 95% of cumulative density as a function of tensile strain.

5.4.2. Mechanism of the local rearrangement of PEDOT

When we closely observed the morphological changes of PEDOT:PSS with the application of strain, boundaries between the PEDOT-rich cores gradually disappeared and combined with each other. The growth of these cores occurred through coalescence or agglomeration, and the median size increased by 85 %, 119 %, and 164 % with strain compared to the initial core sizes. This significant growth of the cores cannot be explained by only mechanical elongation due to tensile stress. For example, at a strain of 42 %, the surface area of the cores increased by 16 % as a result of mechanical deformation, which was much smaller than the real increase of the cores (164%). Hence, the coalescence induced by strain was the main cause for the growth of the PEDOT-rich cores. Our questions are concerned with how increases in the conductive core areas respond to the applied strain and what occurs inside the cores. We believe that the local rearrangement of PEDOT chains occur at the vicinity of the PSS shells when the samples are subjected to strain.

PEDOT:PSS is primarily composed of two parts, which include a PEDOT segment-rich phase and an excess PSS-rich phase. They form the morphology of PEDOT-rich cores and PSS shells, as shown in Figure 5.4. In the core region, the positively charged PEDOT segments are bonded with the negatively charged PSS chains by Coulomb interactions. The excess PSS chains are bonded to each other through hydrogen bonding, which forms the shells. These electronic forces maintain the stability of PEDOT:PSS polymeric structures. When we mechanically stretch the PEDOT:PSS films, the electro-interactions among the PEDOT and PSS chains are significantly influenced by a large distortion of the polymeric structure. As shown in Figure 5.4, during stretching of the films, the inter-distance between the PEDOT-rich

Chapter 5: Growth Mechanism of Strain-Dependent Morphological Changes in PEDOT:PSS Films

cores is gradually closed, and the thickness of PSS shells decreases. Hence, the closer the inter-distance is, the stronger the electro-repulsive forces work among the negatively charged PSS chains. The resultant repulsion leads to electrical and structural instability between the cores. To relieve these electro-repulsive forces, positively charged PEDOT segments should be locally rearranged and migrated near PSS shells. By rearranging the PEDOT segments into the shells, the PSS boundaries between the cores gradually disappear and become PEDOT segments bonded to PSS chains. Therefore, after tensile deformation, initial PEDOT-rich cores divide into two and agglomerate into one by coalescing with each other (Figure 5.4). The increase in the core area is induced by the local rearrangement of PEDOT segments into the PSS shells, which leads to a growth in the conductive region and enhancement of charge transport.

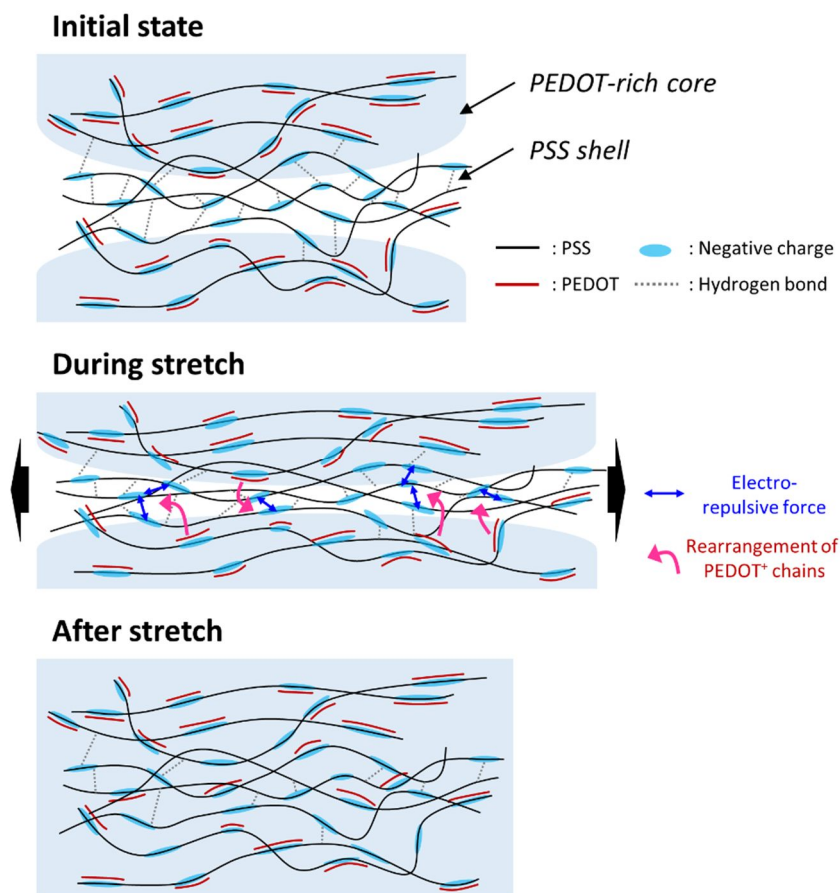


Figure 5.4. Schematic illustration of the evolution procedure of PEDOT-rich cores by mechanical tensile stretching. During the stretching process, a local rearrangement of PEDOT chains occurred, and the PEDOT chains locally migrated to the vicinity of the PSS shells to reduce the electro-repulsive force among the PSS chains. The areas of the PEDOT-rich cores increased after stretching.

5.5. Changes in the chemical environment induced by PEDOT rearrangement

A local rearrangement of PEDOT segments lead to a change in the chemical environment of PEDOT:PSS. To investigate the rearrangement-induced changes in the chemical environment, spectroscopic analyses were conducted using X-ray photoelectron spectroscopy (XPS) and Fourier-transform infrared (FT-IR) spectroscopy. The detailed chemical inter-chain interactions involve PEDOT chains being bonded to PSS chains via Coulomb interactions. The PSS is a doping material for PEDOT and donates a proton with a sulfonate group. However, many PSS chains that are not bonded with PEDOT chains are distributed around the PEDOT-rich cores. The local rearrangement of PEDOT in the PSS shells apparently generates changes in the bonding interactions between PEDOT and the PSS chains.

To examine the electron binding energy changes of PEDOT:PSS with the application of strain, the sulfur atom (S 2p) XPS spectrum was analyzed. Figure 5.5a shows the S 2p binding energy change as a function of the deformation strain. The S 2p line contains a spin-split doublet that consists of S 2p_{1/2} and S 2p_{3/2}. In the spectra of the PEDOT:PSS films, the lower and higher binding energy peaks correspond to the sulfur atoms in PEDOT and PSS, respectively. The binding energy of sulfur in PSS was higher than that of sulfur in PEDOT because PSS sulfur is strongly positive due to the presence of three oxygen atoms in the sulfonate group around sulfur^[80,81]. The distribution of the binding energy of PEDOT was more spread out due to delocalization of the positive charge of PEDOT over several adjacent rings.

Chapter 5: Growth Mechanism of Strain-Dependent Morphological Changes in PEDOT:PSS Films

When we observed changes in the binding energy with the application of strain, the energy distribution shifted to the lower energy side, which means that the energy required to detach the electron decreased due to the applied strain. The change in binding energy of the sulfur in PEDOT as a function of the deformation strain is shown in Figure 5.5b and reveals a decrease in the binding energy with an increase in strain. The binding energy shifted by 0.3 eV after a strain of 16% was applied. Combined with the previous results, the rearrangement of PEDOT into the shells directly affected not only an increase in the core area but also the decrease in binding energy for sulfur in PEDOT. Two factors are known to reduce an atom's binding energy. First, a decrease in the oxidation number causes the binding energy to decrease due to an increase in the screening of the bound electron from the ion core. Second, the local chemical environment also leads to shifts in the binding energy. Changes in electronegativity surrounding the atoms can decrease the energy required to detach electrons due to changes in the electron density of the atoms. Previously, the binding energy of sulfur in PSS-Na has been reported to increase by 0.4 eV compared with that in PSS-H due to an increase in the electronegative effect surrounding the sulfur in PSS^[80]. Here, the latter affects the decrease in the electron binding energy of sulfur in PEDOT. The local rearrangement of PEDOT into the shell leads to a change in the electrons, which leads to an increase of the number of PSS chains around the PEDOT. It draws the outer electron of sulfur in PEDOT to the sides of the PSS chains induced by the increase of electronegativity. Thus, less energy is required to detach the electrons from sulfur in PEDOT.

The bonding energy between constituent atoms in PEDOT:PSS could also be changed with strain because of the rearrangement of PEDOT segments. To verify the changes in bonding energy, FT-IR spectra were measured for the PI substrate and the

Chapter 5: Growth Mechanism of Strain-Dependent Morphological Changes in PEDOT:PSS Films

PEDOT:PSS films after deformation with up to 0, 16, 28, and 42% strain (Figure 5.5c). The peak positions corresponding to the bonding energies of the films are listed in Table 5.1^[82-84]. In particular, to examine the bonding energy changes in sulfur in PEDOT, we observed representative peak positions at approximately 862 and 944 cm^{-1} , which corresponded to the carbon-sulfur (C-S) bonding energy with the application of deformation strain. These peaks shifted to higher bonding energies, as shown in the inset of Figure 5.5c. We also showed that the C-S bonding energy changed in PEDOT as a function of the amount of strain applied, which reflected an increase in bonding energy with strain. This result was caused by the electron drawing effect on the sulfur in PEDOT due to the increase in the number of PSS chains around the PEDOT segments. It can be suggested that the sulfur appeared to be more negative in the C-S bonds, which caused a small vibrational energy increase in the bonding of C-S due to an increase of the dipole moment. This finding means that the mechanical deformation changed the chemical environment PEDOT, which shifted the bonding and binding energies of PEDOT because of the local rearrangement of PEDOT into the PSS shells.

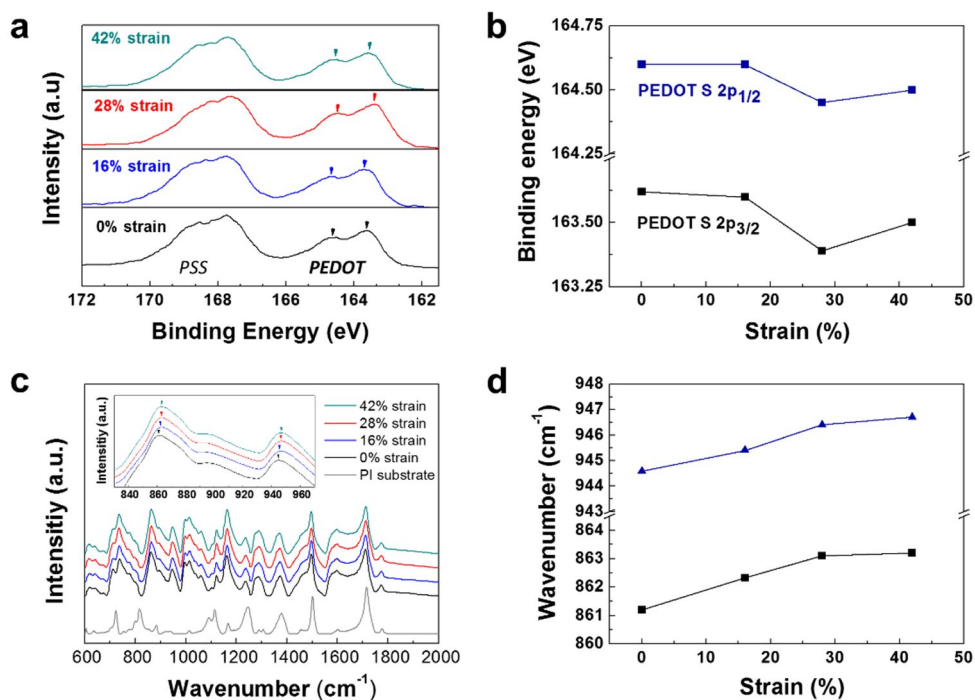


Figure 5.5. Spectroscopic analysis of the changes in bonding energy with tensile strain: (a) XPS spectra of S 2p for PEDOT:PSS films as a function of applied strain (0, 16, 28, and 42%). (b) The change in binding energy of S 2p in PEDOT according to the strain. (c) FT-IR absorption spectra for PEDOT:PSS films with tensile strain and PI substrates. The inset shows the peak shift of C-S bonding. (d) The change in carbon-sulfur (C-S) bonding energy in PEDOT chains as a function of the strain.

Chapter 5: Growth Mechanism of Strain-Dependent Morphological Changes in PEDOT:PSS Films

Table 5.1. Representative FT-IR absorption band for PEDOT:PSS and PI films.

PEDOT:PSS	Wave # (cm ⁻¹)	PI	Wave # (cm ⁻¹)
	709		
C-S (PEDOT)	862	C=O bending	723
	944		
C-C (PEDOT)	1288	C-O-C	1086
C=C (PEDOT)	1496	C-N	1377
S-O (PSS)	1122	C=C	1600
	1162		1714
S-phenyl bonds (PSS)	1037	C=O	1775

5.6. Dependence of changes in resistivity on the weight ratio of PEDOT to PSS

A decrease in the electrical resistance of PEDOT:PSS under tensile strain is mainly caused by an evolution of conductive PEDOT-rich cores through the local rearrangement of PEDOT segments into PSS shells. The rearrangement upon the application of strain is critically influenced by the initial morphology of PEDOT:PSS. To investigate the effects of the morphology of PEDOT:PSS on its resistance change behaviors, we prepared two type of PEDOT:PSS films with different weight ratios of PEDOT to PSS, which were 1:2.5 and 1:6. The relative weight of PSS increased for PEDOT:PSS (1:6) compared with the PEDOT:PSS film with a ratio of 1:2.5 that was used thus far. The increase in the PSS ratio definitely influenced changes in the materials' electrical properties according to the amount of applied strain. Here, we measured the resistance changes for the PEDOT:PSS films with ratios of 1:2.5 and 1:6 under stretched up to rupture strain (65% strain). As shown in Figure 5.6a, major differences were observed in the resistance changes of the two films. First, the 1:6-PEDOT:PSS film had a much higher initial higher electrical resistance than the 1:2.5-PEDOT:PSS film. The initial resistances were 104 M Ω and 0.534 M Ω for the 1:6- and 1:2.5-films, respectively. This was because of a large increase in the PSS weight in the PEDOT:PSS films. The excess PSS worked as an insulative barrier in the form of shells and hindered the charge transport on the films. Hence, a large increase in the initial resistance was observed due to the increase in the PSS weight ratio to PEDOT.

Interestingly, the opposite behavior was observed for resistance changes with tensile strain when the PSS ratio to PEDOT was increased. For the 1:6-PEDOT:PSS films, the resistance gradually increased as the applied strain increased. With an

Chapter 5: Growth Mechanism of Strain-Dependent Morphological Changes in PEDOT:PSS Films

increase in the PSS ratio, the resistance response with the strain was totally different from the previously observed decrease in behavior. It can be inferred that the large increase in the PSS ratio for the PEDOT:PSS films critically influenced the changes in resistance behaviors. To more precisely confirm the opposite behavior, we replotted the resistance change with a relative change in resistivity as a function of strain, as shown in Figure 5.6b. The previously described equation (1) was used for the conversion process. For the conventional 1:2.5-PEDOT:PSS films, the relative changes in resistivity gradually decreased with an increase in the strain. However, the resistivity changes of the 1:6-PEDOT:PSS films was almost invariable when subjected to low amounts of strain (30%) and then steadily increased with an increase strain. The changes in resistivity behavior were totally different from those of the 1:2.5-PEDOT:PSS films. This means that the growth of the conductive regions by the coalescence of the PEDOT-rich cores did not occur with increases in the tensile strain. The morphology was changed to increase the resistivity according to increases in tensile deformation.

Figure 5.6c illustrates the morphological changes of PEDOT:PSS for with weight ratios of 1:2.5 and 1:6 upon being stretched. In the case of the 1:2.5-PEDOT:PSS films, with an increase in the strain of the films, the PEDOT-rich cores coalesced with each other to form large cores. This led to an increase in the conductive regions and enhanced its electrical conductivity. On the other hand, the PEDOT-rich cores of the 1:6-PEDOT:PSS films were relatively small, and the inter-distances were far between the cores due to the large amount of PSS weight in the films. Even when a large amount of strain was applied to the films, coalescence of the cores did not occur. As the strain of the films increased, the cores became elongated in the direction of the stretching, and the inter-distances between the cores simultaneously and gradually

Chapter 5: Growth Mechanism of Strain-Dependent Morphological Changes in PEDOT:PSS Films

became distant. This led to an increase in the PSS insulative barriers, and the transport of mobile charges was prevented with the application of strain. Therefore, the electrical response was critically influenced by the initial morphologies of the PEDOT:PSS films, which exhibited opposite changes in resistance with strain according to the weight ratio of PEDOT to PSS.

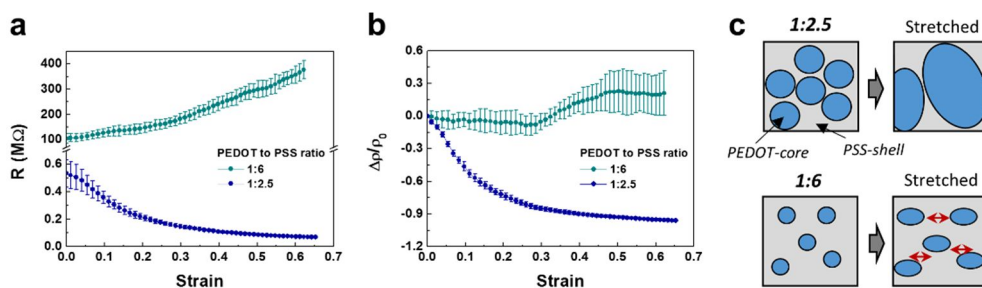


Figure 5.6. Mechano-resistivity changes in PEDOT:PSS films depending on the weight ratio of PEDOT to PSS. (a) Resistance changes of PEDOT:PSS films with tensile strain for PEDOT to PSS ratios of 1:6 and 1:2.5. (b) Relative changes in resistivity as a function of the strain for the 1:6 and 1:2.5 weight ratios. (c) Schematic illustration of the evolution of PEDOT-rich cores with strain dependency on the weight ratio of PEDOT to PSS.

5.7. Summary

The evolution of PEDOT-rich cores was induced by mechanical tensile deformation and exhibited overall growth of the cores due to consumption of the smaller cores by the larger cores. The resultant growth was caused by a local rearrangement of the PEDOT segments into PSS shells to lower the electric repulsive forces between the negatively charged PSS chains near the shells. Transitions in the electron binding and bonding energies were also observed from the changes in the chemical environment of PEDOT:PSS, which was induced only by the application of mechanical strain. With an increase in the conductive PEDOT-rich cores in the films, the electrical resistivity gradually decreased according to the strain due to large increases in the conductive regions. Furthermore, the decrease in resistivity followed the same path as the strain, independent of the thickness of the PEDOT:PSS films, indicating that the growth mechanisms acted equally on PEDOT:PSS regardless of their thickness. When the weight ratio of PSS to PEDOT was increased (1:6-PEDOT:PSS), completely different behaviors were observed in terms of the increase in resistivity in relation to tensile strain because of the enlarged insulating PSS barriers that resulted from the increased PSS ratio in the PEDOT:PSS films. Therefore, the mechanical deformation of PEDOT:PSS directly affected internal morphological changes, and the resultant changes led to transitions in the electrical properties and chemical environments of PEDOT:PSS. An in-depth understanding of the changes in strain-dependent resistivity will enable the use of these films in a wide range of applications, such as strain sensors and actuators, and conductivity modulation tools will help improve the performance of stretchable devices.

CHAPTER 6

Strain-insensitive stretchable electronic conductors: PEDOT-PSS/Acrylamide organogels

6.1. Introduction

Recent developments in electronics have called for stretchable interconnects that transport electrical signals between electroactive components even under various and harsh mechanical deformations^[3,5,6,85-89]. Conventionally, metal-based materials, such as nanowires^[10,67], flakes^[32,59], and composites^[7,11,69], have been used as flexible or stretchable conductors for such flexible interconnects. By designing the structures of the conductors as buckled^[12,15,90] or wavy-shape^[16,57], the stretchable region can be more strategically secured. These structured conductors exhibit high electrical conductivities and device performances under mechanical deformation. However, the stretchability can be constrained according to the structural design under larger mechanical strains. Moreover, when worn or attached onto skin, large mismatches in the mechanical properties of these conductors also result in severe interface delamination between the hard conductors and the soft human body. Therefore,

Chapter 6: Strain-insensitive stretchable electronic conductors: PEDOT-PSS/Acrylamide organogels

naturally soft and biocompatible materials for interconnects that can transport electrical signals are desperately required.

For soft electrically conducting materials, conducting polymers can be utilised due to their electrical conductivity and mechanical flexibility. By introducing a highly cross linkable hydrated polymers, mechanically tough and stretchable hydrogels can be applicable^[91-94]. Recently, by combining conductive polymers, such as polyaniline (PANI), polypyrrole (PPy), and poly(3,4-ethylenedioxythiophene) (PEDOT), with a hydrated matrix polymer, hydrogel-based conductive materials have been produced for functional devices, such as electrical interconnects, supercapacitors, bioelectrodes, and sensors^[95-102]. Conductive hydrogels are highly stretchable and easily deformable materials that can exhibit electrical and ionic conduction. However, despite gelation with conductive polymers, critical issues remain that prevent the use of a conductive hydrogel as an electronic conductor. First, mixed conduction due to the migration of both ions and electrons occurred with the application of a DC voltage. For electronic devices, the electrical conduction should be through electron charge carriers only. However, in most cases, the conductive hydrogels contain mobile ions dispersed in water. The conduction is not purely induced by electron transport but combined with ion transportation. In this case, electrochemical reactions or water electrolysis can occur with the application of a small dc voltage to the hydrogels^[103,104]. Hence, the use of conductive hydrogels is limited by the size of the electrochemical window of the electrode-electrolyte interface. Second, due to the large deformability of the hydrogels, a strain-induced change in the electrical properties occurs during mechanical deformation. A resistance change with strain significantly constrains the circuit design of stretchable devices. Third, long-term environmental instability of the conductive hydrogels occurs because the primary constituent is water. The water inside the

Chapter 6: Strain-insensitive stretchable electronic conductors: PEDOT-PSS/Acrylamide organogels

hydrogels can easily evaporate over time. The loss of the water causes the hydrogels to dry and stiffen, making these conductive hydrogels no longer stretchable polymers.

Here, we fabricated organogel-based strain-insensitive conductors that are electrically conductive and barely dry in ambient air. For electric conduction without electrochemical reactions, extra ions were successfully removed via a dialysis process, and the water in the gels was fully replaced with ethylene glycol (EG), which is an organic solvent. By using closely packed and partially crystallized PEDOT:PSS sheets as a conducting component, an electrical polymeric path was effectively formed inside the gels. Moreover, the change in electrical resistance with tensile strain was minimized without abrupt failure and was almost invariant up to 50% strain. We demonstrated stretchable LED circuits by using the electrically conductive organogels for electronic interconnects.

6.2. Methods

Synthesis: The as-received PEDOT:PSS aqueous solution (Clevios P, Heraeus) was mixed with ethylene glycol (EG, Sigma-Aldrich) with a volume ratio of 8:1. The PEDOT:PSS solute was obtained from PEDOT:PSS solution by using freeze-drying method. We froze the PEDOT:PSS aqueous solution in a freezer (-20 °C) for one day. Subsequently, the frozen solution was placed in freeze dryer machine (FD5508, ilShinBioBase) equipped with vacuum chamber. We lower the vacuum up to 5 mTorr inside the chamber. The solution is dried for 3 days, and then the fully dried PEDOT:PSS solute was obtained. It was dissolved in DI water and EG (8:1) with weights of 0.105, 0.13, 0.155, and 0.18 g for 12-ml solutions. In those solutions,

Chapter 6: Strain-insensitive stretchable electronic conductors: PEDOT-PSS/Acrylamide organogels

acrylamide (AAm, Sigma-Aldrich) monomer was added to reach 2.12 M. The concentration of PEDOT:PSS to PEDOT:PSS plus AAm was varied to 5.49%, 6.83%, 7.90%, and 9.06% for the freeze-dried solutions and 6.72% for the as-received solution. The cross-linker, N,N'-methylenebisacrylamide (MBAAm, Sigma-Aldrich); initiator, ammonium persulphate, (APS, Sigma-Aldrich); and accelerator N,N,N',N'-tetramethylethylenediamine (TEMED, Sigma-Aldrich), whose weight ratios were 0.38 wt. %, 0.55 wt. %, and 0.39 wt. % relative to AAm, respectively, were added into the solution. Subsequently, the solution was poured into a glass mould with dimensions of 50 mm × 75 mm × 1 mm (w × l × t), and then, gelation was conducted on a hotplate at 90 °C for 2 hr. To remove the extra ions and impurities, the synthesised gels were washed in DI water mixed with EG (8:1) for 3 days, changing the solution every day. To selectively evaporate the DI water inside the swelled gels, they were dried in an oven at 60 °C for 4 hr, resulting in PEDOT:PSS-PAAm organogels containing EG as the solvent.

Electrical properties measurements: For measurement of the currents across the PEDOT:PSS-PAAm hydrogel and organogels as functions of voltage, I (current)-V (voltage) sweeps were conducted for the gels with dimensions of 20 mm × 3 mm × 1 mm (w × l × t) using a four-point probe (Keithley 6487 picoammeter, 2000 multimeter, and 6220 current source). The four electrical contacts with the probe tips were made with silver paste, and the I-V curve was measured in the voltage range from -5 to +5 V. The electrical resistivity was calculated using the results from the resistance, which is extracted from the inverse of the slope of the I-V curves and the dimensions of the gels.

We conducted impedance measurement of the PEDOT:PSS hydrogel and organogel (9.06%) within a frequency range from 100 kHz to 0.1 Hz with 10 mV amplitude at 0

Chapter 6: Strain-insensitive stretchable electronic conductors: PEDOT-PSS/Acrylamide organogels

V offset (ZIVE MP2A, Wonatech).

The changes in the electrical resistances of the PEDOT:PSS-PAAm organogels during stretching were measured. Uniaxial stretching tests were conducted on the gels using a tensile machine (MMT-500N, Shimadzu) equipped with an electrically contactable jig for *in situ* resistance measurements (Agilent 34410A multimeter). The gels were cut into dimensions of 8 mm \times 5 mm \times 1 mm ($w \times l \times t$). The electrical contacts were formed with copper foil at each end of the gels before the gels were glued onto acryl clamps. The samples were placed and fixed between two jigs at both ends in the tensile machine. All tests were conducted at room temperature at a displacement rate of 3 mm/min. As the gels were stretched, the electrical resistance was measured once per second until rupture. For a measurement of the change in the resistance during high cycle tensile fatigue, each of the samples was also fixed with the machine, deformed uniaxially up to 50% strain and released to 0% strain for 1000 cycle at 0.05 Hz. The displacement rate was 15 mm/min, and the resistance was measured once per second.

Microstructure analysis: The internal structures of the PEDOT:PSS-PAAm gels were observed using a field-emission scanning electron microscope (FESEM, Carl Zeiss, SUPRA 55VP). The gels were freeze dried for 4 days and then we cut a cross-section of the gels. The gels coated with 3 nm of Pt before the cross sections were imaged.

Mechanical tensile tests: The mechanical properties of the PEDOT:PSS-PAAm organogels were measured using a tensile machine (Instron 3343). The dimensions of the gels were 10 mm \times 10 mm ($w \times l$) rectangles with thicknesses of 1 mm; these samples were glued onto acryl clamps. The samples were placed and fixed between two jigs at both ends in the machine. The displacement rate was 3 mm/min. Tensile

Chapter 6: Strain-insensitive stretchable electronic conductors: PEDOT-PSS/Acrylamide organogels

fatigue tests were also conducted from 50% strain to 0% strain for 1000 cycles at 0.05 Hz. The displacement rate was 15 mm/min. All tests were conducted in air at room temperature.

Environmental stability: The weight change of the EG inside the PEDOT:PSS-PAAm gels was measured in a vacuum chamber as a function of time. The conditions for the measurements were 0.013 atm and room temperature. The gels were cut into 8 mm \times 8 mm ($w \times l$) squares with thicknesses of 1 mm, and the weights of the gels were measured at the following times: 0, 10, 20, 50, 110, 200, 460, and 1320 min. The weight of the EG was measured by subtracting the weight of the completely dried gels from the weights of the gels at each time.

LED demonstration: Ecoflex 0030 elastomer was prepared for use as the stretchable substrate with dimensions of 40 mm \times 10 mm \times 1 mm ($w \times l \times t$). Two LEDs were pinned at each end of the substrate. The PEDOT:PSS (9.06%)-PAAm organogel was cut into a rectangle with dimensions of 27 mm \times 5 mm \times 1 mm ($w \times l \times t$), interconnected between the two LEDs and wired to a 9 V battery.

6.3. Electronic conductor of PEDOT:PSS-PAAm organogel

6.3.1. Demonstration of stretchable LED arrays

Uniformly distributed PEDOT:PSS organogels (PEDOT:PSS-PAAm organogels) were successfully obtained by a gelation of (PEDOT:PSS) dispersed ethylene glycol (EG) solution with polyacrylamide (PAAm). The fabricated PEDOT:PSS-PAAm organogels are electrically conductive and highly stretchable (Figure 6.1). The

Chapter 6: Strain-insensitive stretchable electronic conductors: PEDOT-PSS/Acrylamide organogels

practical use of these organogels was confirmed by the successful lighting of an LED that was partially interconnected with the conductive organogels and electric wires. The LED remains turned on during stretching, twisting, and even with both stretching and twisted of the gels (Figure 6.2). By utilizing a PEDOT:PSS-PAAm organogel as an electrical interconnect, highly stretchable LED arrays were demonstrated. Figure 6.3a illustrates a stretchable LED circuit where two LED lights are interconnected with the conductive PEDOT:PSS-PAAm organogel on an Ecoflex substrate. As shown in Figure 6.3b, a uniform and constant emission of LEDs is realized without electrochemical reaction at the electrode interfaces. Interestingly, the LED is found to function well, even stretched above 200% strain, and it is elastically recovered after being released (Figure 6.3c and movie clip S1 in Supporting Information). In addition to electrical conduction, the mechanical softness of the organogel makes it possible to deform easily in response to the applied stress without rupture. We also demonstrated stretchable 2×3 arrays of LEDs attached to an inflated balloon (Figure 6.4). Under a biaxial deformation on the arrays via expansion of the balloon, the six LEDs remain in operation without mechanical and electrical failures.

**Chapter 6: Strain-insensitive stretchable electronic conductors:
PEDOT-PSS/Acrylamide organogels**

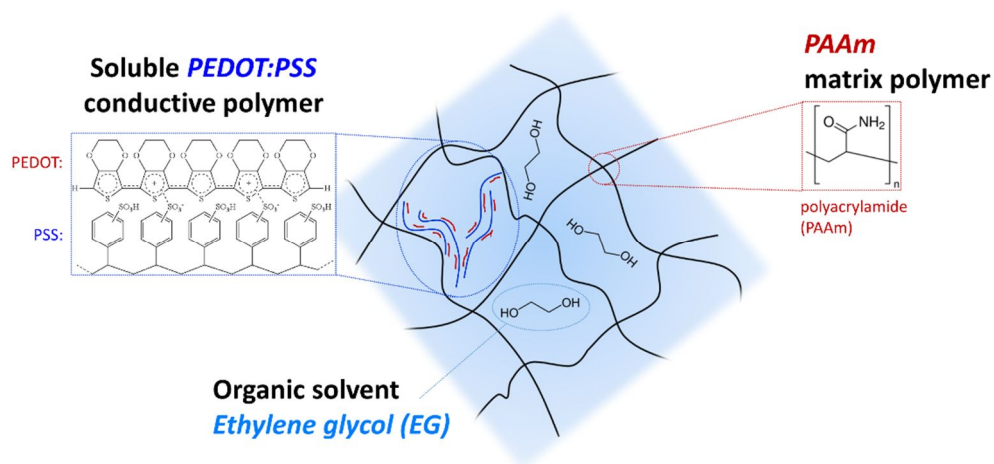


Figure 6.1. Schematic illustration of PEDOT:PSS-PAAm organogel microstructures. Conductive and soluble PEDOT:PSS polymers are dispersed in PAAm matrix polymers, and ethylene glycol organic solvent is the liquid constituent of the organogels.

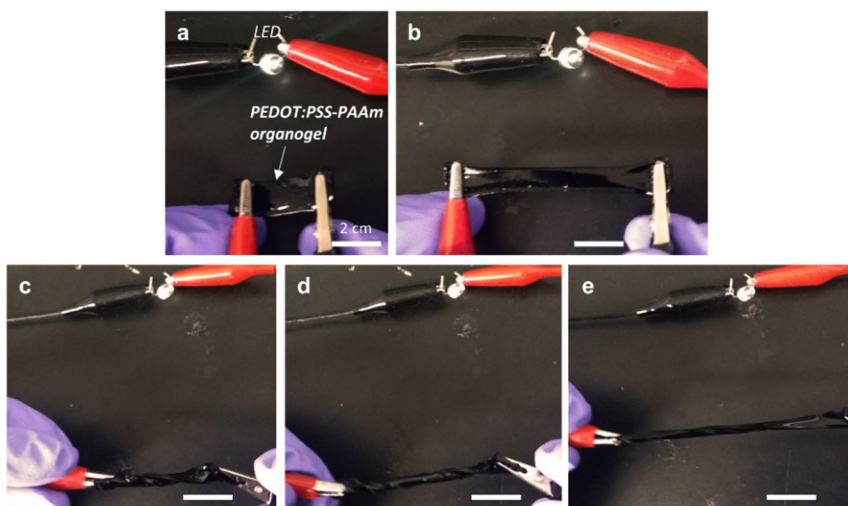


Figure 6.2. Electrical interconnection with PEDOT:PSS-PAAM organogels. (a) LED operation with interconnections containing the organogels while being (b) stretched, twisted by (c) 360° and (d) 720°, and (e) stretched in a twisted state.

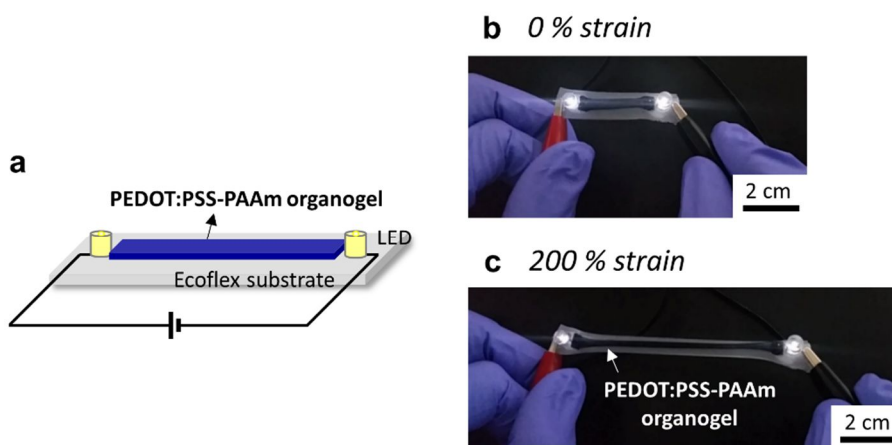


Figure 6.3. Strain-insensitive electronic conductor of a PEDOT:PSS-PAAm organogel without electrochemical reactions. (a) Schematic illustration of the LED integrated circuit. (b) and (c) Optical images of the circuit before and after stretching up to 200% strain, respectively. The LED light interconnected with PEDOT:PSS-PAAm organogel was still operational even with large deformations.

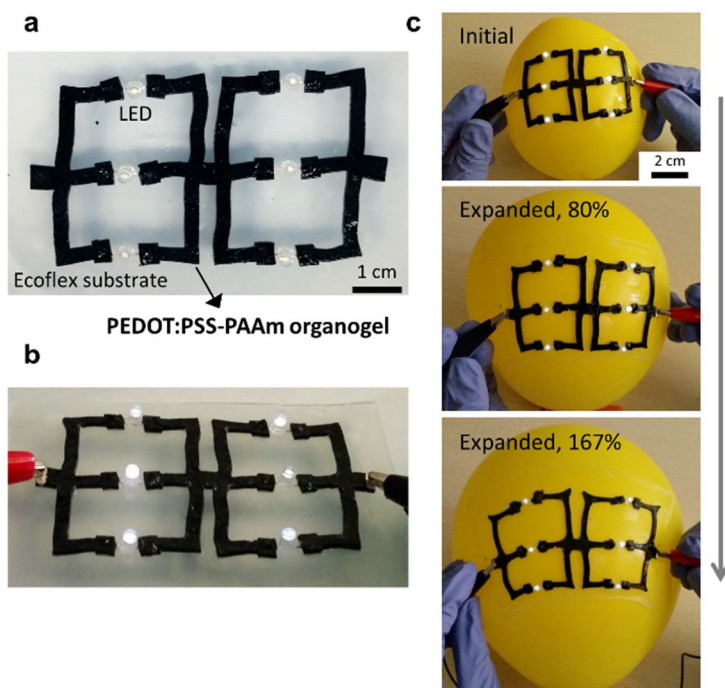


Figure 6.4. Stretchable LED arrays and their response to biaxial stretching on a balloon. (a) Optical image of a stretchable 2×3 array of LEDs interconnected with PEDOT:PSS-PAAm organogels on an Ecoflex substrate. (b) Optical image of the 2×3 LED array showing the emission of the LEDs in a flatted state. (c) Optical images of the stretchable array of LEDs (2×3) attached to a balloon under biaxial expansion (80% and 167%).

6.3.2. Electrical conduction under DC voltage

Conventional conductive hydrogels are mostly composed of water containing extra ions inside the gels. Hence, when an electrical potential is applied to the hydrogels for electrical conduction, not only electric but also ionic conduction occurred by ion migration^[96,100,105]. Moreover, an electrochemically driven current flows due to the reduction of cations, oxidation of anions, or electrolysis of the water inside the hydrogels. The strength of our PEDOT:PSS-PAAm organogels is that they are electrically conductive without ion-derived conduction processes; only electrical conduction occurs through the organogels, even at high applied electrical potentials.

To investigate the electrical conduction behavior of PEDOT:PSS-PAAm organogels, we measured the electric current (I) as a function of voltage (V) by using the four-point probe method. As shown in Figure 6.5a, I-V sweeps of PEDOT:PSS-PAAm organogels were measured as functions of the weight ratio of PEDOT:PSS to PAAm. Interestingly, the electric current is observed to linearly increase with the applied voltage range, as shown in Figure 6.5a, which is representative of ohmic conduction. The current is only induced by electrical conduction through the PEDOT:PSS inside the gel. No electrochemical reactions occurred at the interfaces of the gel and the electrodes, even over the range of applied voltage from -5 V to +5 V. In addition, no damage to the gel was found after the I-V sweep was completed. We also confirmed the electrical conduction of the organogels from the impedance measurement (Figure 6.6). For the PEDOT:PSS hydrogel made from the as-received PEDOT:PSS aqueous solution, it shows large increase of the capacitive reactance when the frequency decreased. It means a capacitive behavior of the hydrogel is observed by an ion migration. Similar behaviors are also observed for the other hydrogel based

Chapter 6: Strain-insensitive stretchable electronic conductors: PEDOT-PSS/Acrylamide organogels

conductors. However, for the PEDOT:PSS organogel, the resistive impedance is not much changed with a large variation of the frequency, and moreover, the capacitive reactance shows very negligible change at even lower frequency. It is typical impedance behavior of electrical conductors. The conduction of the PEDOT:PSS organogels dominantly occurred by electrical migration of PEDOT:PSS polymeric conduction path. Because extra residual ions were removed during the dialysis, ionic conduction was retarded inside the organogels. Moreover, by replacing water with EG as the liquid constituent of the gel, electrochemical reactions generating hydrogen and oxygen did not occur with increasing voltage. However, in the case of PEDOT:PSS-PAAm hydrogels, the electrical current changes irregularly with the applied voltage due to the vigorous electrochemical reactions at the interface of the hydrogel and the electrode (Figure 6.7). A milliampere range current flows irregularly in the voltage range from - 3 V to 4 V, which is indicative of non-ohmic conduction. In addition, during the I-V sweep, bubbles formed due to the generation of gases at the electrical contacts between the hydrogel and the electrodes. The electric current is a faradic current, which is primary caused by redox reactions at the interface. Because there are many hydrogen ions (H^+) dispersed inside the gels, hydrogen gas is evolved at the negative electrode via the reduction of hydrogen ions. Spontaneously, at the positive electrode, the oxidation of water occurs, and then, oxygen gas is evolved. This current is mainly induced by the electrochemical reactions inside the PEDOT:PSS-PAAm hydrogel. As a result, the fabricated PEDOT:PSS-PAAm organogels can serve as electronic conductors without any electrochemical reactions over a wide range of electrical potentials.

As shown in Figure 6.5a, the current level and the slope increased with the weight ratio of PEDOT:PSS due to the increase in the conductive component. The electrical

Chapter 6: Strain-insensitive stretchable electronic conductors: PEDOT-PSS/Acrylamide organogels

percolation was improved inside the organogels with increasing concentration of PEDOT:PSS from 5.49% to 9.06%. However, for the PEDOT:PSS-PAAm organogels made from the as-received PEDOT:PSS solution (6.83%), the slope of the current is lower than in the organogels made from freeze-dried PEDOT:PSS even at high concentrations of PEDOT:PSS. To study the changes in the electrical properties according to the difference between the type of organogel, the electrical resistivity of the PEDOT:PSS-PAAm organogels was compared according to the PEDOT:PSS weight ratio. As shown in Figure 6.5b, the resistivity was plotted as a function of the PEDOT:PSS weight percent using the slope of the I-V curves and the dimension of the gels. The resistivity gradually decreased as a function of the PEDOT:PSS weight ratio. For the organogels fabricated using freeze-dried PEDOT:PSS, the resistivity decreased, from 5,529 Ωcm to 133 Ωcm for 5.49% and 9.06%, respectively. In terms of conductivity, PEDOT:PSS-PAAm organogels (0.01 S/cm) have slightly lower value than the previous works (0.11^[105], 4.3^[97], 0.7^[101], and 0.1 S/cm^[106]). Low conductivity of the organogels is originated from suppressed ionic conduction by replacing water in the hydrogels with EG organic solvent. The electrical percolation in the gels can be greatly improved with a small increase in the PEDOT:PSS content, which leads to the enhancement of the mobile charge transport. Interestingly, compared to the resistivity of the 6.83% (as received) and 6.71% (from freeze dried) samples, the resistivity of the 6.71% sample is much lower than that of the 6.83% gel despite the similar PEDOT:PSS weight ratio.

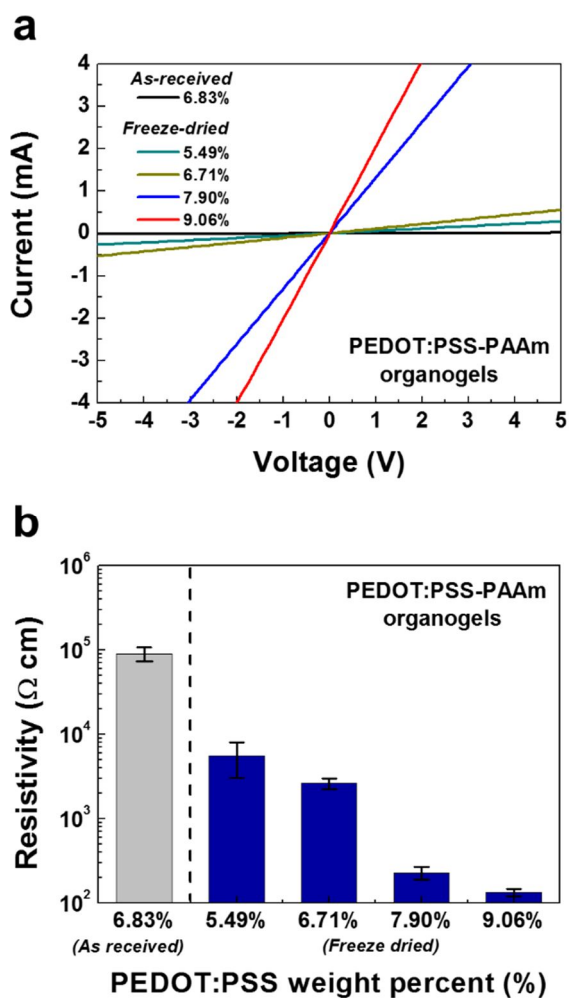


Figure 6.5. I (current) - V (voltage) measurements of (a) PEDOT:PSS-PAAm organogels according to the weight ratio of PEDOT:PSS relative to PEDOT:PSS plus PAAm, which exhibited ohmic electronic conductivity. (b) Electrical resistivity of the organogels as a function of weight ratios.

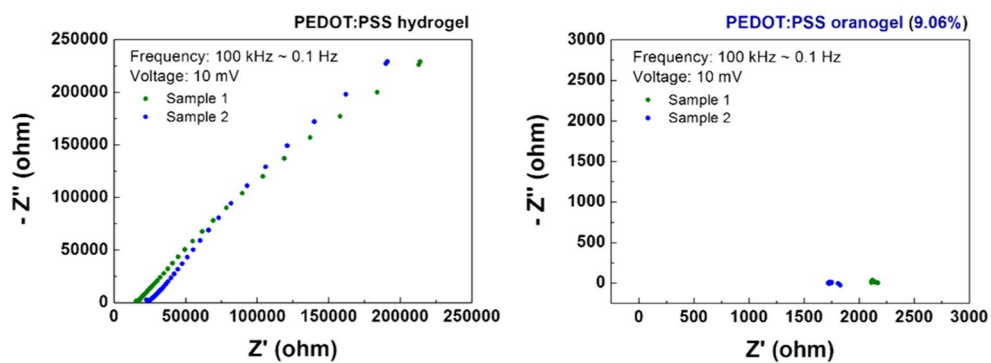


Figure 6.6. Impedance curves of (a) PEDOT:PSS hydrogel and (b) organogel (9.06%) with a frequency ranging from 100 kHz to 0.1 Hz at 10 mV.

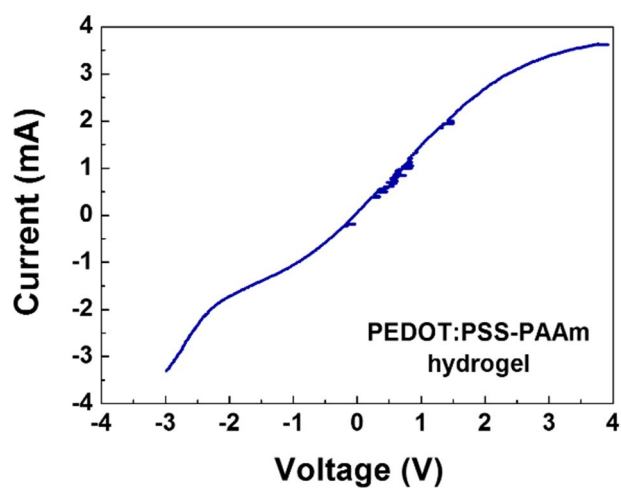


Figure 6.7. Measurement of a I (current) - V (voltage) sweep of the PEDOT:PSS-PAAm hydrogel. Non-ohmic conduction occurred during the current (I) – voltage (V) sweep.

Chapter 6: Strain-insensitive stretchable electronic conductors: PEDOT-PSS/Acrylamide organogels

We also studied the changes in the electrical resistance in the PEDOT:PSS-PAAm organogels during stretching of up to 400% strain. The resistance of the gels was measured *in situ* upon stretching until electrical failure occurred. The normalized resistance change of the gels is plotted as a function of tensile strain in Figure 6.8 for 6.83% (from as received solution), 5.49%, 6.71%, 7.90%, and 9.06% (from freeze-dried solute) PEDOT:PSS-PAAm organogels. The dotted curve is the theoretical resistance increase with strain induced by dimensional change assuming the total volume is conserved. The resistance increase curves of each organogel are located below the theoretical resistance changes. Despite the dimensional change, which is the elongation of length and the reduction of width and thickness of the organogels, the internal percolation path of PEDOT:PSS is well preserved inside the organogels, even under tensile deformation. The inset of Figure 6.8 also shows remarkably low increases of resistance changes with the strain below 100% strain. Interestingly, the percolation path is conserved for larger strains (> 300%) in the freeze-dried PEDOT:PSS organogels than in the as-received PEDOT:PSS organogel. Because the electrical percolation occurs through coarse and freeze-dried PEDOT:PSS, stable electrical percolation can be maintained inside the organogels under large strains. However, electrical rupture occurred at a strain of 150% for the as-received PEDOT:PSS organogel, i.e., the percolation path was disconnected without mechanical rupture of the organogels. We think that the phenomenon is induced by the structural differences between the PEDOT:PSS from the as-received solution and that from the freeze-dried solution.

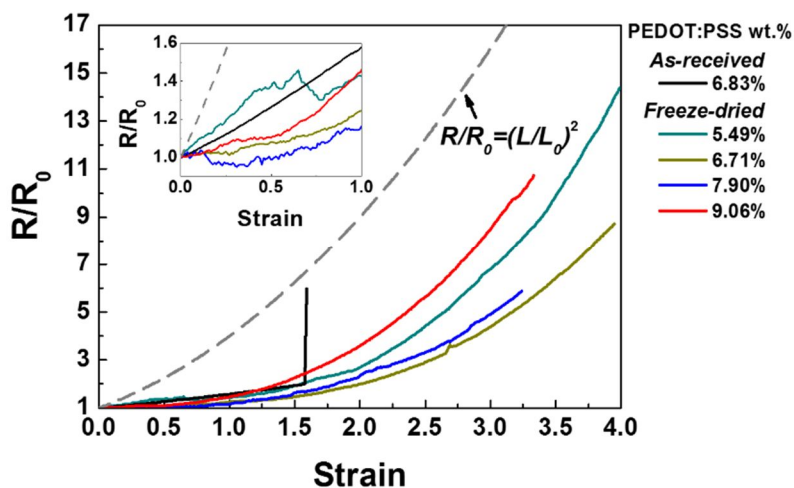


Figure 6.8. Normalized resistance change (R/R_0) plotted during the stretching of PEDOT:PSS organogels with various weight ratios showing insensitive resistance increases under extension. The inset shows increases in resistance changes when the strain was under 100%. The dotted grey line indicates the theoretical resistance change with the change in dimension.

6.4. Fabrication of the organogel with a PEDOT:PSS polymeric path

6.4.1. Formation of polymeric conducting path

The electrically conductive organogels are composed of PEDOT:PSS as the polymeric conducting path and PAAm as the cross-linking polymeric network, which is swelled by EG. The synthetic procedure is divided into four steps: (i) preparation of a PEDOT:PSS solution, (ii) gelation of the PEDOT:PSS solution with PAAm, (iii) dialysis of the synthesized gels, and, finally, (vi) solvent exchange step via the selective evaporation of water. The detailed procedure is shown in Figure 6.9. First, we prepared two types of PEDOT:PSS solutions, which are the as-received PEDOT:PSS solution (Heraeus, Clevios P) and the redispersed freeze-dried PEDOT:PSS solution. The PEDOT:PSS solute was obtained by freeze drying the as-received PEDOT:PSS solution. After the freeze-drying process, the shape of the solute becomes a closely packed sheet, as shown in Figure 6.9. The PEDOT:PSS is aggregated and forms closely packed and ordered PEDOT:PSS layers. To control the concentration of the PEDOT:PSS solution, the solute was redispersed in a mixed solution of EG and DI water with a 1:8 volume ratio. Due to the high solubility of PEDOT:PSS in the solution, a uniformly dispersed PEDOT:PSS-EG solution can be obtained.

For the gelation of the PEDOT:PSS- EG solution, acrylamide (AAm) monomers were used. We prepared different weight ratios of PEDOT:PSS relative to AAm plus PEDOT:PSS weight in the solution. For the as-received PEDOT:PSS solution, 6.83% of PEDOT:PSS is contained in the solution. To control the weight ratio of

Chapter 6: Strain-insensitive stretchable electronic conductors: PEDOT-PSS/Acrylamide organogels

PEDOT:PSS in the gels, different weights of freeze-dried PEDOT:PSS are dissolved in water: 5.49, 6.71, 7.90, and 9.06%. Subsequently, ammonium persulphate (APS) and N,N'-methylenebisacrylamide (MBAAm) was added as an initiator and a cross-linker, respectively, for PAAm. Next, we added N,N,N',N'-tetramethylethylenediamine (TEMED) as an accelerator. The solution was poured into a glass mould and then covered with a glass plate. The solution was cured on a hotplate at 90 °C for 2 hr to fabricate the PEDOT:PSS-PAAm organogel. During polymerization of AAm, extra residual ions (NH_4^+ , HSO_4^+ , and SO_4^{2-}), which are byproducts from the radical initiation of AAm monomers, are also produced in the gel. These ions will lead to ionic conduction inside the gels, and even electrochemical reactions occurred when an electrical voltage was applied. To remove the ions and other impurities inside the gels, dialysis steps are introduced. We made a refining solution that has the same mixing volume ratio of DI water to EG as the initially prepared PEDOT:PSS solution (8:1). By immersing the gels in the EG/DI water solution, the residual ions and impurities inside the gels escaped to the solution via osmotic pressure. After the dialysis, the liquid inside the swelled gels is mixed in the solution of EG and DI water. To fully replace the liquid with EG solvent, selective evaporation of water was conducted by drying the swelled gels in an oven at 60 °C for 4 hr. Because the boiling point of EG, which is 197 °C, is much higher than that of water, the water can be selectively evaporated from the gels. The ultimately fabricated gels are composed of EG as a liquid and uniformly distributed PEDOT:PSS polymers in the cross-linked PAAm networks, i.e., the PEDOT:PSS-PAAm organogel. The fabricated PEDOT:PSS-PAAm organogel is mechanically soft, easily deformable, and electrically conductive, even in the mechanically stretched state.

**Chapter 6: Strain-insensitive stretchable electronic conductors:
PEDOT:PSS/Acrylamide organogels**

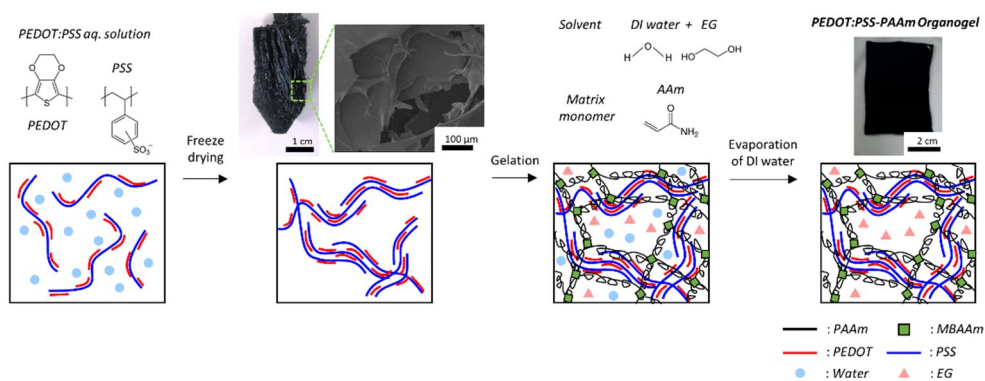


Figure 6.9. Formation of polymeric conducting paths of PEDOT:PSS distributed PAAm organogels. Synthetic procedure of the electrically conductive PEDOT:PSS-PAAm organogels. Closely packed PEDOT:PSS was obtained from freeze drying the as-received PEDOT:PSS aqueous solution. For the gelation process, the PEDOT:PSS solute was mixed with ethylene glycol (EG) diluted with DI water and acrylamide (AAm) matrix monomer. Ammonium persulphate (APS) and TEMED (tetramethylethylenediamine) were used as the initiator and accelerator for the polymerization of acrylamide (AAm) and the N,N'-methylenebisacrylamide (MBAAm) cross-linker, respectively. The conductive paths were formed inside the gels with PEDOT:PSS. The gels were swelled in EG diluted with DI water for dialysis and were then dried in an oven to selectively evaporate the water inside the gels.

6.4.2. Microstructure

To investigate the microstructures of the PEDOT:PSS-PAAm organogels, the cross-sectional morphologies of the 6.83% (from as-received PEDOT:PSS) and 6.71% (from freeze-dried PEDOT:PSS) organogels were observed using a scanning electron microscope (SEM), as shown in Figure 6.10a and 6.10b, respectively. Clear differences are observed in the internal structures of the two samples, and the microstructures are critically correlated with the electrical properties of these two organogels. The PEDOT:PSS organogel made from the as-received solution is composed of uniformly distributed pores with an average size of 20 μm . Inside the pores, net-shaped polymers were interconnected between the inner surfaces of the pores. In contrast, the organogels made from the freeze-dried solute dominantly contain macro-pores with sizes greater than 60 μm . Moreover, it was also observed densely packed pores with sizes less than 1 μm in the high magnitude SEM images in Figure 6.11. Due to the distribution of closely packed PEDOT:PSS inside the gels, a variety of structures, including packed, coiled, and leaf-shaped pores, can be observed. A large difference in the microstructures was observed between the two types of organogels.

The microstructure of the freeze-dried PEDOT:PSS solute is compared with that of bulk PEDOT:PSS, which is the as received PEDOT:PSS solution that was dried in a dry oven at 70 $^{\circ}\text{C}$ for 1 hr. The PEDOT:PSS bulk has no specific structure, with only a flat and smooth surface observed. Hence, the electrical percolation path is formed by completely dissociated PEDOT:PSS chains, the percolation path can be more easily disconnected at lower strain. However, for the freeze-dried PEDOT:PSS, a layered structure that consists of closely packed sheets of PEDOT:PSS was observed (Figure

***Chapter 6: Strain-insensitive stretchable electronic conductors:
PEDOT-PSS/Acrylamide organogels***

6.9). For the as-received PEDOT:PSS solution, the PEDOT:PSS is randomly dispersed in the solution; however, during freeze drying of the PEDOT:PSS solution, the PEDOT:PSS solute became aggregated and formed closely packed and ordered PEDOT:PSS layers. When re-dispersing the PEDOT:PSS solute to form a gel, the coarse and packed PEDOT:PSS layers are not completely broken, and partially crystallized solutes remain in the solution. Because the electrical percolation is composed of coarse and crystallized PEDOT:PSS, the percolation path was enhanced and remained stable in the organogels with uniaxial extension up to large strain.

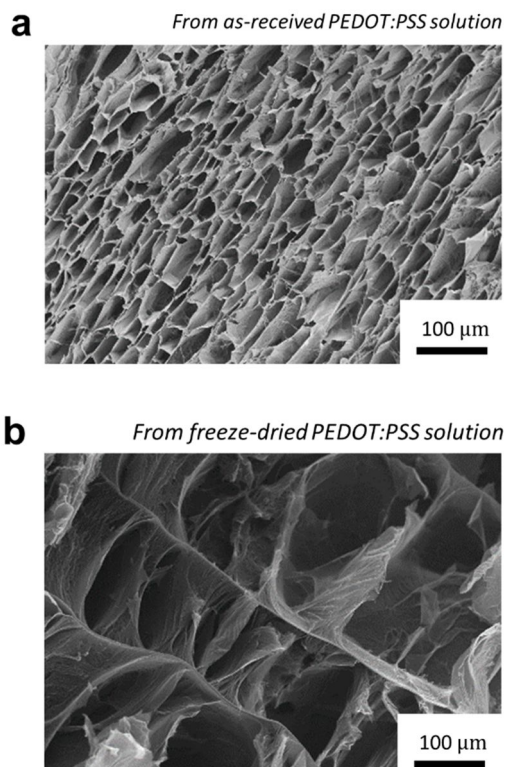


Figure 6.10. SEM images of the cross sections of the PEDOT:PSS-PAAm organogels made from (a) the as-received PEDOT:PSS solution and (b) the freeze-dried PEDOT:PSS solution, respectively. The polymeric conductive path was well formed inside densely packed pores for the organogels made from the freeze-dried PEDOT:PSS solution.

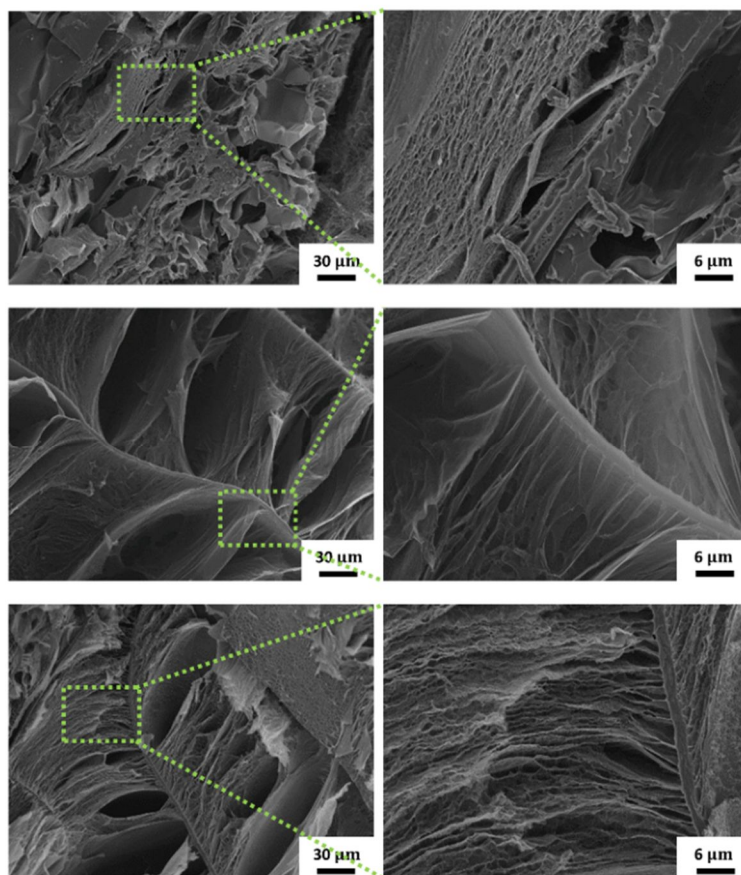


Figure 6.11. Microstructure of an organogel made from freeze-dried PEDOT:PSS solute. Cross-sectional SEM images of the gels at three different points. The magnified images are shown to the right of each image, which correspond to the dotted box.

6.5. Mechanical and electrical response under tensile deformation

6.5.1. Mechanical properties

The fabricated PEDOT:PSS-PAAm organogels are mechanically soft and highly stretchable. To quantify the mechanical properties of the organogels, tensile tests were conducted. As shown in Figure 6.12a, the organogel was glued to two acrylic plates mounted on the tensile machine and then stretched until mechanical rupture occurred. An uniaxial extension of the gels was conducted with a constant rate of 3 mm/min. The stress-strain curves of the PEDOT:PSS-PAAm organogels are obtained according to the various weight ratios of PEDOT:PSS (Figure 6.12b). These organogels are gradually stretched to greater than 350% strain; in fact, stretching of up to 525% strain was achieved for the PEDOT:PSS weight ratio of 5.49%. The tensile strength of the organogels is in the range from 18 kPa to 30 kPa, which are values that are mechanically compatible to human-skin^[107,108]. The stretchability and mechanical strength are dependent on the weight ratio of PEDOT:PSS relative to AAm. As the weight ratio of PEDOT:PSS increased, the stretchability decreased and the strength increased, except for the organogel from the as-received solution.

The mechanical properties (Young's modulus and rupture strain) of PEDOT:PSS-PAAm organogels were compared according to the weight ratio of PEDOT:PSS, as shown in Figure 6.12c. For the PEDOT:PSS-PAAm organogels made from freeze-dried PEDOT:PSS, the strength of the gels is enhanced with increasing weight ratio. The Young's moduli of the organogels increased from 47 kPa to 80 kPa for 5.49% and 9.06%, respectively. However, the rupture strain tends to decrease as the weight ratio

Chapter 6: Strain-insensitive stretchable electronic conductors: PEDOT-PSS/Acrylamide organogels

of PEDOT:PSS increases. Despite the small increase in PEDOT:PSS, the mechanical stretchability and strength is sensitively influenced by the weight ratio of PEDOT:PSS. However, the PEDOT:PSS-PAAm organogels made from the as-received PEDOT:PSS solution has relatively lower mechanical stretchability and Young's moduli than the freeze-dried organogels despite the similar PEDOT:PSS weight ratios. We think that the microstructural differences between the two types of organogel critically influence the mechanical properties. For the organogel from the as-received PEDOT:PSS solution, as shown in Figure 6.10a, a polymeric matrix with uniform size ($\sim 20 \mu\text{m}$) is equally distributed and the PEDOT:PSS chains are randomly dissolved in the pores. However, in the case of the organogel from freeze-dried PEDOT:PSS (Figure 6.10b), a bimodal distribution of the macro-pores ($> 60 \mu\text{m}$) and micro-pores ($< 1 \mu\text{m}$) was observed. In addition, due to the closely packed sheets of PEDOT:PSS inside the gels, a dense and messy polymeric network should form. In other words, the crosslinking between the PAAm network and the PEDOT:PSS is stronger for the freeze-dried organogels than for the as-received gels. With the increase in the PEDOT:PSS weight ratio in the gels, the network is becomes mechanically stronger because of the entanglement among the polymers by physical crosslinking^[109], and the early rupture occurred because of the decrease in the weight ratio of the PAAm networking polymers.

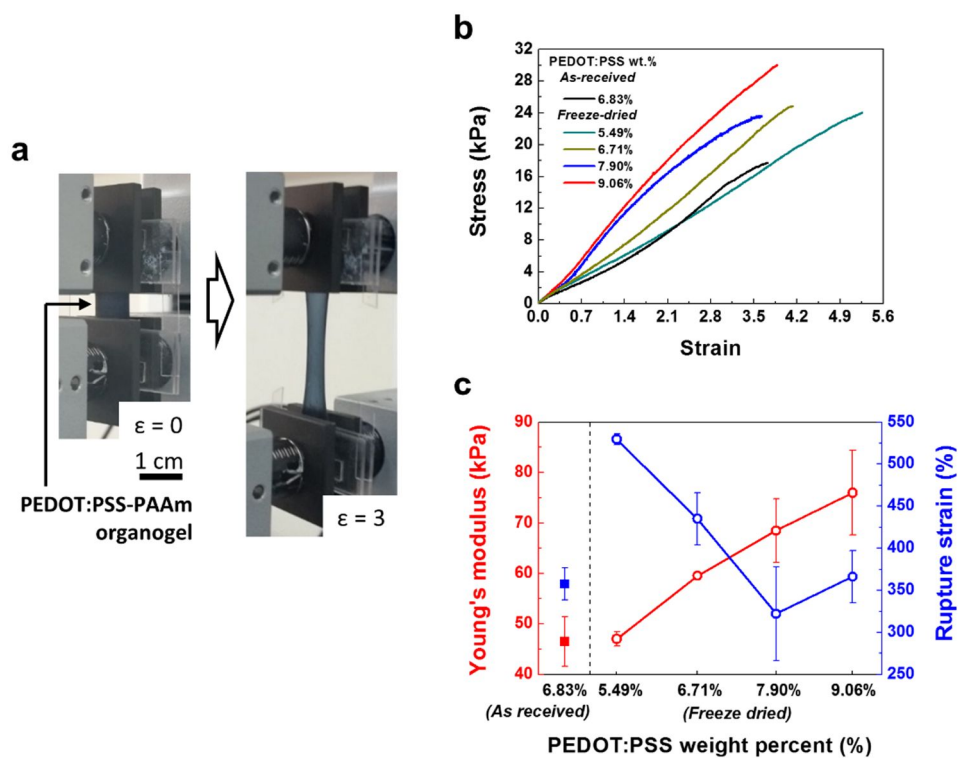


Figure 6.12. (a) A strip of PEDOT:PSS-PAAm organogel in the undeformed state (left) and stretched state up to 300% strain (right). (b) Stress-strain curves for the PEDOT:PSS-PAAm organogels for various weight ratios of PEDOT:PSS until mechanical fracture of each sample occurred. (c) The Young's modulus and rupture strains of the organogels as a function of weight ratios.

6.5.2. Tensile fatigue insensitive changes of electrical properties

To investigate the tensile fatigue of the PEDOT:PSS-PAAm organogels, we applied highly repeated tensile deformation up to 50% strain for 1000 cycles. Every cycle of stress and strain was measured during the tensile fatigue for the PEDOT:PSS (9.06%)-PAAm organogel. As shown in Figure 6.13a, we plotted the stress-strain curves at the 1st, 10th, 100th, 500th, and 1000th cycles as representative cycles. The stress linearly increased and decreased during stretching up to 50% strain and the subsequent release to the load-free state. As the number of fatigue cycles increased, a slight plastic deformation of the organogel occurred after being fully released. A plastic strain of 4% was measured after the 1000th cycle, which is a very small value. Interestingly, regardless of the fatigue cycle, a reversible change in the stress-strain curve can be observed. The unloading path upon release almost follows the loading path upon stretching, even after 1000 cycles. A hysteresis of the curves was not observed during the stretching and releasing cycle. Thus, the mechanical recovery of the organogel was highly reliable with highly repeatable deformation.

We also observed a change in the resistance of the PEDOT:PSS (9.06%)-PAAm organogel depending on the tensile fatigue. The resistance was measured *in situ* during repeated strain from 50% to 0% for 1000 cycles. The normalized resistance change was plotted as a function of the fatigue cycle, as shown in Figure 6.13b. During the cycle, the resistance of the organogel initially decreased up to the 50th cycle and then gradually increased with the deformation cycle. After the 1000th fatigue cycle was completed, the resistance increased by up to 57% compared with the initial resistance. Despite the good mechanical recovery of the PEDOT:PSS-PAAm organogel during the fatigue, the path of electrical percolation was influenced by the repeated

Chapter 6: Strain-insensitive stretchable electronic conductors: PEDOT-PSS/Acrylamide organogels

deformation, which leads to a permanent degradation of the electrical conduction. For the initial cycle up to the 50th cycle, the resistance decreased with the cycle number, which indicated that the percolation path is slightly enhanced by the repeated deformation during the initial cycles. However, as the number of fatigue cycles increased, the degradation of the percolation path mainly occurred with the cycle.

When we observed the variation in the resistance for one cycle, the resistance barely changed during stretching to and releasing from 50% strain, independent of the cycle number (Figure 6.13b). To investigate the resistance change with strain at each cycle, we plotted the normalized resistance change as a function of strain in the 1st, 10th, 100th, 500th, and 1000th cycles, as shown in Figure 6.13c. Although the initial resistances are different, depending on the cycle number, a reversible recovery of the resistance change can be observed for a one-cycle deformation. The resistance change is almost invariant with the strain, and a minor hysteresis with a resistance change of less than 10% was observed only for the 1st cycle. Despite an overall increase in the resistance after the fatigue cycle, the resistance change during each cycle was not significant, regardless of the fatigue cycle. In other words, the electrical percolation path is stably maintained inside the PEDOT:PSS-PAAm organogel during a single deformation when stretched to and released from 50% strain. The conductive paths formed with the coarse and crystallized PEDOT:PSS are preserved during the deformation, with a degradation of the path only occurring under mechanical fatigue.

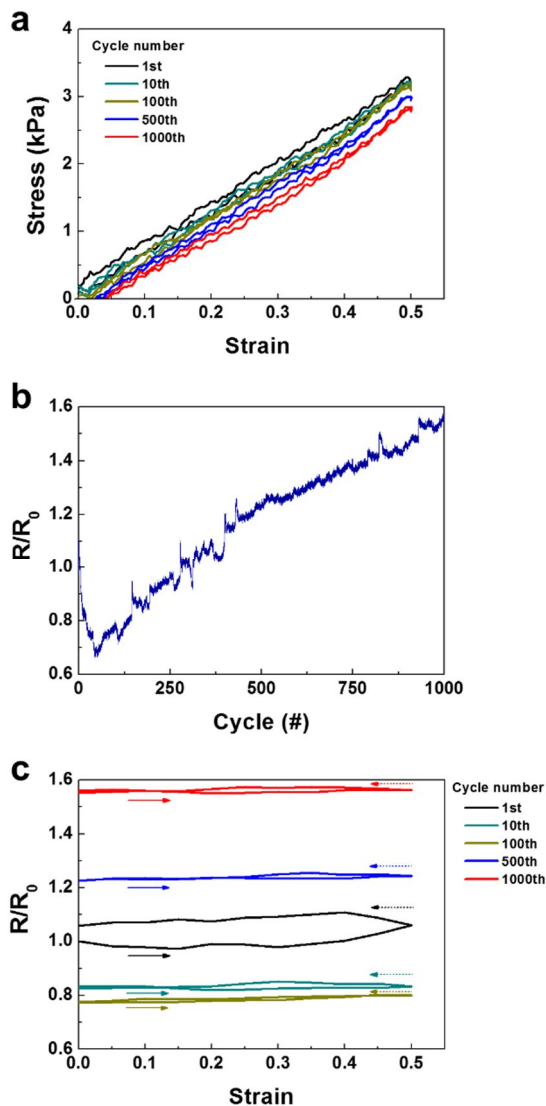


Figure 6.13. Fatigue tests for PEDOT:PSS (9.06%)-PAAm organogels after 1000 cycles of repeated tensile deformations of up to 50% strain. d) Stress-strain curves from the 1st, 10th, 100th, 500th and 1000th cycles. e) Resistance changes as a function of fatigue cycle up to the 1000th cycle. f) Resistance change-strain curves from the 1st, 10th, 100th, 500th and 1,000th cycles, which exhibited stretch-insensitive resistance change up to 50% strain within a cycle.

6.6. Environmental stabilities of the organogels

It is important to improve the environmental stability of conductive gels for their long-term use in air. The major problem is evaporation of the constituent liquids in the gels during exposure to air. Keeping the liquid inside the gels is essential for maintenance of the gel form. By using EG as the liquid constituent for the gels, we can expect long-term stability in ambient conditions. We compared the states of a hydrogel and the organogels of PEDOT:PSS-PAAm after exposure to air. The samples were cut into squares, and the states of the gels were determined at the start of the test and after one day (Figure 6.14a). In the case of the hydrogel, it was fully dried out and became a hard bulk polymer after only one day. In contrast, the organogels almost maintained their initial state, as shown in Figure 6.14a. The shrinkage of the gel was not observed after one day due to the lack of evaporation of the EG solvent; the gel was still moist and maintained mechanical stretchability.

To quantify the stability of the PEDOT:PSS-PAAm organogels, the weight loss of the liquid constituent inside the gels was measured as a function of time. PEDOT:PSS-PAAm hydrogels and PEDOT:PSS-PAAm organogels were prepared with various weight ratios of PEDOT:PSS. We measured the weight change of the liquid (w/w_0) with time. The initial and present weights are denoted by w_0 and w , respectively. As shown in Figure 6.14b, the experimental conditions are very harsh, with the experiment conducted in a vacuum chamber at a pressure lower than atmospheric pressure (0.013 atm). Figure 6.14c shows the weight change of the constituent liquids, i.e., water or EG, for each gel as a function of time. For the PEDOT:PSS-PAAm hydrogels, the weight of water inside the gels rapidly decreased, with the water completely evaporating within 3 hr. The hydrogel becomes a brittle

***Chapter 6: Strain-insensitive stretchable electronic conductors:
PEDOT-PSS/Acrylamide organogels***

bulk polymer in the fully dried state. In contrast, the PEDOT:PSS-PAAm organogels remain in the gel state for longer than 3 hr under the vacuum state. Although the organogels were under vacuum, 60 wt.% of the solvent remained in the organogels after 22 hr. The lack of evaporation is mainly due to the extremely low vapor pressure of the EG solvent. The vapor pressures of water and EG are 17.3 and 0.06 mm Hg at 20 °C^[110], respectively. Compared with water, EG barely evaporates in ambient air. Therefore, the organogels can retain the constituent liquid for a long time, and the maintenance of the gel state is even better when using EG. By introducing EG, which has a low vapor pressure, into the PEDOT:PSS gels, we can ensure the superior long-term stability of the conductive gels compared with other typical conductive hydrogels.

Chapter 6: Strain-insensitive stretchable electronic conductors: PEDOT-PSS/Acrylamide organogels

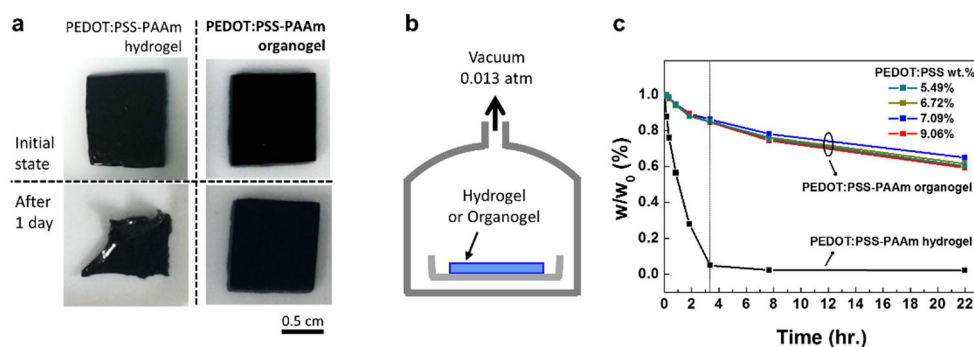


Figure 6.14. Environmentally stable PEDOT:PSS-PAAm organogels. (a) Photographs of the PEDOT:PSS-PAAm hydrogel and organogel before and after being dried in air for 1 day. (b) Schematic illustration of the experimental set-up for measurements of the weight changes of the gels in a vacuum chamber (0.013 atm). (c) Relative changes in the solvent weight (w/w_0 (%)) inside the PEDOT:PSS-PAAm hydrogel and PEDOT:PSS-PAAm organogels of various weight ratios in a vacuum chamber as a function of time at room temperature. The weights of the initial and present amounts of solvent are indicated with w_0 and w , respectively. The organogels contained above 60% of EG, even after 22 hr in the vacuum chamber.

6.6. Summary

Highly stretchable and electrically conductive PEDOT:PSS-PAAm organogels are successfully fabricated by using PEDOT:PSS conductive polymers and the highly cross-linkable PAAm polymer. Initially, by gelation of PEDOT:PSS solute dissolved solution mixed with EG solvent using PAAm, the PEDOT:PSS uniformly dispersed PAAm gels can be obtained. Subsequently, through dialysis and liquid exchange with EG, electrically conductive PEDOT:PSS-PAAm organogels with ionic conduction excluded are finally produced. Electrical percolation paths were formed with a polymeric path with closely packed PEDOT:PSS inside the organogels. Thus, the polymeric conducting path is well maintained during stretching up to large strains (> 300%), and a strain-insensitive resistance change is achieved up to 50% strain within fatigue cycle. The strength of the large stretchability and high electrical conductivity enable these conductive organogels to be utilised as electrical interconnects or electrodes for stretchable electronic devices. Due to the softness and easy formability of the gels, they can be patterned into various structural forms and attached onto any arbitrary shape. The potential applications of these organogels are numerous, e.g., in human-wearable and attachable electronic devices as an essential component that transports electrical signals with long-term stability.

CHAPTER 7

Conclusion

7.1. Conclusion

This study investigated the overall correlation of mechanical deformation and electrical properties of PEDOT:PSS conductive polymers. Based on an in-depth understanding of the dependency of mechanical strain, highly stretchable and electrically conductive PEDOT:PSS gel-type materials were successfully developed. As electronic and stretchable conductors, PEDOT:PSS are mechanically soft and easily processable materials that have use in various applications in the fields of organic electronics and bioelectronics.

Precise predictions of such strain-dependent behavior are of particular importance in the fabrication of flexible or stretchable electronics. The underlying principles were fully investigated for the PEDOT:PSS films by decoupling the intrinsic and extrinsic properties upon being stretched. This revealed that strain-induced morphological transformations led to significant decreases in the conductivity of PEDOT:PSS films. This unusual phenomenon offers the new possibility of mechanically and reversibly

Chapter 7: Conclusion

controlling the conductivity of such films. First, by mechanical matching PEDOT:PSS and the compliant substrate, crack-free PEDOT:PSS films subjected to more than 60 % strain was successfully demonstrated. This marks an important step toward the development of stretchable electronics. Second, the strain-driven transformation of PEDOT:PSS led to a large decrease in the materials' intrinsic resistivity by up to 90%, which was induced by a growth in the conductive regions that were composed of PEDOT-rich cores. These strain-induced conductivity changes will allow these materials to be used in numerous potential applications, including the development of flexible strain sensors, tunable conductivity tools, and the development of stretchable conductors.

Based on an in-depth understanding of the mechanical and electrical properties of PEDOT:PSS and fundamental studies on the chemical syntheses of soft gel materials, a new class of PEDOT:PSS electronic conductor was generated using a stretchable, electrochemical reaction-free, and electro-conductive PEDOT:PSS organogel. The organogel electronic conductor was electrically conductive even under DC voltages of up to ± 5 V without any electrochemical reactions. This voltage window had not been explored for conventional conductive gels. Furthermore, the electrical resistance was insensitively changed by stretching the material above 350% strain by forming a polymeric conducting path with closely packed PEDOT:PSS in the gel. In particular, no increase in resistance was observed when the materials were subjected to a strain of up to 50% during deformation cycles. These functions were maintained with long-term environmental stability with exposure to air. This unprecedented electronic organogel conductor should enable researchers to design and tailor entirely new classes of conductive organic hybrid materials that should also result in the development of a new research area regarding biocompatible electronic devices.

7.2. Future work and recommendations

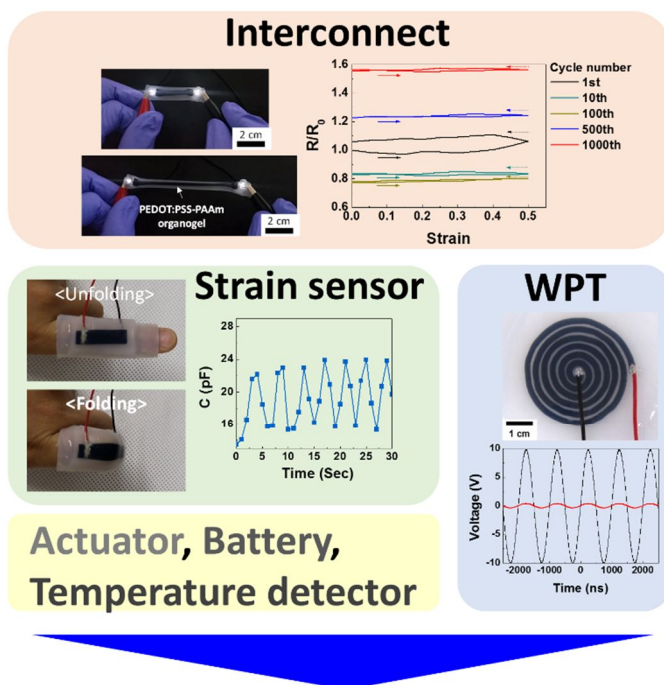
The development of PEDOT:PSS-based organogels was demonstrated for use in stretchable electronic devices. Recently, we made highly stretchable and biocompatible strain sensors. By using two parallel conductive organogels embedded in an insulated Ecoflex mold, capacitive type strain sensors were fabricated. The degree of stretching and compressive strain could be measured above 200% strain with changes in the capacitance. This device could be attached to bare skin, such as fingers, elbows, and knees, which required a large mechanical deformation. In addition, we demonstrated wireless power transmission with the PEDOT:PSS organogels that were patterned in a coil shape. By using a magnetic induction method, high frequency AC voltage could be directly transmitted from the transmitter to the receiver coils without any hazards to the human body. This enabled their integration with soft elastomeric substrates and allowed them to freely interconnect with PEDOT:PSS organogel conductors.

The utility of this material will be demonstrated by incorporating it into various electronic devices, such as a batteries, temperature detectors, and actuators (Figure 7.1). Because most part of electronics are composed of PEDOT:PSS organogel conductors, such devices could be considered one-component electronic devices. Therefore, with the integration of electronic devices based on soft PEDOT:PSS organogel, fully stretchable and biocompatible electronics-integrated soft artificial skins can be developed.

Further studies are also required to demonstrate the properties of PEDOT:PSS organogel-based electronic systems. It is essential to enhance the electrical conductivity of these organogels. By incorporating additional metallic particles,

Chapter 7: Conclusion

nanowires, or CNTs, which have high conductivity, the conductivity of organogels could be improved by several orders of magnitude. The development of electrical contact materials is important. To electrically connect soft organogel conductors and hard metallic conductors, the contact materials should be mechanically compatible, electrochemically stable, and allow for ohmic conduction. PEDOT:PSS is expected to be a very suitable conductor for use as contact materials due to its electronic and ionic conductivity. For the development of electronic functional devices, soft conductive gel-based diodes, amplifiers, or transistors are important parts for the design of electronic circuits. To realize these devices, pn junctions must be formed. Hence, the development of n-type conductive gels should be investigated. All soft and human compatible functional devices will be enabled by combining n-type gels and p-type PEDOT:PSS gels. This will promote studies on human-applicable soft gel electronic materials for use in attachable or implantable devices, such as bio-electrodes, sensors, stimulators, and actuators. The combination of organic and bioelectronics fields will facilitate the progress of synergistic studies to add new bio-functionalities and develop new classes of soft materials that will also support the new area for biocompatible electronic devices.



Electronics-integrated artificial soft skins

Figure 7.1. Integration of PEDOT:PSS-PAAm organogel-based electronics, including interconnects, a strain sensor, wireless power transfer (WPT), battery, temperature detector, actuator, and other devices on soft elastomeric substrates.

References

- [1] U. Lang, N. Naujoks, J. Dual, *Synth. Met.* **2009**, *159*, 473.
- [2] A. M. Nardes, M. Kemerink, R. A. J. Janssen, *Phys. Rev. B* **2007**, *76*, 085208.
- [3] M. Drack, I. Graz, T. Sekitani, T. Someya, M. Kaltenbrunner, S. Bauer, *Adv. Mater.* **2014**, *27*, 34.
- [4] R.-H. Kim, D.-H. Kim, J. Xiao, B. H. Kim, S.-I. Park, B. Panilaitis, R. Ghaffari, J. Yao, M. Li, Z. Liu, V. Malyarchuk, D. G. Kim, A.-P. Le, R. G. Nuzzo, D. L. Kaplan, F. G. Omenetto, Y. Huang, Z. Kang, J. a Rogers, *Nat. Mater.* **2010**, *9*, 929.
- [5] D.-H. Kim, N. Lu, R. Ma, Y.-S. Kim, R.-H. Kim, S. Wang, J. Wu, S. M. Won, H. Tao, A. Islam, K. J. Yu, T. Kim, R. Chowdhury, M. Ying, L. Xu, M. Li, H.-J. Chung, H. Keum, M. McCormick, P. Liu, Y. Zhang, F. G. Omenetto, Y. Huang, T. Coleman, J. A. Rogers, *Science* **2011**, *333*, 838.
- [6] M. Kaltenbrunner, T. Sekitani, J. Reeder, T. Yokota, K. Kuribara, T. Tokuhara, M. Drack, R. Schwödiauer, I. Graz, S. Bauer-Gogonea, S. Bauer, T. Someya, *Nature* **2013**, *499*, 458.

- [7] S. Yun, X. Niu, Z. Yu, W. Hu, P. Brochu, Q. Pei, *Adv. Mater.* **2012**, *24*, 1321.
- [8] S. Han, S. Hong, J. Ham, J. Yeo, J. Lee, B. Kang, P. Lee, J. Kwon, S. S. Lee, M.-Y. Yang, S. H. Ko, *Adv. Mater.* **2014**, *26*, 5808.
- [9] K. H. Kim, M. Vural, M. F. Islam, *Adv. Mater.* **2011**, *23*, 2865.
- [10] J. Ge, H. Bin Yao, X. Wang, Y. D. Ye, J. L. Wang, Z. Y. Wu, J. W. Liu, F. J. Fan, H. L. Gao, C. L. Zhang, S. H. Yu, *Angew. Chemie - Int. Ed.* **2013**, *52*, 1654.
- [11] M. S. Lee, K. Lee, S. Y. Kim, H. Lee, J. Park, K. H. Choi, H. K. Kim, D. G. Kim, D. Y. Lee, S. Nam, J. U. Park, *Nano Lett.* **2013**, *13*, 2814.
- [12] F. Xu, X. Wang, Y. Zhu, Y. Zhu, *Adv. Funct. Mater.* **2012**, *22*, 1279.
- [13] Z. Xu, Z. Liu, H. Sun, C. Gao, *Adv. Mater.* **2013**, *25*, 3249.
- [14] U.-H. Shin, D.-W. Jeong, S.-H. Kim, H. W. Lee, J.-M. Kim, *ACS Appl. Mater. Interfaces* **2014**, *6*, 12909.
- [15] J. Zang, S. Ryu, N. Pugno, Q. Wang, Q. Tu, M. J. Buehler, X. Zhao, *Nat. Mater.* **2013**, *12*, 321.

- [16] B. Y. Ahn, E. B. Duoss, M. J. Motala, X. Guo, S.-I. Park, Y. Xiong, J. Yoon, R. G. Nuzzo, J. A. Rogers, J. A. Lewis, *Science* **2009**, *323*, 1590.
- [17] A. N. Aleshin, S. R. Williams, A. J. Heeger, *Synth. Met.* **1998**, *94*, 173.
- [18] L. Rebouta, L. Rubio-Peña, C. Oliveira, S. Lanceros-Mendez, C. J. Tavares, E. Alves, *Thin Solid Films* **2010**, *518*, 4525.
- [19] S.-I. Na, S.-S. Kim, J. Jo, D.-Y. Kim, *Adv. Mater.* **2008**, *20*, 4061.
- [20] K. E. Aasmundtveit, E. J. Samuelsen, L. A. A. Pettersson, O. Inganäs, T. Johansson, R. Feidenhans'l, *Synth. Met.* **1999**, *101*, 561.
- [21] T. Takano, H. Masunaga, A. Fujiwara, H. Okuzaki, T. Sasaki, *Macromolecules* **2012**, *45*, 3859.
- [22] Q. Wei, M. Mukaida, Y. Naitoh, T. Ishida, *Adv. Mater.* **2013**, *25*, 2831.
- [23] Y. Niquet, C. Delerue, C. Krzeminski, *Nano Lett.* **2012**, *12*, 3545.
- [24] D. R. Cairns, R. P. Witte, D. K. Sparacin, S. M. Sachsman, D. C. Paine, G. P. Crawford, R. R. Newton, *Appl. Phys. Lett.* **2000**, *76*, 1425.
- [25] T. Li, Z. Y. Huang, Z. C. Xi, S. P. Lacour, S. Wagner, Z. Suo, *Mech. Mater.* **2005**, *37*, 261.

- [26] S. P. Lacour, D. Chan, S. Wagner, T. Li, Z. Suo, *Appl. Phys. Lett.* **2006**, *88*, 204103.
- [27] N. Lu, X. Wang, Z. Suo, J. Vlassak, *Appl. Phys. Lett.* **2007**, *91*, 221909.
- [28] B. Erdem Alaca, M. T. a. Saif, H. Sehitoglu, *Acta Mater.* **2002**, *50*, 1197.
- [29] N. Cordero, J. Yoon, Z. Suo, *Appl. Phys. Lett.* **2007**, *90*, 111910.
- [30] J. Sun, N. Lu, J. Yoon, K.-H. Oh, Z. Suo, J. J. Vlassak, *J. Mater. Res.* **2009**, *24*, 3338.
- [31] T. Sekitani, Y. Noguchi, U. Zschieschang, H. Klauk, T. Someya, *Proc. Natl. Acad. Sci. U. S. A.* **2008**, *105*, 4976.
- [32] K.-Y. Chun, Y. Oh, J. Rho, J.-H. Ahn, Y.-J. Kim, H. R. Choi, S. Baik, *Nat. Nanotechnol.* **2010**, *5*, 853.
- [33] Z. Yu, L. Li, Q. Zhang, W. Hu, Q. Pei, *Adv. Mater.* **2011**, *23*, 4453.
- [34] T. Someya, T. Sekitani, S. Iba, Y. Kato, H. Kawaguchi, T. Sakurai, *Proc. Natl. Acad. Sci. U. S. A.* **2004**, *101*, 9966.
- [35] D.-H. Kim, J. Song, W. M. Choi, H.-S. Kim, R.-H. Kim, Z. Liu, Y. Y. Huang, K.-C. Hwang, Y. -w. Zhang, J. a Rogers, *Proc. Natl. Acad. Sci.* **2008**, *105*,

18675.

- [36] J. a Rogers, T. Someya, Y. Huang, *Science* **2010**, 327, 1603.
- [37] S. Kirchmeyer, K. Reuter, *J. Mater. Chem.* **2005**, 15, 2077.
- [38] Y.-J. Lin, F.-M. Yang, C.-Y. Huang, W.-Y. Chou, J. Chang, Y.-C. Lien, *Appl. Phys. Lett.* **2007**, 91, 092127.
- [39] J. Huang, P. F. Miller, J. S. Wilson, a. J. de Mello, J. C. de Mello, D. D. C. Bradley, *Adv. Funct. Mater.* **2005**, 15, 290.
- [40] J. Y. Kim, J. H. Jung, D. E. Lee, J. Joo, *Synth. Met.* **2002**, 126, 311.
- [41] S. K. M. Jönsson, J. Birgersson, X. Crispin, G. Greczynski, W. Osikowicz, A. W. Denier van der Gon, W. R. Salaneck, M. Fahlman, *Synth. Met.* **2003**, 139, 1.
- [42] J. Ouyang, Q. Xu, C.-W. Chu, Y. Yang, G. Li, J. Shinar, *Polymer (Guildf)*. **2004**, 45, 8443.
- [43] G. Latessa, F. Brunetti, A. Reale, G. Saggio, A. Di Carlo, *Sensors Actuators B Chem.* **2009**, 139, 304.
- [44] S. Takamatsu, T. Takahata, M. Muraki, E. Iwase, K. Matsumoto, I.

- Shimoyama, *J. Micromechanics Microengineering* **2010**, *20*, 075017.
- [45] D. J. Lipomi, J. A. Lee, M. Vosgueritchian, B. C. Tee, J. A. Bolander, Z. Bao, *Chem. Mater.* **2011**, *24*, 373.
- [46] V. Vijay, A. D. Rao, K. S. Narayan, *J. Appl. Phys.* **2011**, *109*, 084525.
- [47] H. Hillborg, J. F. Ankner, U. W. Gedde, G. D. Smith, H. K. Yasuda, K. Wikstro, **2000**, *41*, 6851.
- [48] P. Görrn, S. Wagner, *J. Appl. Phys.* **2010**, *108*, 093522.
- [49] D. Y. W. Yu, *J. Appl. Phys.* **2004**, *95*, 2991.
- [50] A. M. Nardes, R. a. J. Janssen, M. Kemerink, *Adv. Funct. Mater.* **2008**, *18*, 865.
- [51] R. Jalili, J. M. Razal, P. C. Innis, G. G. Wallace, *Adv. Funct. Mater.* **2011**, *21*, 3363.
- [52] J.-H. Huang, D. Kekuda, C.-W. Chu, K.-C. Ho, *J. Mater. Chem.* **2009**, *19*, 3704.
- [53] U. Lang, E. Müller, N. Naujoks, J. Dual, *Adv. Funct. Mater.* **2009**, *19*, 1215.
- [54] D. Tahk, H. H. Lee, D.-Y. Khang, *Macromolecules* **2009**, *42*, 7079.
- [55] Y. Cao, P. Smith, A. J. Heeger, *Synth. Met.* **1991**, *43*, 181.

- [56] S. J. Pomfret, P. N. Adams, N. P. Comfort, A. P. Monkman, *Polymer (Guildf)*. **2000**, *41*, 2265.
- [57] S. P. Lacour, S. Wagner, Z. Huang, Z. Suo, *Appl. Phys. Lett.* **2003**, *82*, 2404.
- [58] N. Lu, Z. Suo, J. J. Vlassak, *Acta Mater.* **2010**, *58*, 1679.
- [59] C. F. Guo, T. Sun, Q. Liu, Z. Suo, Z. Ren, *Nat. Commun.* **2014**, *5*, 3121.
- [60] C. S. Smith, *Phys. Rev.* **1954**, *94*, 42.
- [61] J. T. Lenkkeri, *Phys. Status Solidi* **1986**, *136*, 373.
- [62] R. He, P. Yang, *Nat. Nanotechnol.* **2006**, *1*, 42.
- [63] M. J. Knight, *J. Vac. Sci. Technol.* **1969**, *6*, 706.
- [64] S. Sugiyama, M. Takigawa, I. Igarashi, *Sensors and Actuators* **1983**, *4*, 113.
- [65] P. F. French, A. G. R. Evans, *Solid. State. Electron.* **1989**, *32*, 1.
- [66] A. Partridge, S. Member, J. K. Reynolds, B. W. Chui, E. M. Chow, A. M. Fitzgerald, L. Zhang, N. I. Maluf, T. W. Kenny, *J. Microelectromechanical Syst.* **2000**, *9*, 58.
- [67] H. Wu, D. Kong, Z. Ruan, P.-C. Hsu, S. Wang, Z. Yu, T. J. Carney, L. Hu, S. Fan, Y. Cui, *Nat. Nanotechnol.* **2013**, *8*, 421.

- [68] Y. Yu, J. Zeng, C. Chen, Z. Xie, R. Guo, Z. Liu, X. Zhou, Y. Yang, Z. Zheng, *Adv. Mater.* **2014**, *26*, 810.
- [69] M. Park, J. Im, M. Shin, Y. Min, J. Park, H. Cho, S. Park, M.-B. Shim, S. Jeon, D.-Y. Chung, J. Bae, J. Park, U. Jeong, K. Kim, *Nat. Nanotechnol.* **2012**, *7*, 803.
- [70] Y. Zhu, F. Xu, *Adv. Mater.* **2012**, *24*, 1073.
- [71] J. Di, D. Hu, H. Chen, Z. Yong, M. Chen, Z. Feng, Y. Zhu, Q. Li, *ACS Nano* **2012**, *6*, 5457.
- [72] Y. H. Kim, C. Sachse, M. L. Machala, C. May, L. Müller-Meskamp, K. Leo, *Adv. Funct. Mater.* **2011**, *21*, 1076.
- [73] P. Docampo, J. M. Ball, M. Darwich, G. E. Eperon, H. J. Snaith, *Nat. Commun.* **2013**, *4*, 2761.
- [74] S. Savagatrup, A. S. Makaram, D. J. Burke, D. J. Lipomi, *Adv. Funct. Mater.* **2014**, *24*, 1169.
- [75] M. Kaltenbrunner, M. S. White, E. D. Głowacki, T. Sekitani, T. Someya, N. S. Sariciftci, S. Bauer, *Nat. Commun.* **2012**, *3*, 770.

- [76] S. Takamatsu, T. Takahata, M. Muraki, E. Iwase, K. Matsumoto, I. Shimoyama, *J. Micromechanics Microengineering* **2010**, *20*, 075017.
- [77] F.-C. Tang, J. Chang, F.-C. Wu, H.-L. Cheng, S. L.-C. Hsu, J.-S. Chen, W.-Y. Chou, *J. Mater. Chem.* **2012**, *22*, 22409.
- [78] T. Yasuda, L. Han, T. Tsutsui, *J. Photopolym. Sci. Technol.* **2009**, *22*, 713.
- [79] Y.-Y. Lee, J.-H. Lee, J.-Y. Cho, N.-R. Kim, D.-H. Nam, I.-S. Choi, K. T. Nam, Y.-C. Joo, *Adv. Funct. Mater.* **2013**, *23*, 4020.
- [80] G. Greczynski, T. Kugler, W. R. Salaneck, *Thin Solid Films* **1999**, *354*, 129.
- [81] G. Greczynski, T. Kugler, M. Keil, W. Osikowicz, M. Fahlman, W. . Salaneck, *J. Electron Spectros. Relat. Phenomena* **2001**, *121*, 1.
- [82] M. Garg, J. K. Quamara, *Indian J. Pure Appl. Phys.* **2007**, *45*, 563.
- [83] C. Sriprachuabwong, C. Karuwan, A. Wisitsorrat, D. Phokharatkul, T. Lomas, P. Sritongkham, A. Tuantranont, *J. Mater. Chem.* **2012**, *22*, 5478.
- [84] Y. Xiao, J.-Y. Lin, S.-Y. Tai, S.-W. Chou, G. Yue, J. Wu, *J. Mater. Chem.* **2012**, *22*, 19919.

- [85] D. J. Lipomi, M. Vosgueritchian, B. C.-K. Tee, S. L. Hellstrom, J. a Lee, C. H. Fox, Z. Bao, *Nat. Nanotechnol.* **2011**, *6*, 788.
- [86] C. Keplinger, J.-Y. Sun, C. C. Foo, P. Rothmund, G. M. Whitesides, Z. Suo, *Science* **2013**, *341*, 984.
- [87] T. Yamada, Y. Hayamizu, Y. Yamamoto, Y. Yomogida, A. Izadi-Najafabadi, D. N. Futaba, K. Hata, *Nat. Nanotechnol.* **2011**, *6*, 296.
- [88] G. a Salvatore, N. Münzenrieder, T. Kinkeldei, L. Petti, C. Zysset, I. Strebel, L. Büthe, G. Tröster, *Nat. Commun.* **2014**, *5*, 2982.
- [89] I. R. Mineev, P. Musienko, A. Hirsch, Q. Barraud, N. Wenger, E. M. Moraud, J. Gandar, M. Capogrosso, T. Milekovic, L. Asboth, R. F. Torres, N. Vachicouras, Q. Liu, N. Pavlova, S. Duis, A. Larmagnac, J. Voros, S. Micera, Z. Suo, G. Courtine, S. P. Lacour, *Science* **2015**, *347*, 159.
- [90] Y. Sun, W. M. Choi, H. Jiang, Y. Y. Huang, J. a Rogers, *Nat. Nanotechnol.* **2006**, *1*, 201.
- [91] K. J. Henderson, T. C. Zhou, K. J. Otim, K. R. Shull, *Macromolecules* **2010**, *43*, 6193.

- [92] J.-Y. Sun, X. Zhao, W. R. K. Illeperuma, O. Chaudhuri, K. H. Oh, D. J. Mooney, J. J. Vlassak, Z. Suo, *Nature* **2012**, *489*, 133.
- [93] T. L. Sun, T. Kurokawa, S. Kuroda, A. Bin Ihsan, T. Akasaki, K. Sato, M. A. Haque, T. Nakajima, J. P. Gong, *Nat. Mater.* **2013**, *12*, 932.
- [94] T. Baumberger, C. Caroli, D. Martina, *Nat. Mater.* **2006**, *5*, 552.
- [95] D. Mawad, E. Stewart, D. L. Officer, T. Romeo, P. Wagner, K. Wagner, G. G. Wallace, *Adv. Funct. Mater.* **2012**, *22*, 2692.
- [96] H. Ding, M. Zhong, Y. J. Kim, P. Pholpabu, A. Balasubramanian, C. M. Hui, H. He, H. Yang, K. Matyjaszewski, C. J. Bettinger, M. Science, T. Beijing, X. Road, F. Avenue, U. States, B. Engineering, C. Engineering, M. Avenue, *ACS Nano* **2014**, *8*, 4348.
- [97] S. Naficy, J. M. Razal, G. M. Spinks, G. G. Wallace, P. G. Whitten, *Chem. Mater.* **2012**, *24*, 3425.
- [98] S. Sekine, Y. Ido, T. Miyake, K. Nagamine, M. Nishizawa, *J. Am. Chem. Soc.* **2010**, *132*, 13174.
- [99] S. Ghosh, O. Inganäs, *Adv. Mater.* **1999**, *11*, 1214.

- [100] G.-P. Hao, F. Hippauf, M. Oschatz, F. M. Wisser, A. Leifert, W. Nickel, N. Mohamed-Noriega, Z. Zheng, S. Kaskel, *ACS Nano* **2014**, *8*, 7138.
- [101] J. Hur, K. Im, S. W. Kim, J. Kim, D. Chung, T. Kim, K. H. Jo, J. H. Hahn, Z. Bao, S. Hwang, N. Park, *ACS Nano* **2014**, *8*, 10066.
- [102] L. Li, Y. Wang, L. Pan, Y. Shi, W. Cheng, Y. Shi, G. Yu, *Nano Lett.* **2015**, *15*, 1146.
- [103] M. Bassil, J. Davenas, M. EL Tahchi, *Sensors Actuators B Chem.* **2008**, *134*, 496.
- [104] H. Kang, S. Hwang, J. Kwak, *Nanoscale* **2015**, *7*, 994.
- [105] L. Pan, G. Yu, D. Zhai, H. R. Lee, W. Zhao, N. Liu, H. Wang, B. C.-K. Tee, Y. Shi, Y. Cui, Z. Bao, *Proc. Natl. Acad. Sci.* **2012**, *109*, 9287.
- [106] Y. Shi, M. Wang, C. Ma, Y. Wang, X. Li, G. Yu, *Nano Lett.* **2015**, *15*, 6276.
- [107] P. G. Agache, C. Monneur, J. L. Leveque, J. De Rigal, *Arch. Dermatol. Res.* **1980**, *269*, 221.
- [108] X. Liang, S. A. Boppart, *IEEE Trans. Biomed. Eng.* **2010**, *57*, 953.
- [109] J. P. Gong, *Soft Matter* **2010**, *6*, 2583.

[110] D. R. Lide, *CRC Press. Boca Raton, FL, 2005. 2005, CRC Press,.*

요약 (국문초록)

최근 전도성 고분자는 큰 기계적 변형이 노출되는 유연 및 신축성 소자 구현을 위한 전도 물질로써 다양하게 활용되고 있다. 탄성 변형을 영역과는 달리 큰 변형율에 의한 소성 변형이 소자에 가해질 경우에 결함발생, 구조적 및 형상적 변화, 인접 물질간 영향 등 외부적 요소의 복합적 작동으로 인한 전기적 특성의 변화가 발생하게 된다. 그러므로, 각 요소의 영향을 구별하고 기계적 변형에 의한 내재적 전기적 특성의 변화 메커니즘을 규명하는 것은 향후 신축성 전극 재료 개발을 위하여 매우 중요하다. 전극 소재로써 적용이 가능한 대표적 전도성 고분자인 poly(3,4-ethylenedioxythiophene):poly(styrenesulfonate) (PEDOT:PSS)를 활용하여 큰 변형율로 신축이 가능한 새로운 종류의 신축성 전극 구현을 연구 개발을 수행하였다. 첫째, 필름 형태의 PEDOT:PSS 전극에 기계적 물성(Poisson's ratio and elastic modulus)이 매칭된 polyimide (PI) 기판을 적용하여 60% 변형율 이상에서도 버클이나 크랙과 같은 결함 생성이 없는 PEDOT:PSS 전극을 개발하였다. 흥미롭게도 원액 PEDOT:PSS 필름의 경우 인장 변형에 따라서 80% 이상의 비저항 감소가 발생하였고, 디메틸설폭사이드 (DMSO) 첨가를 통한 화학적 처리 후 PEDOT:PSS-DMSO 필름의 경우 변형율에 관계없이 비저항이 거의 일정한 것을 관찰 할 수 있었다. 화학적 처리를 한 필름은 DMSO 용매로 인해 PEDOT 과 PSS 가 해리된 구조를 갖고, 인장에 따라서도 전기 전도 경로가 달라지지 않는 몰포로지를 갖는 것을 확인하였다. 반면, 원액의 필름의 경우 인장 변형에 따라 전도성의 PEDOT-rich 코어 영역 성장이 크게 일어 난 것을 밝혀 냈다. 이를 통해 최초로 PEDOT:PSS 의 인장 변형에 따른 메커니즘을 밝혀 냈고, 향후 기계적 변형 의존성을 이용한 전기 전도 조절 방법으로 활용 가능성을 제시하였다. 신축에 따라서도 전기 전도가 달라지지 않는 화학적 처리를 한

PEDOT:PSS 를 활용하여, 소프트 한 젤 물질을 이용한 PEDOT:PSS 기반 신축전극 개발을 수행하였다. 젤의 원초적인 소프트 한 성질 덕분에 제작된 신축 전극은 신체 피부와의 적합성이 우수하고 큰 변형 하에서도 결함 없는 탄성적 변형이 가능하다. 또한 전기 전도 측면에서 PEDOT:PSS 의 화학적 처리를 통해 높은 전도도 확보가 가능하다. 액상의 PEDOT:PSS 와 유기용매 에틸렌글리콜을 젤 형성을 위한 폴리아크릴아마이드 (PAAm) 가교 고분자에 고루 분산시켜 PEDOT:PSS-PAAm 에틸렌글리콜 젤을 합성하였다. 젤 용매로써 에틸렌글리콜 유기용매를 사용한 오가노젤 형태로 제작을 하여, 장기간 노출 시 용매의 증발이 거의 발생하지 않아 안정성이 뛰어나고 직류 전원에서도 전기화학 반응이 없는 신축 전기 전도체를 개발하였다. 제작된 젤은 350% 이상의 큰 변형율에서도 전기 전달이 안정적으로 수행한다. 이것은 젤 내부에 패킹된 PEDOT:PSS 고분자 전도 경로를 형성하여 변형에 따라서도 전도경로가 유지되기 때문이며, 전기 저항의 변화가 형상변화에 의한 이론적 증가보다 훨씬 낮게 변화하는 것을 확인하였다. 심지어 50% 변형율에서 반복적인 변형을 가하더라도 전기저항의 변화가 거의 나타나지 않는 변형에 둔감한 거동을 얻어 내었다. 향후 PEDOT:PSS 신축 전극은 고 신축성으로 인해 복잡하고 다양한 표면을 덮을 수 있는 인체 접촉 및 삽입 식 전자 소자에 전극을 다양한 활용이 기대된다. 본 연구는 향후 새로운 형태의 오가닉 하이브리드 전극 물질 개발이나 생체적합 형 전자 소자 분야 활용 분야에 활용 가능할 것으로 기대한다.

표제어: 전도성 고분자; PEDOT:PSS; 기계적 매칭; 물포로지 변화; 기계-전기적 특성; 신축성 전기 전도체; 변형 둔감성;

학 번: 2010-20623